Western Graduate&PostdoctoralStudies

Western University
Scholarship@Western

Electronic Thesis and Dissertation Repository

10-2-2012 12:00 AM

Load-Sharing of Toe-Nailed, Roof-to-Wall Connections under Extreme Wind Loads in Wood-Frame Houses

Mohammad Khan, *The University of Western Ontario*

Supervisor: Dr. Gregory A. Kopp, *The University of Western Ontario*

A thesis submitted in partial fulfillment of the requirements for the Master of Engineering Science degree in Civil and Environmental Engineering

© Mohammad Khan 2012

Follow this and additional works at: https://ir.lib.uwo.ca/etd

Part of the Civil Engineering Commons, Other Civil and Environmental Engineering Commons, and the Structural Engineering Commons

Recommended Citation

Khan, Mohammad, "Load-Sharing of Toe-Nailed, Roof-to-Wall Connections under Extreme Wind Loads in Wood-Frame Houses" (2012). *Electronic Thesis and Dissertation Repository*. 895.
https://ir.lib.uwo.ca/etd/895

This Dissertation/Thesis is brought to you for free and open access by Scholarship@Western. It has been accepted for inclusion in Electronic Thesis and Dissertation Repository by an authorized administrator of Scholarship@Western. For more information, please contact wlswadmin@uwo.ca.

Load-Sharing of Toe-Nailed, Roof-to-Wall Connections under Extreme Wind Loads in Wood-Frame Houses

(Spine title: Load-Sharing Between Roof-to-Wall Connections)

(Thesis format: Monograph)

by

Mohammad Abrar Alam Khan

Department of Civil and Environmental Engineering

Faculty of Engineering

A thesis submitted in partial fulfillment

of the requirements for the degree of

Master of Engineering Science

The School of Graduate and Postdoctoral Studies

The University of Western Ontario

London, Ontario, Canada

© Mohammad Abrar A. Khan 2012

THE UNIVERSITY OF WESTERN ONTARIO
School of Graduate and Postdoctoral Studies

CERTIFICATE OF EXAMINATION

Supervisor

Dr. Gregory A. Kopp

Examiners

Dr. F. Michael Bartlett

Dr. Hanping Hong

Dr. W. John Braun

The thesis by
Mohammad Abrar Alam Khan

Entitled:

Load-Sharing of Toe-Nailed, Roof-to-Wall Connections under Extreme Wind Loads in Wood-Frame Houses

is accepted in partial fulfillment of the
requirements for the degree of
Master of Engineering Science

Date

Chair of the Thesis Examination Board

Abstract

A typical wood frame house roof consists of trusses which are nailed to the top-plates of the wall assembly. These are known as roof-to-wall connections (RTWCs). A load-sharing mechanism is developed between adjacent RTWCs via roof elements such as roof-sheathing, fascia beams, etc., during high wind loads. An experimental setup was developed to observe the load-sharing behavior between seven connections. To mimic the roof bending stiffness in the direction perpendicular to the trusses, two steel beams with representative bending stiffness were connected across the RTWCs in a simple way. Identical ramp and identical fluctuating wind loads were applied to all the connections simultaneously. Two types of beams were used for these loading types. The bending stiffness of the stiffer beams is four times higher than the bending stiffness of the less stiff beams. Individual RTWCs were also subjected to identical ramp and fluctuating wind loads to define the load-displacement behavior of toe-nail connections and to make comparisons with the results found from the RTWCs of the systems. From the tests conducted it was found that individual connections displacement variability for the same applied loads is reduced by the system (i.e., beams) due to load-sharing between the connections through the beams. Load-sharing is greatest during the short duration, damaging peak loads. Load-sharing changes and increases continuously with the permanent displacements during damaging peak loads. Due to higher flexural rigidity of the stiffer beams, load-sharing or load re-distribution is higher between the RTWCs than for the less stiff beams.

KEYWORDS: Wood-frame house, roof-to-wall connection, load-sharing, extreme wind loads

Acknowledgments

The author would like to express his sincere gratitude to his supervisor Dr. Gregory A. Kopp for his continuous support and guidance throughout the graduate studies at the University of Western Ontario. The author would also like to acknowledge Dr. David J. Henderson and Dr. Murray J. Morrison for their technical assistance in developing the experimental setup and helpful discussion with the test results. The author also likes to thank Mr. Tushar Kanti Guha for many interesting discussions.

The author appreciates the help of Mr. Andrew Klazinga for aiding in purchasing of the test materials and helping in operating the laboratory instrumentations. The author would also like to thank Mr. Craig Wood, Mr. Curtis Williams, Mr. Jefferson Scarrow and Mr. Athiban Pandiarajan for helping in constructing the test specimens and also conducting some of the tests.

This work was funded by NSERC under the Strategic Project Grants program and by the Institute for Catastrophic Loss Reduction (ICLR). Much of the infrastructure for this research was provided by grants and support from the Canada Foundation for Innovation, the Ontario Innovation Trust, and the Insurance Bureau of Canada. The author is grateful to Mr. Chris Vandalaar of University Machine Services who constructed the test rigs used herein.

Lastly, and most importantly, the author wishes to thank his parents, Mohammad Hiron Khan and Shirin Khan for raising him with love and support. This thesis is humbly dedicated to them.

TABLE OF CONTENTS

CERTIFICATE OF EXAMINATION ..... **II**

ABSTRACT ..... **III**

ACKNOWLEDGMENTS ..... **IV**

TABLE OF CONTENTS ..... **V**

LIST OF TABLES ..... **VIII**

LIST OF FIGURES ..... **IX**

CHAPTER 1: INTRODUCTION **1**

1.1 WIND LOADS ON LOW-RISE BUILDING 2

1.2 ROOF FAILURES & TOE-NAIL CONNECTIONS 3

1.3 VERTICAL LOAD PATH OF A RESIDENTIAL HOUSE 5

1.4 LOAD-SHARING BETWEEN ADJACENT RTWCS 7

1.5 RESEARCH OBJECTIVES 7

CHAPTER 2: LITERATURE REVIEW **9**

2.1 INTRODUCTION 9

2.2 RESPONSE BEHAVIOR OF INDIVIDUAL TOE-NAIL CONNECTIONS 9

2.3 LOAD-SHARING BEHAVIOR BETWEEN ADJACENT RTWCS 11

2.3.1 FULL-SCALE, GABLE ROOF TESTS OF MORRISON (2010) AND MORRISON ET AL. (2012) 12

2.3.2 FULL-SCALE HIP ROOF TESTS BY HENDERSON ET AL. (2011) AND KOPP ET AL. (2012) 15

2.4 SUMMARY 16

CHAPTER 3: EXPERIMENTAL SET-UP **17**

3.1 INTRODUCTION 17

3.2 SIMPLIFICATION OF THE ROOF SYSTEM 17

3.3 TEST SET-UP 19

3.4 DATA ACQUISITION 22

3.5 RAMP LOADS 23

3.6 FLUCTUATING WIND LOADS 24

3.7 FORCE BALANCE BETWEEN THE NET APPLIED LOAD AND NET MEASURED LOAD 27
3.8 TEST MATRIX 29

CHAPTER 4: TOE-NAIL TEST RESULTS 31

4.1 INTRODUCTION 31
4.2 RAMP LOADS APPLIED TO INDIVIDUAL TOE-NAILS 31
4.2.1 BI-LINEAR LOAD-DISPLACEMENT MODEL 33
4.2.2 CURVILINEAR LOAD-DISPLACEMENT MODEL 35
4.2.3 STATISTICS OF THE FITTED PARAMETERS FOR THE BI-LINEAR MODEL 38
4.2.4 DISTRIBUTION OF THE FITTED PARAMETERS FOR THE BI-LINEAR MODEL 40
4.2.5 CORRELATION BETWEEN PARAMETERS FOR THE BI-LINEAR MODEL 43
4.3 FLUCTUATING WIND LOADS ON INDIVIDUAL TOE-NAILS 44
4.4 COMPARISON OF LOAD-DISPLACEMENT BEHAVIOR IN THE INDIVIDUAL AND SYSTEM TESTS 48
4.4.1 INITIAL SLOPE 48
4.4.2 FAILURE CAPACITY (FC) AND FAILURE DISPLACEMENT (DC) 49
4.4.3 DISTRIBUTIONS OF FAILURE CAPACITY (FC) AND FAILURE DISPLACEMENT (DC) 53
4.5 FAILURE TYPES 58
4.6 MOISTURE CONTENT 59
4.7 CONCLUSIONS 60

CHAPTER 5: ANALYSIS OF LOAD-SHARING 61

5.1 INTRODUCTION 61
5.2 LOAD-SHARING BETWEEN STRONGER AND WEAKER CONNECTIONS FOR RAMP LOADS 62
5.3 EFFECT OF BEAM BENDING STIFFNESS ON LOAD-SHARING FOR IDENTICAL RAMP LOADS 67
5.4 LOAD-SHARING FOR FLUCTUATING WIND LOADS 74
5.4.1 VARIATION OF DISPLACEMENTS FOR RTWCS WITHIN THE SYSTEM 81
5.4.2 EFFECT OF BENDING STIFFNESS ON THE TIME DURATION TO FAILURE 84

CHAPTER 6: CONCLUSIONS & RECOMMENDATIONS 87

6.1 CONCLUSIONS 87
6.2 RECOMMENDATIONS FOR FUTURE RESEARCH 89

REFERENCES 91

APPENDIX A 95

A.1 CONSTRUCTION OF SPECIMENS 95

APPENDIX B 97

B.1 LOAD CELLS CALIBRATION 97

B.2 PRESSURE TRANSDUCER CALIBRATION 98

B.3 LINEAR VARIABLE DIFFERENTIAL TRANSFORMER (LVDT) CALIBRATION 100

APPENDIX C 102

C.1 MEASUREMENT UNCERTAINTY 102

C.2 PRECISION UNCERTAINTY (LINEARITY ERROR) FOR LOAD SENSORS 102

C.3 BIAS UNCERTAINTY FOR LOAD SENSORS 103

APPENDIX D 105

D.1 ROOF IDEALIZATION 105

D.2 FLEXURAL RIGIDITY OF LESS STIFF BEAMS 108

D.3 FLEXURAL RIGIDITY OF STIFFER BEAMS 109

APPENDIX E 110

E.1 ILLUSTRATION OF TWO-SAMPLE T-TEST 110

E.2 ILLUSTRATION OF ONE-WAY ANALYSIS OF VARIANCE (ANOVA) 111

E.3 ANDERSON-DARLING GOODNESS-OF-FIT TEST 114

CURRICULUM VITAE 116

LIST OF TABLES

Table 3.1 Test duration for different wind speeds. 26

Table 3.2 Test matrix for the current project 30

Table 4.1 Statistics of the load-displacement model for all 8kN/min ramp loading test (arbitrary estimation) 39

Table 4.2 Statistics of the load-displacement model for all 8kN/min ramp loading test (data-driven estimation) 39

Table 4.3 Correlation coefficients between different parameters for ramp loading tests (arbitrary estimation) 44

Table 4.4 Statistics of the failure capacities & failure displacements for different test types 53

Table 4.5 Anderson-Darling critical value and Anderson-Darling statistics for failure capacities & failure displacements for different test types 54

Table 4.6 Mean and standard deviation of the failure capacities for different failure types and different test types 59

Table 5.1 Mean displacement (D) and coefficient of variation (COV) of mean displacements at different time segments (groups) for the individual and system fluctuating wind loading tests 83

Table C.1 Uncertainties associated with individual Tension Load Cells (TLC). 103

Table C.2 Uncertainties associated with individual Bending Beam Load Cells (BLC). 104

LIST OF FIGURES

Figure 1.1 Global roof failure of a gable roof house (July 4, 2010; Raymore, Saskatchewan; photo courtesy of G.A. Kopp). 4

Figure 1.2 Failure of a group of trusses during a tornado (June 23, 2010; Midland, Ontario; photo courtesy of M.J. Morrison). 4

Figure 1.3 Shingle, sheathing and flushing loss on the upper roof (August 20, 2009; Vaughan, Ontario; photo courtesy of G.A. Kopp). 5

Figure 1.4 Vertical load path for a residential wood-frame house. 6

Figure 2.1 Load-displacement behavior of toe-nail connection. (a) Tri-linear model (Shanmugam et al., 2009), (b) Non-linear model given by Foschi (2000). 10

Figure 2.2 Estimated reaction loads vs. measured displacement for RTWC 'S3' for full scale gable roof test for different wind speeds (from Morrison et al., 2012). 14

Figure 2.3 Measured loads vs. displacement for a single toe-nailed RTWC (from Morrison & Kopp, 2011). 14

Figure 2.4 Measured displacement and reaction time histories of two adjacent, toe-nailed connections in a wood-framed, hip roof (from Henderson et al., 2011). 16

Figure 3.1 (a) Roof components that are considered to idealize the roof bending stiffness, (b) skeleton of a roof which shows that the trusses are nailed to the top plate (c) experimental test specimen which can replicate the roof bending stiffness (through beams) and truss spacing. 18

Figure 3.2 Experimental setup: seven test rigs one beside another. By changing the spacing of the test rigs on center distance between the RTWCs can be adjusted. 20

Figure 3.3 Experimental setup: test setup under the airbags. The load is applied through the airbags which connect the RTWC by tension load cell. Bending beam load cells measure the actual reaction load to the connection. Displacement transducer measures the vertical displacement of the connection from the smooth plain surface. 20

Figure 3.4 Photograph of the data acquisition system. 23

Figure 3.5 PLA generated 8kN/min ramp loads to one RTWC and compared to the demand force. 24

Figure 3.6 Foot print of the truss layout of the gable roof and the estimated reaction load to RTWC 'S3' for different wind speeds (from Morrison, 2010). This particular 'S3'

fluctuating wind loading history will be applied identically to the RTWCs within a system in the present study. 27

Figure 3.7 Net applied load & net measured load vs. time for one system test where identical 8kN/min ramp loads were applied to each of the connections within the system. 28

Figure 3.8 Net load differences vs. time for the same experiment shown in Figure 3.7. . 28

Figure 4.1 Load-displacement curve of 35 individual RTWCs for 8kN/min ramp loads and the mean load-displacement curve calculated from these test results..... 32

Figure 4.2 Load-displacement curve for one RTWC for 8kN/min ramp loads (experimental) and the idealized bi-linear model (broken lines). 34

Figure 4.3 Bi-linear nail withdrawal model for a RTWC. 34

Figure 4.4 Load-displacement curve for one RTWC for 8kN/min ramp load and idealized curvilinear load-displacement model (broken lines)..... 36

Figure 4.5 Curvilinear nail-withdrawal model for RTWC (adapted from He (2010)). 36

Figure 4.6 Mean capacity curve from 35 ramp loading tests and the fit to the theoretical capacity curve. 37

Figure 4.7 Normal, Log-normal, Gumbel and Weibull probability paper for initial slope (Ko). 41

Figure 4.8.a Theoretical and Empirical cumulative distribution function for (a) yield capacity (Fy), (b) yield displacement (Dy) and (c) initial slope (Ko) (for arbitrary estimation)..... 42

Figure 4.8.b Theoretical and Empirical cumulative distribution function for (d) failure capacity (Fc), (e) failure displacement (Fc) and (f) secondary slope (K1) (for arbitrary estimation)..... 42

Figure 4.9 Applied fluctuating wind loads to a RTWC (a) and the response of vertical displacement for that applied fluctuating wind loading (b). 45

Figure 4.10 Fluctuating wind loading time history used in the individual toe-nail tests as well as in the system tests. The damaging peaks (20) are marked by the black circles. .. 45

Figure 4.11 Load-displacement behavior for two RTWCs for fluctuating wind loads (experimental): (a) the connection fails at the maximum applied load; (b) the connection fails at a lower applied load than the maximum loads. 46

Figure 4.12 Regression analyses between the failure capacity and ultimate capacity for realistic wind load. 47

Figure 4.13 Measured loads vs. displacement for seven RTWCs in the less stiff system during one ramp loading test. Squares indicate the failure capacity (Fc) and failure displacement (Dc) for each connection; circles indicate the yield capacity (Fy) at fixed yield displacement ($Dy = 1.22mm$). 49

Figure 4.14 Box-and-whisker diagrams for failure capacities from the six test types. 50

Figure 4.15 Box-and-whisker diagrams for failure displacements from the six test types. 51

Figure 4.16 Probability density function (PDF) of failure capacities of six different test types. 55

Figure 4.17 Cumulative distribution function (CDF) of failure capacities of six different test types..... 56

Figure 4.18 Probability density function (PDF) of failure displacements of six different test types..... 56

Figure 4.19 Cumulative distribution function (CDF) of failure displacements of six different test types. 57

Figure 4.20 Different types of toe-nail connection failure (s-nail split failure is not shown here) 58

Figure 5.1 Load-sharing schematic diagram between two RTWCs. 62

Figure 5.2 Applied (P) and measured load (R) time series for RTWC#03~RTWC#05; RTWC#03 and RTWC#05 constructed with 3 nails whereas RTWC#04 constructed with 4 nails. 64

Figure 5.3 (a) Applied load (P) vs. displacement (D); (b) measured load (R) vs. displacement (D); and (c) load difference (ΔR) vs. displacement (D) for RTWC#03~RTWC#05 for the same experiment of Figure 5.2. 65

Figure 5.4 Applied (P) and measured (R) load time series for RTWC#03~RTWC#05; RTWC#03 and RTWC#05 constructed with 3 nails whereas RTWC#04 constructed with 2 nails. 66

Figure 5.5 Applied load vs. displacement (a) and measured load vs. displacement (b) for RTWC#03~RTWC#05 for the same experiment of Figure 5.4. 67

Figure 5.6 Applied and measured load time series for RTWC#03~RTWC#05 for the less stiff system. 69

Figure 5.7 Applied load (P) vs. displacement (D) and measured load (R) vs. displacement (D) for RTWC#03~RTWC#05 for the same experiment as Figure 5.6. 70

Figure 5.8 Applied (P) and measured (R) load time series for RTWC#03~RTWC#5 for stiffer system. 71

Figure 5.9 Applied load and measured load vs. displacement for RTWC#03~RTWC#05 for the same experiment of Figure 5.8. 72

Figure 5.10 Applied load (a), load difference (b) and displacement (c) time series for one toe-nail connection (RTWC#05) in the less stiff system for identical fluctuating 'S3' wind loads 76

Figure 5.11 (a) Applied load (P4, P5 & P6) and measured load (R5); (b) load difference (ΔR5) and (c) displacement (D5) for t=588s to 592s for the same experiment shown in Figure 5.10. 77

Figure 5.12 Load-displacement behavior for the same connection shown in Figure 5.10. 77

Figure 5.13 Load difference vs. time (a, c) and Displacement vs. time (b, d) for RTWC#03 and RTWC#04 respectively for one fluctuating wind loading system test with 6.35cm x 6.35cm x 0.476cm beams. 78

Figure 5.14 Load difference vs. displacement for seven RTWCs within the less stiff system during one experiment. 80

Figure 5.15 Load difference vs. displacement for seven RTWCs within the stiffer system during one experiment. 81

Figure 5.16 Box-and-whisker diagrams for mean displacements at different time segments (groups) mentioned in Table 5.1 for (a) individual fluctuating, (b) less stiff system fluctuating and (c) stiffer system fluctuating wind loads. 82

Figure 5.17 (a) Displacement vs. time for all the connections in the less stiff system during one fluctuating wind loads test. (b) Inset showing the same plot from 1490s to1520s. 86

Figure 5.18 (a) Displacement vs. time for all the connections in the stiffer system during one fluctuating wind loads test. (b) Inset showing the same plot from 1785s to1815s. ... 86

Figure A.1 Construction of a roof-to-wall toe nail connection. 95

Figure B.1 Load cell calibration technique 97

Figure B.2 A plot of voltage excitation measurements versus corresponding applied load with a least-squares line overlaid. 98

Figure B.3 Experimental set up for pressure transducer calibration. 99

Figure B.4 A plot of voltage excitation measurements versus corresponding applied pressure with a least-squares line overlaid. 100

Figure B.5 LVDT calibration technique. 100

Figure B.6 A plot of voltage excitation measurements versus corresponding displacement with a least-squares line overlaid. 101

Figure D.1 Roof system. The truss of the roof is nailed to the top plate by three-12d nails (toe-nail). The end of the trusses is interconnected via a fascia beam. 105

Figure D.2 Roof sheathing and fascia beam are considered for roof bending stiffness. 105

Figure D.3 Cross section of 5000mm long, 9mm thick roof sheathing and 2x4 fascia beam. 106

Figure D.4 Cross sections of the steel beams which have been used in the present study (less stiff system and stiffer system). 108

Chapter 1: INTRODUCTION

Hurricanes and other natural extreme wind events have caused extensive property damage to wood-frame residential construction in the past two decades in the United States and Canada. Insured damage estimated by *Georgia Insurance Information Service* (GIIS, 2004) claimed that Hurricane Hugo (1989) cost US$5.4 billion to insurance companies, most of which were residential damage claims. Hurricane Andrew (1992), Hurricane Iniki (1992) and Hurricane Opal (1995) produced insured property losses estimated at US$17.7 billion, US$1.8 billion and US$2.2 billion respectively. The deadliest, Hurricane Katrina (2005), exceeded all the previous damage records (US$81 billion, Knabb et al., 2005). The actual cost of the total damage would be, of course, even higher than the insured damage. Pielke et al. (2008) estimated the normalized mainland U.S. hurricane damage from 1900-2005 and mentioned that the current trend in the increasing population and infrastructure in coastal regions increases the likelihood of annual losses. The current upward trend in sea surface temperatures (Trenberth, 2005) is raising the probability of stronger hurricanes and its associated losses in the twenty first century (Emanuel, 2005). All these prediction of higher losses for upcoming hurricanes has made mitigation strategies more important than ever (Guikema, 2009 and Board on Natural Disasters, 1999).

Most residential structures in North America are made of wood-frame construction and these tend to be among the most vulnerable to high winds. Failures to such structures mostly initiate within the building envelope, especially the roof, since it experiences the highest wind loads. The progression of the roof failure increases when

there are openings on windward walls. Windborne debris impacts on windows and doors (HUD, 1993 and Minor, 1994) also increases the openings of the building envelope. Thus, internal pressurization (Kopp et al., 2008) raises the wind loading substantially which increases the likelihood of total roof failure. Water penetration through the openings also causes extensive interior damage and the contents of the house (Sparks et al., 1994).

1.1 Wind loads on low-rise building

Severe wind storms, such as landfalling hurricanes, tornadoes, downbursts, etc., are associated with highly varying turbulent wind fields. These fluctuating winds and building aerodynamics are responsible for generating spatially and temporally varying pressures on the building surfaces (Surry et al., 1999). Wind loads on the roof of a low rise building depends on many parameters, such as roof slope and shape, building height, upstream exposure, as well as wind velocity, direction and duration (Ginger and Holmes, 2003; Ho et al., 2005; Zisis and Stathopoulos, 2009; Kopp et al., 2011). The load path of a light frame house is not well defined due to the redundant structural members in a simple house, and the role of internal linings and architectural features distributing loads to other structural members. As a result, the structural analysis of light frame houses is not straightforward (Reardon and Henderson, 1996). Due to this complexity in analysis, residential framing and building guidelines are often prescriptive and based on simplified engineering analysis (Henderson et al., 2011).

1.2 Roof failures & toe-nail connections

Damage investigations after severe windstorms have shown that roof sheathing failures (Lee and Rosowsky, 2005) and global roof failures (Kopp et al., 2011) are common. Historically, toe-nail connections are used as a hold down connection for the roof trusses to the top plate of the wall assembly of low-rise wood-frame houses, which are known as roof-to-wall connections (RTWC). Figures 1.1 to 1.3 show photographs of roof failures, which were taken during damage surveys of tornadoes that struck at different locations in Canada. These figures show that toe-nails are the main fasteners that hold down the roof to the wall and global roof failure (whole roof blown off) and sheathing failure (partial roof failure) has been often found to be very common. In particularly Figure 1.1 and 1.2 shows that the roof trusses and the roof sheathings actually acting as a rigid frame during failure. So, the entire roof system actually acts as a unit for these particular types of failures. However, in this present study, only the mechanism of global roof failure will be studied thoroughly. Although, now it is a reasonably common practice to use hurricane straps in hurricane prone regions after Hurricane Andrew (1992), there are many existing houses or houses in non-hurricane prone areas where the roof system depends on toe-nail connection capacity and its behavior. After Hurricane Andrew in 1992, improved building code provisions (1994) were implemented in South Florida. Over 80% of the existing homes today were constructed before the improved building code provisions (US Census Bureau 2003) in hurricane-prone regions. A major source of damage and economic loss during hurricanes are from existing single-family residential homes.

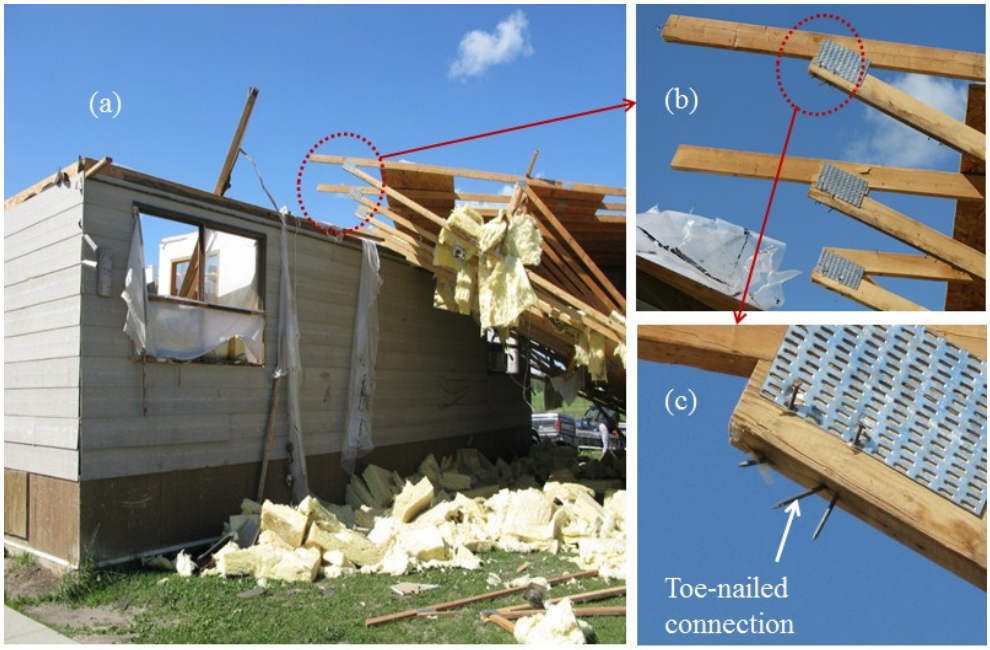

Figure 1.1 Global roof failure of a gable roof house (July 4, 2010; Raymore, Saskatchewan; photo courtesy of G.A. Kopp).

Figure 1.2 Failure of a group of trusses during a tornado (June 23, 2010; Midland, Ontario; photo courtesy of M.J. Morrison).

Figure 1.3 Shingle, sheathing and flushing loss on the upper roof (August 20, 2009; Vaughan, Ontario; photo courtesy of G.A. Kopp).

1.3 Vertical load path of a residential House

In the building system, the interconnected elements must sustain the uplift load and transfer it to the ground. Figure 1.4 shows a schematic diagram of the vertical load path of a residential wood frame house. The wind-generated suction creates uplift loads on the surface of the roof. The roof sheathing (plywood or Oriented Strand Board (OSB)), which are nailed (or screwed) to the top chords of the trusses, transfers this load to the top plate, which is attached to the wall assembly. The trusses are usually nailed to the top plate by three 8d or 12d nails (Ontario Building Code, 2006).

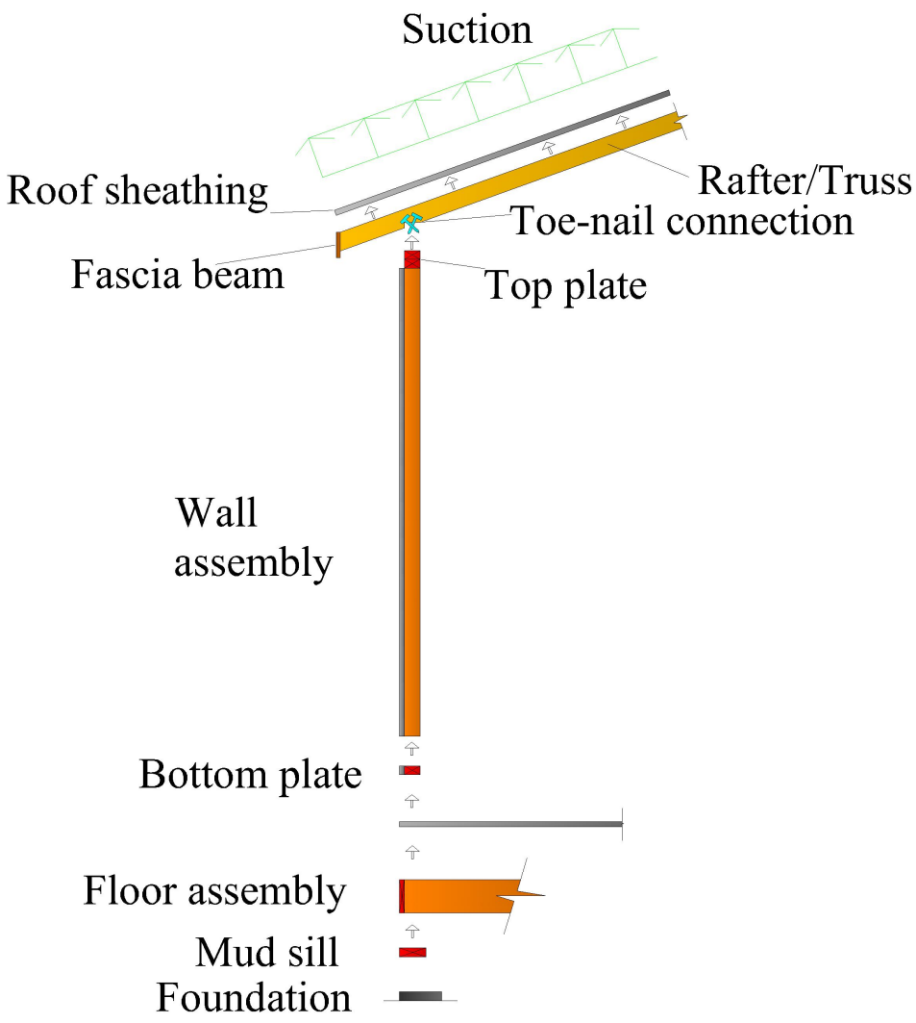

Figure 1.4 Vertical load path for a residential wood-frame house.

This load is transferred from the top plate, through the wall assembly, to the foundation (through the bottom plate, floor assembly and mud sill). To perform well, this load path must be continuous during the extreme wind loading. However, roof-to-wall connections (RTWCs) are considered to be a weak link in the vertical load path (Shanmugam et al., 2009). Most of the cases roof failures initiate at these connections (Reardon et al., 1999).

1.4 Load-sharing between adjacent RTWCs

Since the trusses and the roof sheathing act as a rigid frame during high winds, the entire roof system acts as a unit. So, the wind-induced uplifting load can be distributed in the transverse direction along the roof surface through the roof components. Due to high variability of toe-nail connections load-displacement behavior, even for the same applied loading history different connection may have different displacement magnitude. As a result of these differential displacements between RTWCs load will be transferred or shared to adjacent connections to satisfy moment equilibrium. As a result, the load distributions in wood frame houses are complex. The estimated wind load on each RTWC may be different than the actual reaction load due to load-sharing between multiple connections through the roof elements. The response of the RTWCs for wind loading is largely unknown due to Load-sharing (Morrison and Kopp, 2011; Morrison et al., 2012).

1.5 Research Objectives

Thus, the objective of the current project is to study the load-sharing behavior between adjacent RTWCs in a gable roof by developing an experimental setup which is able to adjust the "roof" stiffness in a simple way in order to better understand the interactions between roof stiffness, truss spacing and connection behavior under realistic fluctuating wind loading as well as gradually increasing ramp loading. To represent the roof bending stiffness two steel beams are fastened across the RTWCs. Two types of paired beams are used in this study. The bending stiffness of the stiffer beams is four times higher than the bending stiffness of the less stiff beams. The primary goal of this

project is to understand the effect of beams bending stiffness on load-sharing between the RTWCs. To do so, the spacing between the RTWCs were kept fixed and the loading history were also kept identical and simultaneous (either ramp loads or fluctuating wind loads) while the beams interconnect the RTWCs. The load-displacement behavior of individual toe-nail connections will be studied extensively.

Chapter 2: LITERATURE REVIEW

2.1 Introduction

As discussed in Chapter 1, the response of the RTWCs for wind loading is complex due to load-sharing. However, to understand the load-sharing behavior, it is also important to understand the individual connection response due to wind loading. A brief history of toe-nail studies will be presented here, followed by a discussion on the load-sharing behavior in wood-frame houses found in the literature.

2.2 Response behavior of individual toe-nail connections

Roof-to-wall connections have been the subject of several studies such as Riley and Sadek (2003), Cheng (2004), Reed et al. (1997), Shanmugam et al. (2009), and Morrison and Kopp (2011). Among them, Shanmugam et al. (2009) applied very small (3 cycle) cyclic loading to the in-situ RTWCs. Morrison and Kopp (2011) applied realistic fluctuating fluctuating wind loads to the RTWCs. The rest of the authors did apply gradually increasing displacement to the connection (typically 2.54 to 6.35 mm/min) and measured the required force to displace the connection. Cheng (2004) examined the variability associated with the construction of toe-nail connections such as the number and type of nails, the type and size of the lumber, the method of nailing, etc., which changes the failure capacity as well as connection behavior significantly. The mean maximum withdrawal capacity (failure capacity) from these studies range from 1130N to 2900N depending on the above mentioned factors.

The load-displacement behavior of these connections has been proposed to be nonlinear (Riley and Sadek, 2003) or tri-linear (Shanmugam et al., 2009) as shown in Figure 2.1. He (2010) adopted and modified load-displacement behavior as a non-linear spring for a single nail for predicting the uplift capacity of a roof panel which was originally given by Foschi (2000). Findings from Morrison and Kopp (2011) demonstrate that it takes many incremental peaks to fail a connection during realistic wind loading (Figure 2.3 and Figure 4.8). The mean failure capacity of a toe-nail connection does not depend on the loading rate (Rosowsky and Reinhold, 1999; Morrison and Kopp, 2011). Toe-nail behavior is highly variable and the coefficient of variations of the parameters which define the load-displacement behavior is high (Shanmugam et al., 2009). Morrison and Kopp (2011) also demonstrated that the effect of missing nails during construction of toe-nail connection can significantly reduce the roof's hold down capacity. This finding is also consistent with He (2010) who found that, a single missing nail in a roof panel can reduce the panel uplifting capacity by 10%.

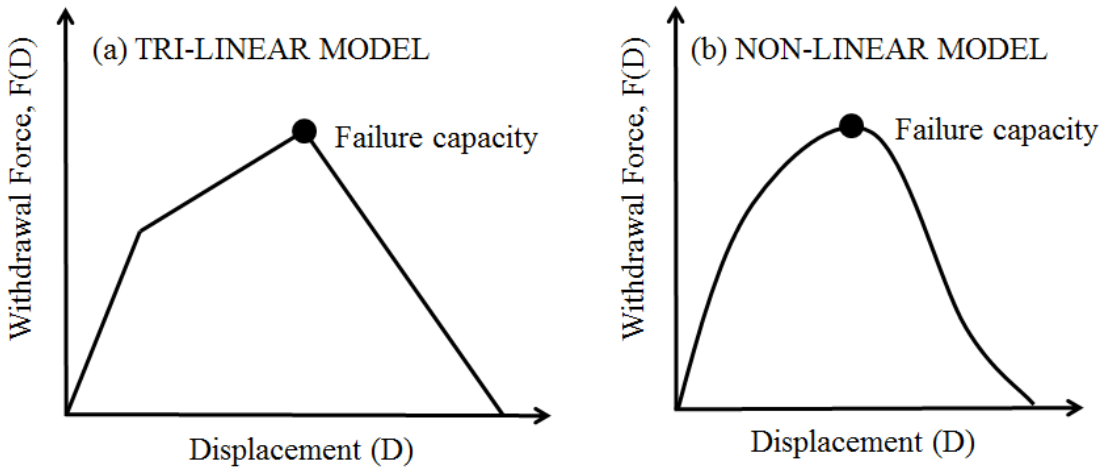

Figure 2.1 Load-displacement behavior of toe-nail connection. (a) Tri-linear model (Shanmugam et al., 2009), (b) Non-linear model given by Foschi (2000).

2.3 Load-sharing behavior between adjacent RTWCs

As described in Chapter 1, wind load is distributed to multiple toe-nail connections in low-rise residential buildings because the roof components work as a system or a unit to resist wind loading. Since, the load-displacement behavior of individual toe-nail connection is highly variable as described above; the stronger connections take up more of the load compared to an adjacent weak connection during high wind through structural elements such as roof-sheathing, fascia beam etc. Thus, the individual connection stiffness, stiffness of the roof and the truss spacing could play a great role for this load-sharing behavior (Wolfe and LaBissoniere, 1991).

Significant structural roof tests have been conducted to find the structural influence functions which indicate the load-sharing between adjacent RTWCs (Wolfe and LaBissoniere, 1991; Mani, 1997). Wolfe and LaBissoniere (1991) mentioned that when an individual truss is subjected to its design load along the truss top chord, 40 to 70 percent of the load is distributed to the adjacent trusses. They speculated that, by applying point load to single truss at a time and measuring the reaction load to all the trusses and then by superimposing the assembly reactions measured for each truss load, the reaction response characteristics of the assembly under full assembly load may be determined. They also argued that, load-sharing does not occur until any connection deflects relative to its adjacent connections. Load-sharing (i.e., load distribution between connections) must increase with roof stiffness and decrease with an increase of truss spacing. Load-sharing also reduces the variability of the system compared to that of the individual connections and, so, increases the minimum overall load-bearing capacity of the structure.

Reed et al. (1997) studied the uplift capacity of light-frame rafter-to-top plate connections both individually and in a system. In the system, they used roof sheathing and sub fascia members between seven rafter-to-top plate connections to replicate the roof system. By measuring the applied required loads to fail the whole system and dividing that by the total number of toe-nail connection with in the system they found that the average toe-nail failure capacity (2.99kN) was significantly higher than the average single toe-nail capacity (1.92kN). They demonstrated that this increase in capacity is due to the load-sharing between the toe-nail connections. However, due to the insufficient number of tests and lacking actual measured reaction loads they could not comment on the load-sharing extensively.

A recent study by Mensah et al. (2011) reported a database-assisted design methodology to predict wind-induced structural behavior by determining the influence surfaces of a 1/3-scale, light-frame, model wood building. The challenge is that the use of such influence functions is limited, considering that incremental damage of connections appears to change the load-sharing (Henderson et al., 2011; Morrison et al., 2012).

2.3.1 Full-scale, gable roof tests of Morrison (2010) and Morrison et al. (2012)

Morrison (2010) and Morrison et al. (2012) applied realistic fluctuating wind loads to a full-scale gable roof. They used the air-box method (Kopp et al., 2010), but with many different sized and shaped air-boxed which were attached to the surface of the roof (Kopp et al. 2010; Morrison, 2010). By generating realistic, fluctuating, full-scale pressures via the air-boxes, they were able to apply both temporally and spatially varied wind loads to the roof of the house. Two basic parameters were known for this test,

namely, (i) the pressures applied to the roof, and (ii) the displacements of each of the RTWC under the applied wind load. However, the actual reactions at the connections were not measured, so they estimated to the applied loads via the tributary area method. From this study, it was found that (i) displacements of top plates and at the 1st-to-2nd floor connections were negligible compared to the displacements at the RWTCs, and that (ii) the roof trusses acted approximately as rigid members. They also demonstrated that with the incremental displacement of the toe-nail connection from the top plate, load-sharing between adjacent connections changes throughout the loading time history. There was notable hysteresis associated with the connections as they yielded. These authors also point out that, depending on the roof stiffness, ultimate roof failures occur when multiple connections fail simultaneously, possibly up to entire roof. They also found that the uplift capacity of the roof based on estimated wind loads is significantly higher than that predicted using the actual individual connection results, a result which can only be explained by the substantial load-sharing (and the fact that the trusses on the gable end had additional capacity due to being fastened along the end wall). Figure 2.2 shows the estimated reaction load vs. displacement for different wind speed for one particular roof-to-wall connection. From this figure it can be seen that for the connection's 10~15mm displacement from the top plate the estimated (tributary area) applied load ranged from 6~7kN, which is quite a large load for a toe-nail connection to bear. However, when a similar estimated wind load was applied to individual toe-nail connections, they were found to fail on average at an applied load of 2.8kN (Figure 2.3). Since the actual full-scale house had poorer quality connections (Morrison, 2010), it is evident that the simple

tributary area method significantly overestimates the reaction, again indicating substantial load-sharing occurs with the neighbouring connections.

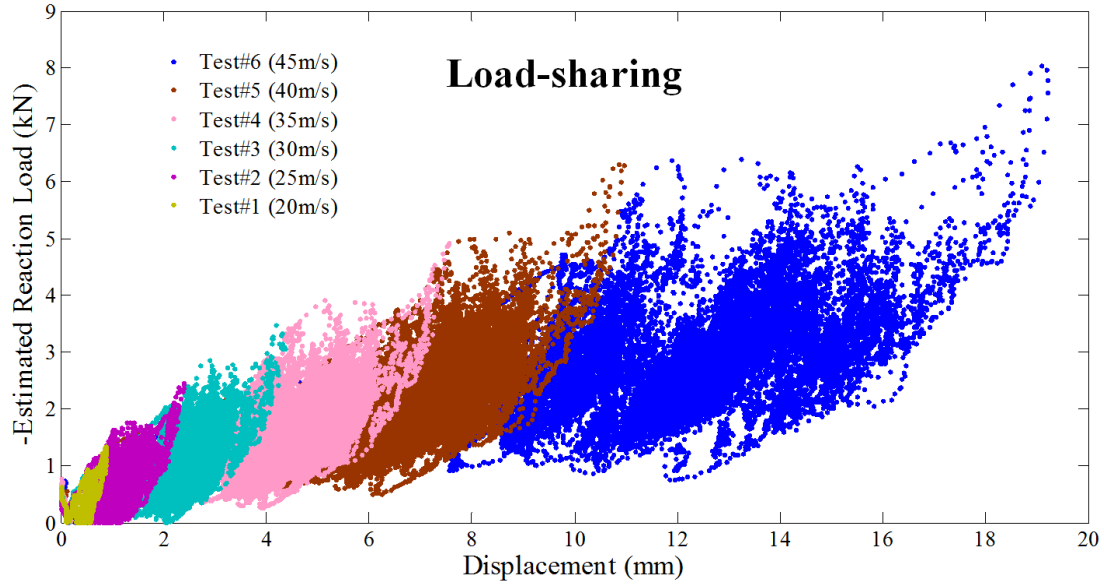

Figure 2.2 Estimated reaction loads vs. measured displacement for RTWC 'S3' for full scale gable roof test for different wind speeds (from Morrison et al., 2012).

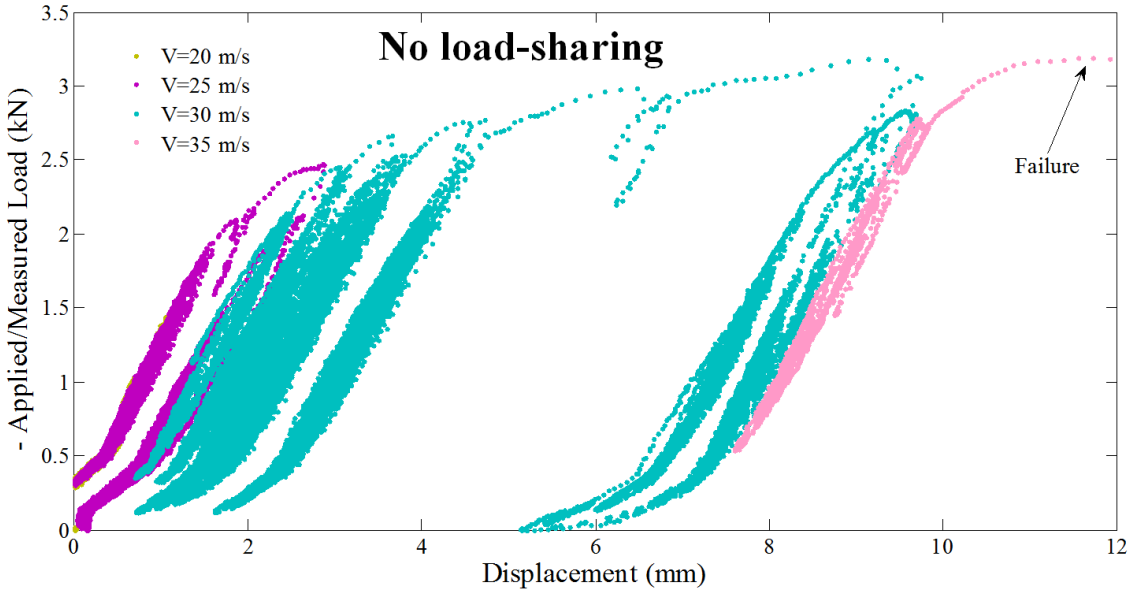

Figure 2.3 Measured loads vs. displacement for a single toe-nailed RTWC (from Morrison & Kopp, 2011).

2.3.2 Full-scale hip roof tests by Henderson et al. (2011) and Kopp et al. (2012)

Henderson et al. (2011) and Kopp et al. (2012) conducted full-scale tests on a timber-framed hip roof with spatially and temporally varying wind loads. The main objective of these tests was to monitor the load transfer mechanism within the roof frame and at the top plate level. By applying patch loading at different locations with the air boxes, the influence functions of certain RTWCs were determined and used to find the calculated applied reactions. The actual load was measured by load cells. It was found from these full-scale tests that the load ratio (i.e., measured load/applied load) between the measured load and calculated applied load between adjacent connections changes with the incremental displacement of any connection. Figure 2.4 shows the load, displacement, and load ratio time series for two adjacent trusses (labelled as LN07 & LN08 in the figures) to top plate connections (RTWCs). From the figure, at around 660s, an incremental displacement occurred due to applied peak load at LN07. The load ratio also changes at that time. The load ratio of the adjacent connection (LN08) also changes with incremental displacement of LN07 at that time. This test also confirmed that, spatially varying peak loads are shared by several RTWCs and the failure mechanism of a roof depends on the partial increments of the toe-nail connections which are consistent with Morrison (2010) and Morrison et al. (2012).

Although, these tests confirmed the load-sharing behavior between the adjacent toe-nail connections, they were unable to demonstrate the load-sharing relationships pertaining to roof stiffness, truss spacing, wind loading and the connections behavior.

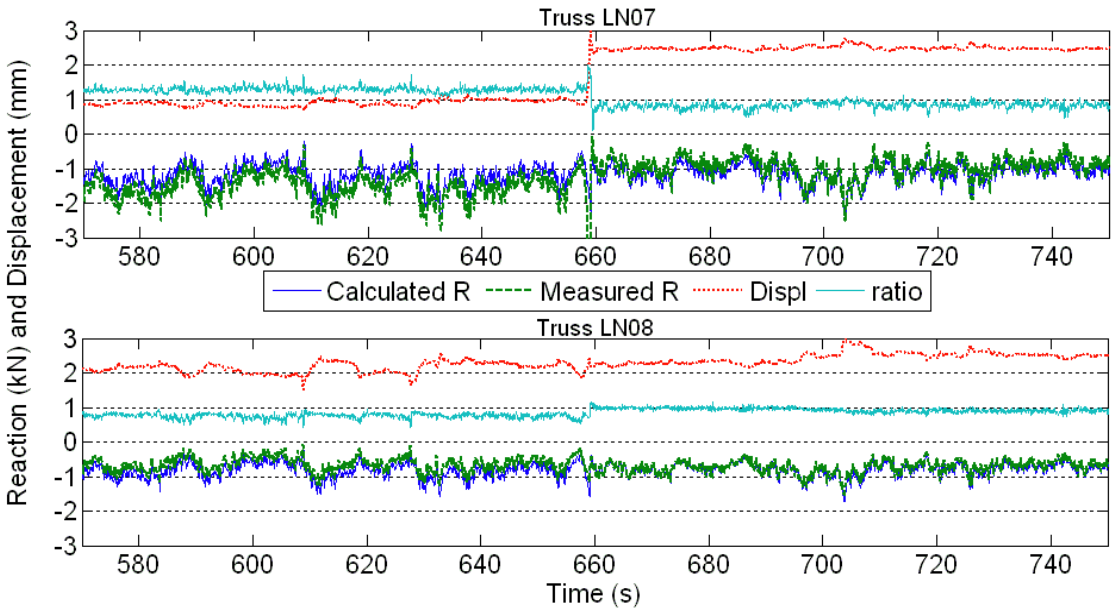

Figure 2.4 Measured displacement and reaction time histories of two adjacent, toe-nailed connections in a wood-framed, hip roof (from Henderson et al., 2011).

2.4 Summary

From the studies on load-sharing described above it can be summarized that load-sharing between RTWCs occur due to differential displacements between adjacent connections. Since the applied load is distributed between adjacent toe-nail connections a particular connection may sustain higher applied load than its failure capacity. Load-sharing changes with any connections permanent withdrawal. From literature, it has been found that toe-nail load-displacement behavior, roof stiffness (in the direction perpendicular to the trusses), distance between trusses and wind loads to the roof are the primary elements which affect load-sharing between connections, and, ultimately, the response of the roof.

Chapter 3: EXPERIMENTAL SET-UP

3.1 Introduction

In this chapter, a detailed description of the simplifications to the roofing system, the major assumptions associated with these simplifications, the details of the test set-ups, wind loading protocols, etc., are presented.

3.2 Simplification of the roof system

As discussed in the previous chapter, the major factors that affect the load-sharing at the RTWCs are the (i) connection load-displacement behavior and variability, (ii) the applied load at each RTWC, and (iii) the bending stiffness of the roof in the direction perpendicular to the trusses, for a given truss spacing. The major components in the roof that contribute to the roof bending stiffness are the roof sheathing, fascia, gable end bracing, and perhaps the drywall connected to the ceiling. To idealize the roof bending stiffness in the current experiments, this stiffness was simulated in a highly idealized way as two steel beams, illustrated in Figure 3.1 (a & c). Note that, the actual roof stiffness is challenging to identify due to inherent complexity of a simple roof system. Thus, the bending stiffness of the steel beams used herein is not equivalent to the actual stiffness of a simple gable roof as described in Appendix D. Two different sizes of paired beams are used in the current experiments. The less stiff beam has a cross section of 3.8cm x 3.8cm x 0.635cm and flexural rigidity (EI) of 23.1kN-m^2 (see Appendix D for details). The stiffer beam has a cross section of 6.35cm x 6.35cm x 0.476cm and flexural rigidity (EI) of 91kN-m^2 (see Appendix D for details). As stated above, it is obvious that the roof

stiffness idealized herein is not accurate enough to represent all of the details in the load transfer of a real structure; however, the simplification of the roof stiffness will provide specific information, which appeared to be important during the roof failures observed by Morrison et al. (2012).

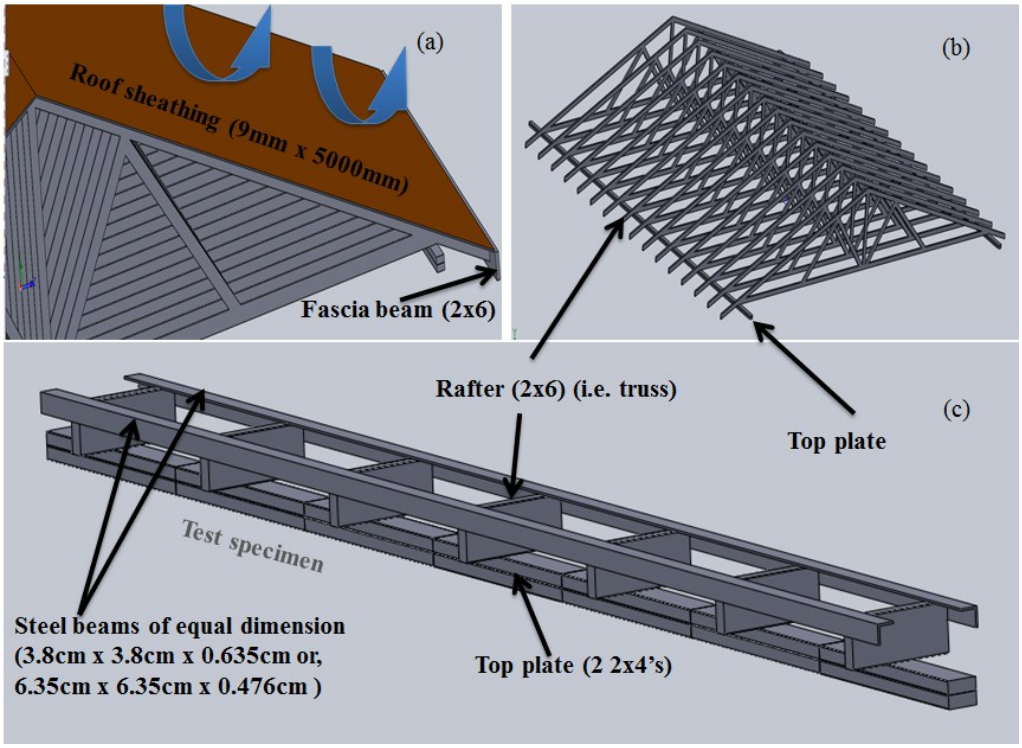

Figure 3.1 (a) Roof components that are considered to idealize the roof bending stiffness, (b) skeleton of a roof which shows that the trusses are nailed to the top plate (c) experimental test specimen which can replicate the roof bending stiffness (through beams) and truss spacing.

It is to be noted that, the idealization herein has considered the load distribution only in one direction (i.e. along the direction of the top plate). However, in reality load can be distributed along the truss direction (i.e. normal direction to the top plate). Lateral movement or sway of the building has been ignored explicitly in this present experimental setup. These idealizations of the structure will be justified by comparing the

current experimental results with those of Morrison (2010), Morrison et al. (2012) and Henderson et al. (2011).

The experimental set-up should also be able to handle variable truss spacing. Depending on the type of structure the truss spacing can be varied from 600mm to 900mm (e.g., Ontario Building Code, 2006). The truss spacing should be considered as a factor which could have a certain impact on load-sharing. In reality it has been observed that during extreme wind, depending on the roof stiffness, load can typically be shared at up to three or four trusses (Wolfe and LaBissoniere, 1991) or more (Morrison et al., 2012), for typical construction practice.

3.3 Test set-up

In the current test set-up, toe-nailed RTWC can be tested individually or as a system. A steel frame test rig is used to withdraw an individual connection (see Figure 3.2), using exactly the same approach as Morrison and Kopp (2011). The loads are applied to the specimen by controlling the pressure inside of the airbag, which is then mechanically attached to the toe-nail specimen, as shown in Figure 3.3. Two 2x4, 0.6m long wood pieces attached by nails, representing the top plate, are mounted on the bending beam load cells. One 2x6, 0.3m long wood section representing the rafter (truss) of the house is nailed to the middle of attached wood lumbers (top plate). Three 12d twisted shank nails (length: 82.6mm, shank diameter: 2.87mm) are used for the connection. The lumber used for the experiments was No.2 grade Spruce-Pine-Fir, with a moisture content varying between about 6 – 14%.

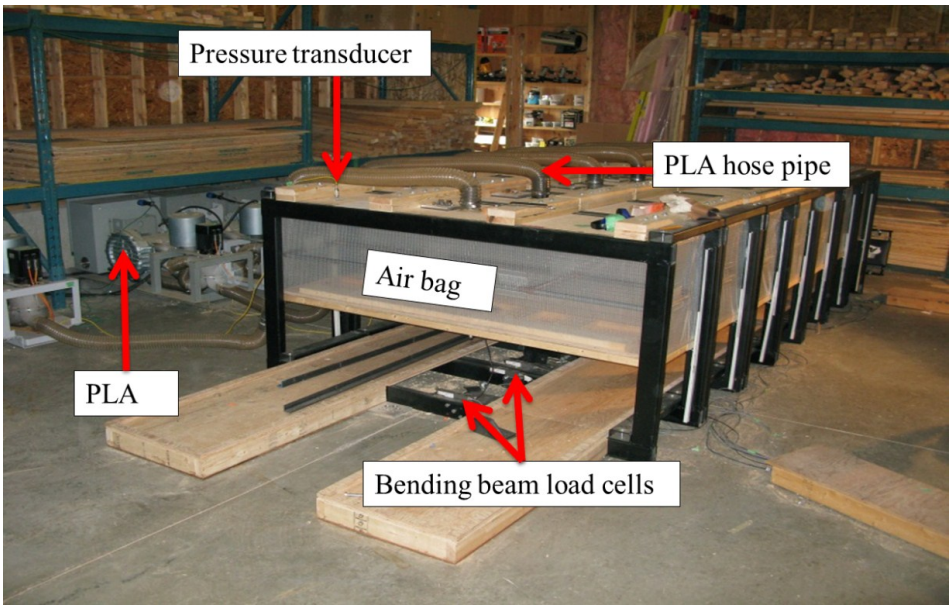

Figure 3.2 Experimental setup: seven test rigs one beside another. By changing the spacing of the test rigs on center distance between the RTWCs can be adjusted.

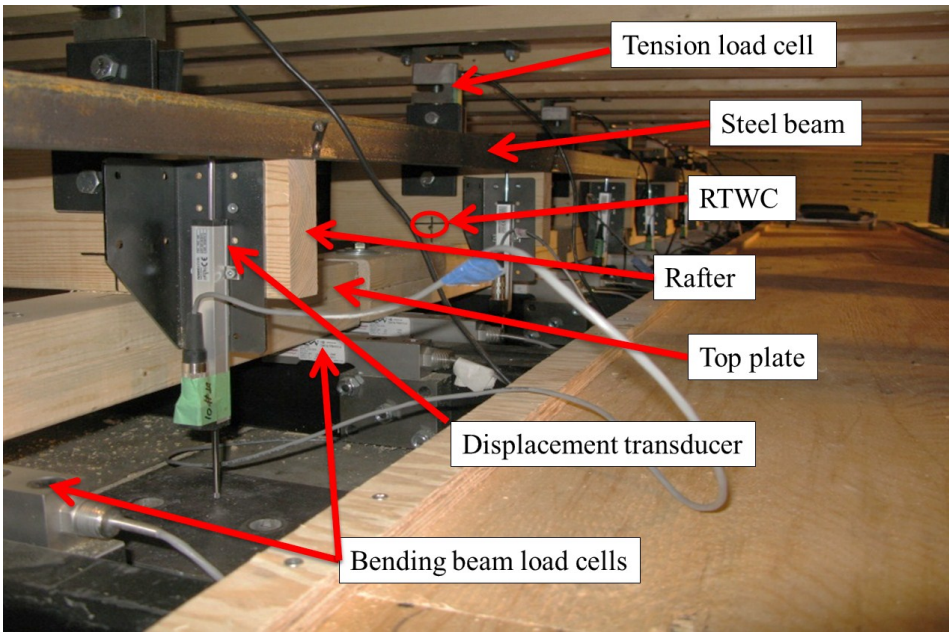

Figure 3.3 Experimental setup: test setup under the airbags. The load is applied through the airbags which connect the RTWC by tension load cell. Bending beam load cells measure the actual reaction load to the connection. Displacement transducer measures the vertical displacement of the connection from the smooth plain surface.

To avoid construction variability as much as possible, similar methods and workmanship were used to make each of the RTWCs – see Appendix A for details.

Tension load cells were used to monitor the applied load to the individual RTWC, but these also act as the connections between the airbags and the rafters. Displacement transducers (DT) are used to monitor the vertical displacement of the RTWC from the top-plate, with the tip of the DT placed on a hard, rigid surface. The withdrawal design capacity of the steel frame test rig is 10kN. Pressure loading actuators (PLA) are used to apply the demand load. A detailed study of PLA can be found in Kopp et al. (2010, 2012).

The nails were driven pneumatically with an inclination angle of 45 degree to the rafter and a height of 25.4mm (one inch) from the top plate, consistent with the National Design Specification for Wood Construction (NDS; 2005). Due to the inclination of the nails, each nail will not be subjected to pure withdrawal load. Although, most roof slopes vary between 3/12 to 6/12, the RTWC considered here is consistent with 'ASTM D 1761-06 Standard Test Methods for Mechanical Fasteners in Wood'. Since the objective of this project is to investigate the Load-sharing mechanism, the shear load is ignored explicitly. The tests are conducted using exactly the same approach as Morrison and Kopp (2011).

Load-sharing can be occurred up to three to four consecutive truss-to-wall connections on either side of a particular connection (Wolfe and LaBissoniere, 1991). So, it was decided to investigate the load transfer mechanism between seven RTWCs. Reed et al. (1997) also dealt with seven RTWCs as discussed in Chapter 2. To do so, seven steel frame airbag loading systems were built (as shown in Figure 3.2). They were placed

beside each other such that the RTWCs are on 0.6m centers. The two steel beams (stiffeners) are attached across the top of the rafters by screws. Details can be seen in Figures 3.1 – 3.3.

As mentioned above, there are four basic parameters which can be controlled during the experiments: the RTWCs, truss spacing, bending stiffness of the steel beams, and the wind load applied to each RTWC. In this current project two types of beams are used and for each set of beams the RTWCs and the loading system are considered to be the only variables, while the truss spacing are held constant. As well, it was decided that a ramp and a fluctuating wind loads will be applied to all of the RTWCs. Ramp loading tests are important because they give the primary indication of the toe-nail connection behavior. Although, the failure capacity of an individual toe-nail connection is independent of the loading rate, it was decided that an identical 8kN/min ramp load should be applied to each of the connections. The fluctuating wind loads used for this experiment was the same as described in Morrison and Kopp (2011). However, a brief description of these loading time series will be given later on in this chapter.

3.4 Data acquisition

National Instruments hardware (Figure 3.4) and LabVIEW system design software are used to acquire the data from the sensors. In total, 35 sensors were used during each experiment. Among them, 7 tension load cells measure the applied load, 14 bending beam load cells (2 for each RTWC) measure the actual reaction load, while 7 displacement transducers monitor the displacement of each RTWC during the experiment. There are another 7 pressure transducers for each nail-rig. Each of the

pressure transducers are used to monitor the pressure inside the airbag in a way such that the airbag produces the demanded uplift as monitored by the tension load cell. Measurement and automation software are used to create the experimental task so that all the sensors can work simultaneously. Calibration coefficients such as real slopes and real intercepts for each sensor were determined carefully – see Appendix B for details. The data were recorded at a sampling frequency of 100Hz.

Figure 3.4 Photograph of the data acquisition system.

3.5 Ramp loads

PLA and flexible airbag is used to apply load to the specimen as described above. Since the PLA creates suction inside the airbag and it initially needs to adjust the required flow rate, it produces higher load than the demand load during start-up. To avoid this, no load is applied during first 5 sec and then 3kN/min ramp load is applied for 10 sec (up to 0.5kN). After that 8kN/min ramp load is applied up to failure of the RTWC. Although,

3kN/min ramp load is applied initially (for the purpose of control) this loading history will be referred to as the "8kN/min ramp load" for simplicity. However, it is to be noted that when the connection fails, i.e., after the maximum applied load, the PLA shows uncontrolled behavior and cannot generate the demand force (e.g., Figure 3.5). Since we are interested in the behavior of toe-nail connection up to the failure capacity (i.e., maximum load it can sustain), after that point no data are required and will not be used in the analyses. However, the PLA can fairly accurately generate the demand load up to failure capacity of a connection, as shown in the figure.

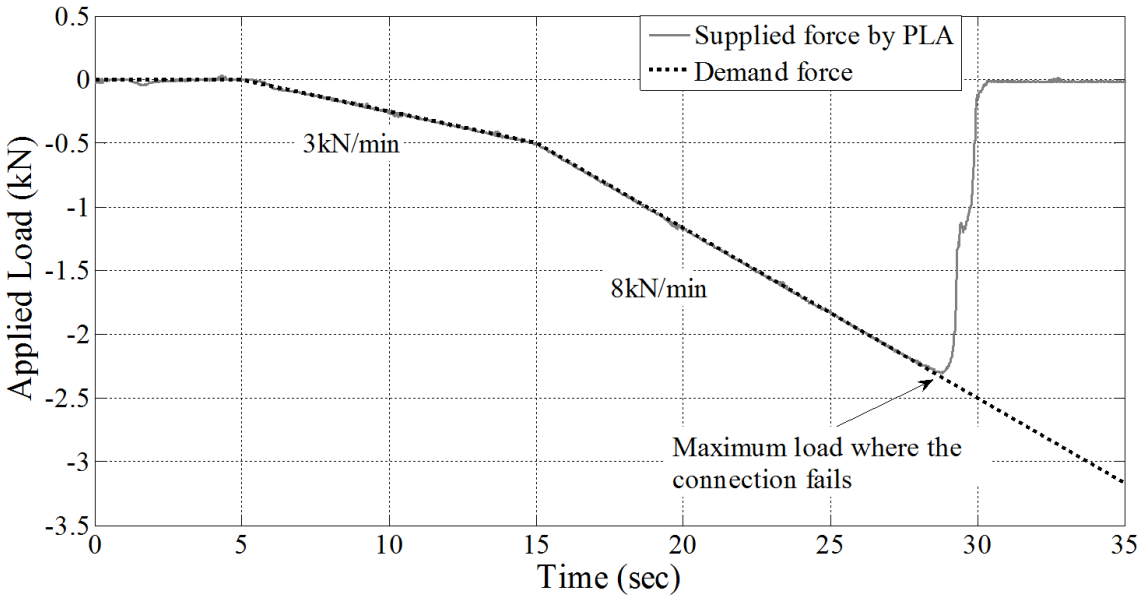

Figure 3.5 PLA generated 8kN/min ramp loads to one RTWC and compared to the demand force.

3.6 Fluctuating wind loads

In this section a brief discussion is presented on how and why the fluctuating wind loading history was chosen. The fluctuating wind loading history was chosen from a full-scale test house for a particular connection for different wind speeds. The full scale

test house is a typical two-storey wood frame, brick veneer gable roof house. The plan dimensions (Figure 3.6) of the house are 9.0m by 8.9m with an eaves height of 8.0m and a roof slope of 4:12. The extension of the roof overhangs the external wall of the house on all sides by approximately 0.61m. The prefabricated trusses were spaced at 0.61m on centers and the connections between the trusses to the top plates are the common standard toe-nail connections. The plywood thickness for roof sheathing is 9mm. The end of all trusses are connected to a long 2x6 wood fascia as shown in Figure 3.1(a) which increases the structural integrity and roof stiffness of the house. The layout of the trusses and naming conventions are presented in the Figure 3.6. There are 16 roof trusses used for the test house. So, in total there are 32 RTWCs in the house which is ranged from N2 to N17 in the northern wall and S2 to S17 in the southern wall. The trusses N2S2 and N17S17 are gable end trusses. This is the same house tested by Morrison (2010).

Wind tunnel tests were performed, as described by Morrison (2010), on a 1:50 scale model gable roof house for different wind angles ranging from 0^o to 90^o at a mean roof height wind speed of 9.6 m/s. The scaling law for converting the wind tunnel test results into a full scale test is (Simiu and Scanlan, 1996):

$$\left(\frac{VT}{L}\right)_{Model-scale} = \left(\frac{VT}{L}\right)_{Full-scale}$$

Where, V stands for velocity, T stand for time and L stands for length scale. In this particular project, the full-scale test duration of 15minutes for 20m/s wind velocity was selected. From the scaling law, the model-scale duration is 37.5 seconds. A representative wind tunnel pressure time series data for 37.5 seconds was chosen. Now,

considering the model scale test duration as constant the duration for 25 m/s, 30 m/s, 35 m/s, 40 m/s and 45 m/s wind speeds are determined (Table 3.1).

Table 3.1 Test duration for different wind speeds.

Scaling Wind Speed, V (m/s)	Test Duration, T (s)
20	900
25	720
30	600
35	514
40	450
45	400

Once the pressure data are known for the different wind speeds, the time-varying reaction load at each of the RTWCs can be calculated by the summation of moments (SOM) method or by the uplift of each truss by tributary area approach (Morrison, 2010). The wind angle (40^o) which produces the maximum reaction at a single RTWC was chosen for angle of attack. It was observed that RTWC 'S2' experience the maximum load for high wind. But, it should be noted that 'S2' has a higher surface area due to the overhanging roof. The gable end trusses connections are stronger compared to the other connections. So, it was decided that 'S3' fluctuating wind loads (as shown in Figure 3.6) will be applied identically to each of the RTWC in the present study. More details on loading history of the house can be found in Morrison (2010), and identical loads to his are used herein.

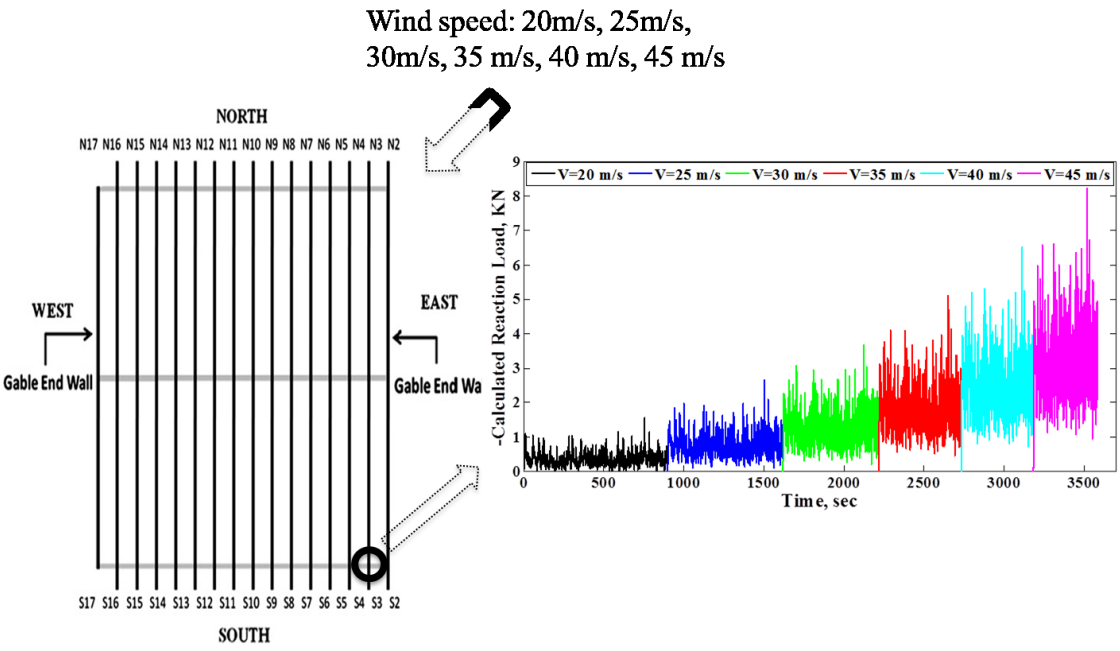

Figure 3.6 Foot print of the truss layout of the gable roof and the estimated reaction load to RTWC 'S3' for different wind speeds (from Morrison, 2010). This particular 'S3' fluctuating wind loading history will be applied identically to the RTWCs within a system in the present study.

3.7 Force balance between the net applied load and net measured load

The calibration of the load cells and uncertainty associated with the measurements are important parameters to be considered in the tests. So the uncertainty analysis and calibration of the sensors were done very carefully [Appendix B & Appendix C]. Since this is a physical system, ideally, the summation of the applied load by the tension load cells for all the seven RTWCs within a system should be equal to the summation of the measured load by the bending beam load cells for all the RTWCs. Figure 3.7 shows the force balance between net applied load and net measured load for an identical 8kN/min ramp load applied to each of the RTWCs within the system. Ideally, the load difference between the net measured load and net applied load should be zero.

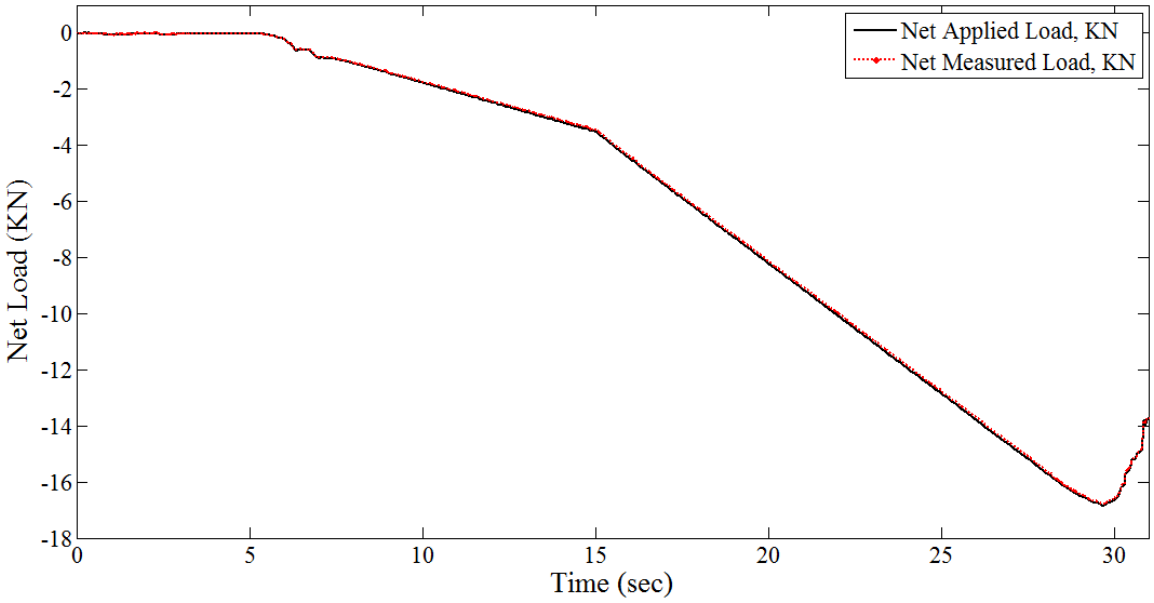

Figure 3.7 Net applied load & net measured load vs. time for one system test where identical 8kN/min ramp loads were applied to each of the connections within the system.

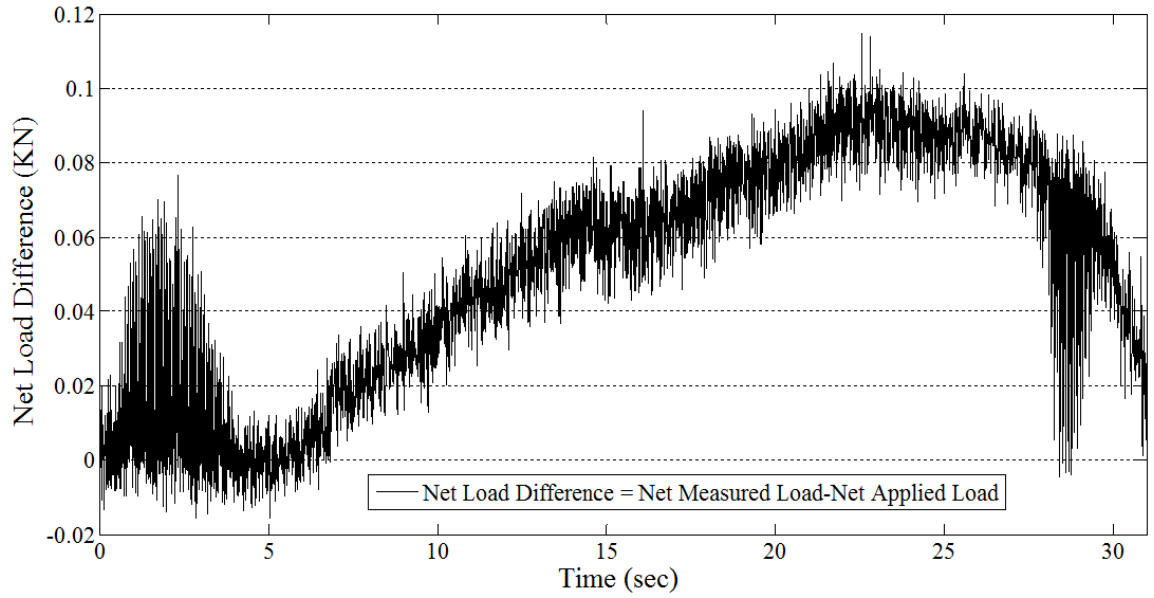

Figure 3.8 Net load differences vs. time for the same experiment shown in Figure 3.7.

The mean uncertainty associated with the tension load cells were 0.059kN and for the bending beam load cells were 0.041kN – see Appendix C for details. However, in the

analysis, the net load difference is distributed to each of the bending beam load cells by their measurement uncertainty so that the net measured load is equal to the net applied load. Figure 3.8 shows that the net load difference is negligible compared to the individual load cells measurement uncertainty. Thus, the test set-up and instrumentation can be considered to be sufficiently accurate.

3.8 Test matrix

Several experiments were conducted to characterize the Load-sharing behavior. Table 3.2 shows the summary of the tests conducted. Individual tests were performed to characterize the toe-nail behavior and to compare the results with toe-nails while they are in a system. In total 35 RTWCs were subjected to ramp loads individually and 35 RTWCs were subjected to fluctuating wind loads individually. Five repetitive tests for each loading types and system types were conducted. Note that, system means when seven RTWCs are interconnected via two steel beams at the edge of the rafters as shown in Figure 3.1(c). So, for five repetitive tests for any particular loading and a particular system type there are 35 (7x5) RTWCs in total.

Table 3.2 Test matrix for the current project

Test type	Identical 8kN/min ramp loads (# of toe-nail connections)	Identical fluctuating wind loads (# of toe-nail connections)
Individual	35	35
Less stiff system ($EI=23.1 kN\text{-}m^2$)	35 (7x5)	35 (7x5)
Stiffer system ($EI=91 kN\text{-}m^2$)	35 (7x5)	35 (7x5)

Other than the above mentioned test matrix, two system tests with stiffer beams (6.35cm x 6.35cm x 0.476cm) were performed for identical 8kN/min ramp loads applied to each of the connections within the system. In these tests, all the RTWCs were made with three 12d nails, except RTWC#04. In the first test, RTWC#04 was made with four 12d nails (stronger connection) and in the second test RTWC#04 was made with two 12d nails (weak connection). These tests were conducted to understand the load-sharing between the strong and weak connections within a system.

Chapter 4: TOE-NAIL TEST RESULTS

4.1 Introduction

In this chapter the results of the individual and system tests described in Chapter 3 will be discussed. From the individual ramp loading tests, a load-displacement model will be proposed, with the statistics of different parameters being given. The response of individual toe-nail due to fluctuating will loads will be discussed briefly. Following this, failure details and capacities will be examined.

4.2 Ramp loads applied to individual toe-nails

Individual RTWCs were subjected to 8kN/min ramp loads. In total, 35 samples were tested. Figure 4.1 shows the load-displacement curves of 35 individual RTWCs for 8kN/min ramp loads and the mean load-displacement curve calculated from these test results. The calculation procedure of mean load-displacement curve is explained in Section 4.2.2 in this Chapter. From the experiments, the load-displacement behavior of toe-nail connections has been found non-linear. This figure also shows that, even though each of the RTWCs were constructed with 3-12d twisted shank nails and subjected to identical 8kN/min ramp loads there is a high variability between the load-displacement curve of individual RTWCs. Load-displacement behavior of toe-nail connections has been frequently used for modeling of the roof system of wood-frame, low-rise houses. The load-displacement character of toe-nails has been examined in several studies and, in most cases the nail withdrawal behavior has been simplified so as to avoid complexity in numerical analysis.

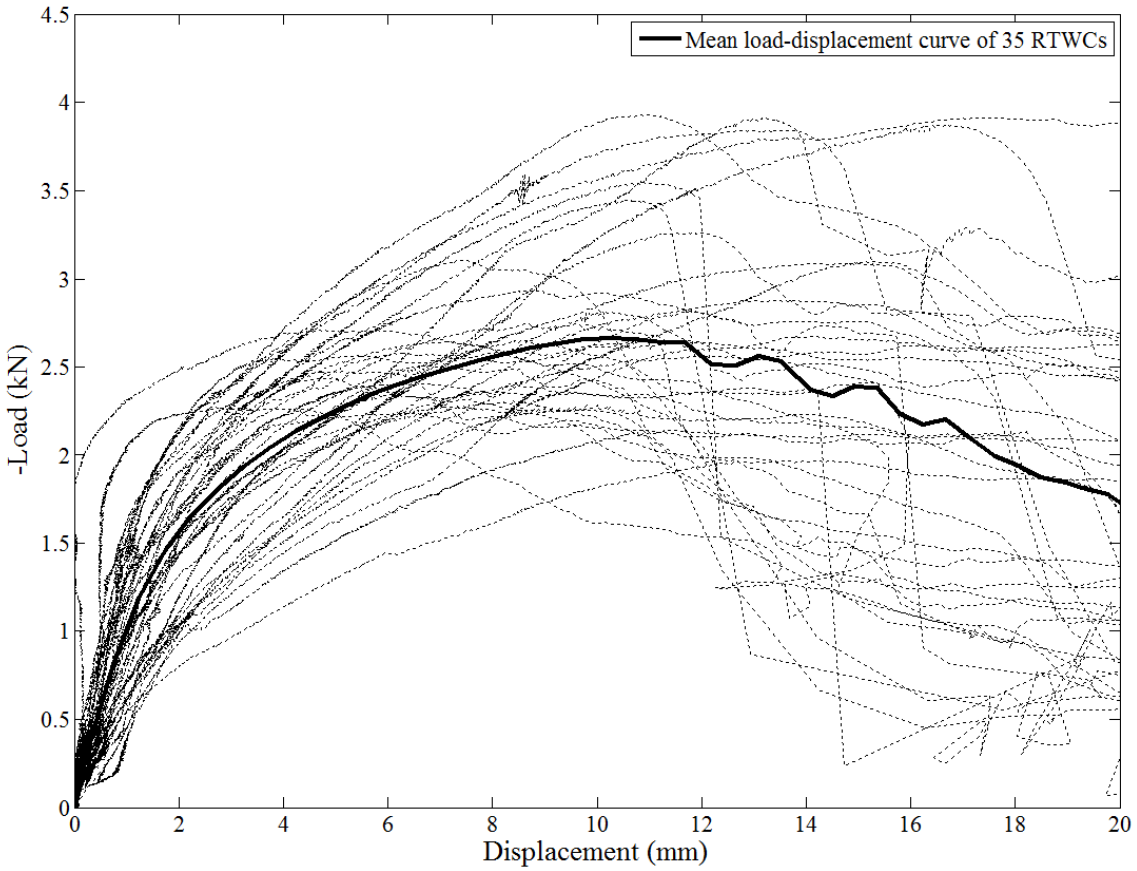

Figure 4.1 Load-displacement curve of 35 individual RTWCs for 8kN/min ramp loads and the mean load-displacement curve calculated from these test results

Chui et al. (1998) and Groom and Leichti (1993) have defined the nail-withdrawal with elasto-plastic and piecewise linear (e.g. tri-linear) models respectively. However, they defined the load-displacement up to the maximum resisting load of a connection and did not consider the strain softening effect (i.e. negative stiffness after maximum resisting load) of nail withdrawal. Shanmugham et al. (2009) developed the relation of load-displacement of toe-nail connection as a tri-linear model up to ultimate nail withdrawal displacement where all the strength is lost. Riley and Sadek (2003) proposed a non-linear model. He (2010) considered the load-displacement behavior as non-linear spring and adapted and modified the equations originally given by Foschi (2000).

In this present study the load-displacement behavior of RTWCs has been proposed as piecewise linear (e.g. bi-linear) model and curvilinear model up to maximum withdrawal capacity of toe-nail connection. These models will be discussed in details in this section and the statistics of different parameters which define these models will be given from the experimental results.

4.2.1 Bi-linear load-displacement model

In the bi-linear model it is proposed that the load-displacement relationship is linear up to yield capacity (F_y) and after that point the load-displacement behavior is also assumed as linear, but with a different slope, up to failure capacity (F_c). Failure capacity is the maximum load a connection can withstand. The parameters which define the model are initial slope (K_o), secondary slope (K_1), yield capacity (F_y), yield displacement (D_y), failure capacity (F_c) and failure displacement (D_c) which are shown in Figures 4.2 – 4.3. Since any connection's actual behavior is nonlinear, the secant stiffness is taken as the representative initial stiffness. Failure displacement is the displacement of the connection at failure capacity and yield displacement is the displacement of the connection at yield capacity. The load-displacement relationship can be described as:

$$K_o = \frac{F_y}{D_y} \quad [4.1]$$

$$K_1 = \frac{F_c - F_y}{D_c - D_y} \quad [4.2]$$

$$F(D) = DK_o;\ \ where, D \leq D_y \quad [4.3]$$

$$F(D) = F_y + (D - D_y)K_1;\ \ where, D_y < D \leq D_c \quad [4.4]$$

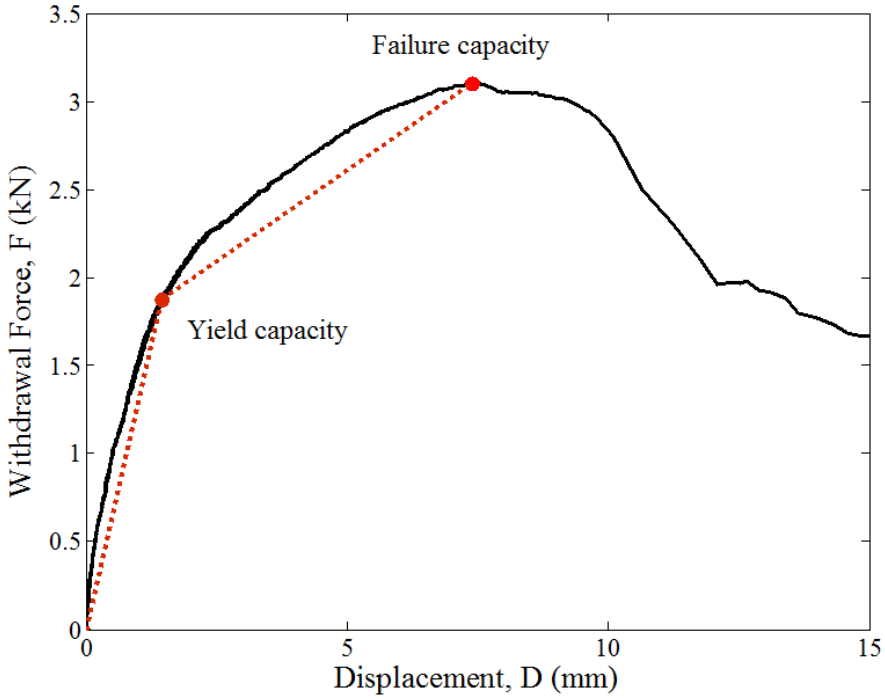

Figure 4.2 Load-displacement curve for one RTWC for 8kN/min ramp loads (experimental) and the idealized bi-linear model (broken lines).

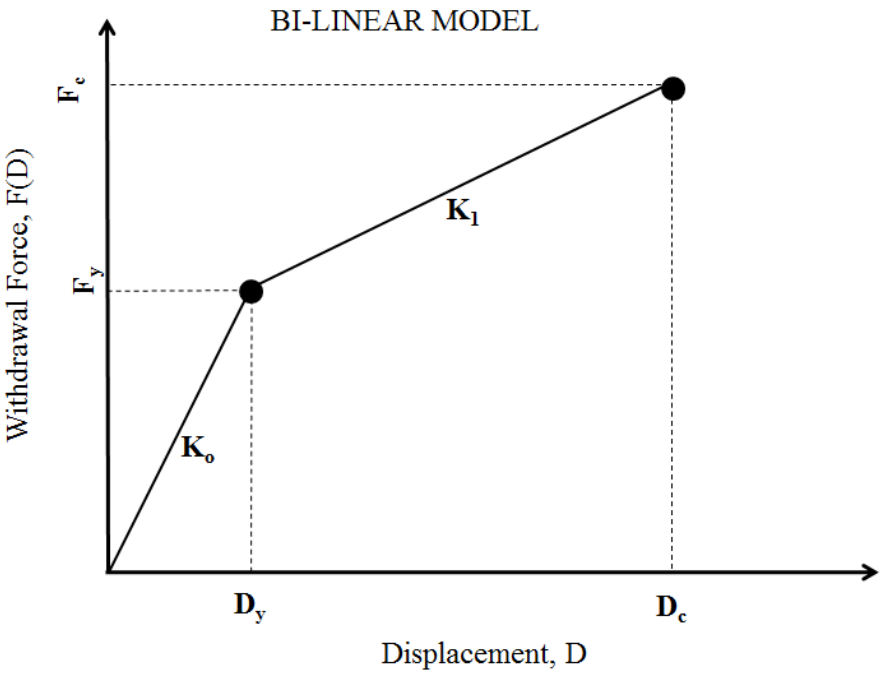

Figure 4.3 Bi-linear nail withdrawal model for a RTWC.

4.2.2 Curvilinear load-displacement model

The load-displacement behavior of toe-nail connection can also be defined as a curvilinear model, as illustrated in Figures 4.4 – 4.5. In this model, it is proposed that the load-displacement relationship is linear up to yield capacity (F_y). After that point, it follows non-linear behavior up to failure capacity (F_c) (Figure 4.5). The relationships between loads and displacement, adapted from He (2010), are given as:

$$F(D) = K_o D;\ \ where, D \leq D_y \qquad [4.5]$$

$$F(D) = F_y + \left[Q_o + Q_1\left(D - D_y\right)\right]\left[1 - \exp\left(\frac{K_o\left(D_y - D\right)}{Q_o}\right)\right];\ \ where, D_y < D \leq D_c \qquad [4.6]$$

The intercept and the asymptotic slope of the curve, Q_o and Q_1, respectively, can be estimated by fitting Equations 4.5 & 4.6 with the experimentally found mean capacity curve (Figure 4.6) through regression analysis.

Figure 4.6 shows the mean capacity curve from 35 ramp loading tests and the theoretical capacity curve, which is derived from Equation 4.5 and 4.6 by regression analysis of the experimental data. To find the experimental mean capacity curve, for each 0.5mm incremental displacement, the load from every ramp test was averaged at the corresponding displacement. The resulting values of the parameters, obtained by regression analysis, are $Q_o = 0.9KN$ and $Q_1 = 0.09KN/mm$ for $K_o = 1KN/mm$, $D_y = 1mm$ and $D_c = 10.24mm$.

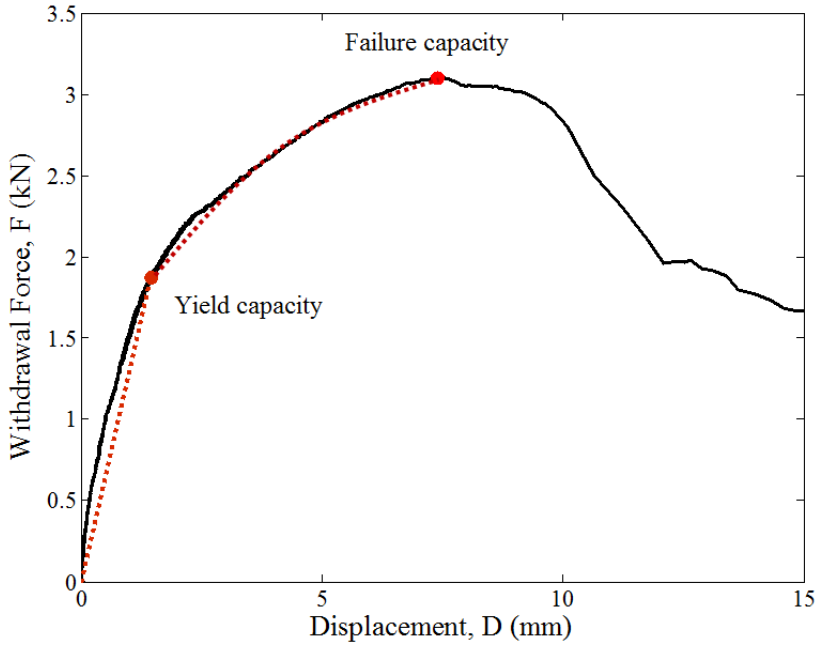

Figure 4.4 Load-displacement curve for one RTWC for 8kN/min ramp load and idealized curvilinear load-displacement model (broken lines).

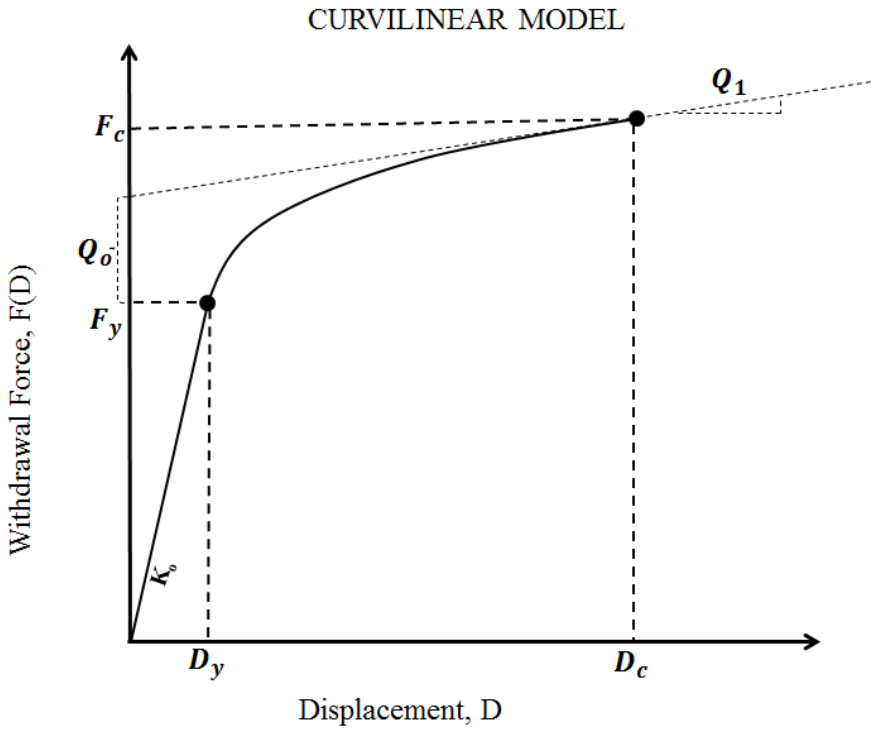

Figure 4.5 Curvilinear nail-withdrawal model for RTWC (adapted from He (2010)).

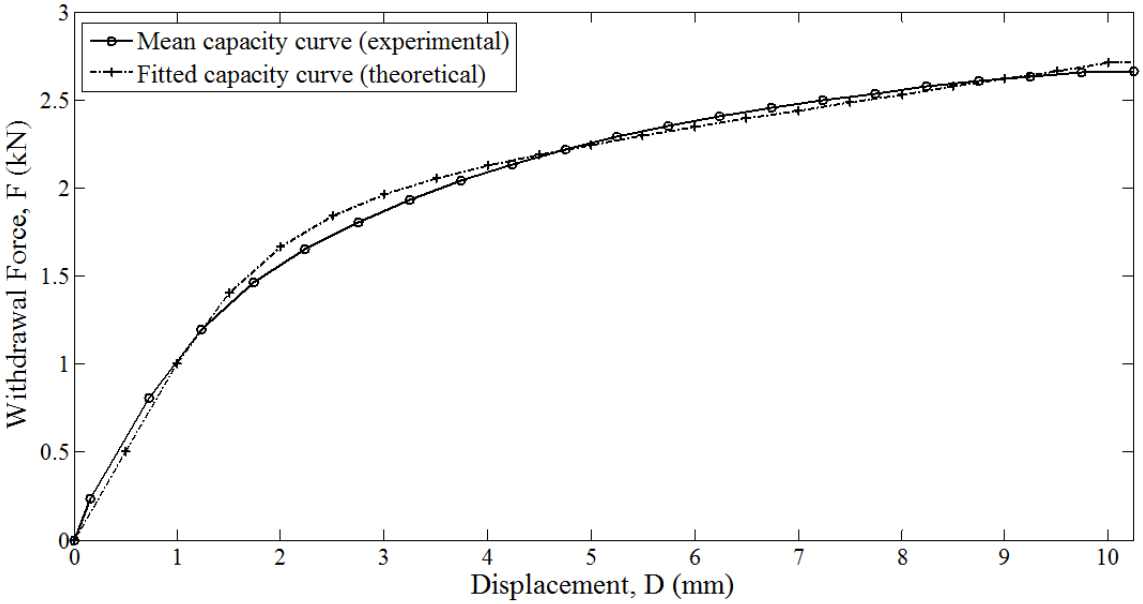

Figure 4.6 Mean capacity curve from 35 ramp loading tests and the fit to the theoretical capacity curve.

Now by assuming Q_o and Q_1 as constant in Equation 4.6 and by varying K_o, D_y and D_c within their bound range (Table 4.1 and 4.2) a series of toe-nail load-displacement curves can be produced numerically. To predict the load-displacement behavior of a toe-nail connection, if it is assumed that the parameters K_o, D_y and D_c are known, F_y can be estimated from Equation 4.5 by letting, D equal to D_y. Similarly, F_c can be calculated from Equation 4.6 by setting, D equal to D_c. Alternatively, if K_o, F_y and F_c are assumed to be known, the corresponding displacements of the connection can be obtained from the measurements for different loads. Table 4.1 & 4.2 could be used to supply the known values in Equations 4.5 & 4.6 and predict the load-displacement behaviors of these particular types of toe-nail connections.

4.2.3 Statistics of the fitted parameters for the bi-linear model

Statistics for the six parameters are presented in Tables 4.1 and 4.2. In Table 4.1, D_y is chosen manually (arbitrary estimation) whereas in Table 4.2, D_y is assumed to be constant 1.22mm (data-driven estimation) and the corresponding load is considered as yield capacity for each sample. The reason behind choosing 1.22mm is that, it is the mean value for yield displacement for arbitrary estimation. Other than this, Shanmugham et al. (2009) proposed the yield displacement for three 16d nails (length=88.9mm, diameter=3.33mm) as 1.6mm, which is higher than the present study, but reasonable given their longer nail length and higher diameter. However, since three 12d nails (length=82.6mm, diameter=2.87mm) are used in the present study, it appears to be a reasonably a good approximation to take 1.22mm as the mean yield displacement in the present study.

The initial and secondary slopes are calculated by using Equation 4.1 and 4.2, respectively. A null hypothesis was formed to investigate if there is any statistically significant difference in means between the arbitrary estimation and data-driven estimation for yield capacity, initial slope and secondary slope. A two-sample t-test (e.g. Spiegel, 1990) was used to check the null hypothesis that the mean values are equal for both methods. It was found that there is no difference between the mean values of the parameters for the arbitrary and data-driven estimation. The reader is referred to Appendix E for a description of the statistical methods.

From Tables 4.1 and 4.2, it can be seen that the coefficient of variation (COV) for the failure capacity has the smallest value (0.20) of all of the parameters. It is to be noted

that, the minimum value for the secondary slope in present study is very low which intrinsically means that toe-nail connections behavior could also be defined as an elastic-plastic behavior. Although great attempts were made to make the toe-nail connections identical in the present study, the variations in the parameters (i.e. COV) indicate the high variation of toe-nail load-displacement properties.

Table 4.1 Statistics of the load-displacement model for all 8kN/min ramp loading test (arbitrary estimation)

Statistics	Yield capacity, F_y (kN)	Yield displacement, D_y (mm)	Initial slope, K_o (kN/mm)	Failure capacity, F_c (kN)	Failure displacement, D_c (mm)	Secondary slope, K_1 (kN/mm)
Mean	1.17	1.22	1.06	2.84	10.57	0.19
Maximum	2.26	2.15	2.61	3.93	17.48	0.28
Minimum	0.59	0.55	0.46	1.97	5.06	0.05
Standard Deviation	0.36	0.41	0.47	0.57	3.41	0.06
COV	0.31	0.33	0.45	0.20	0.32	0.31
Statistical Distribution (ADs)	LN (0.72)	N (0.27) LN (0.35)	N (0.65) LN (0.32)	LN (0.61)	N (0.42) LN (0.58)	N (0.46)

Table 4.2 Statistics of the load-displacement model for all 8kN/min ramp loading test (data-driven estimation)

Statistics	Yield capacity, F_y (kN)	Yield displacement, D_y (mm)	Initial slope, K_o (kN/mm)	Failure capacity, F_c (kN)	Failure displacement, D_c (mm)	Secondary slope, K_1 (kN/mm)
Mean	1.19	1.22	0.97	2.84	10.57	0.18
Maximum	2.36	n/a	1.93	3.93	17.48	0.29
Minimum	0.55	n/a	0.45	1.97	5.06	0.03
Standard Deviation	0.45	n/a	0.37	0.57	3.41	0.06
COV	0.38	n/a	0.38	0.20	0.32	0.33

4.2.4 Distribution of the fitted parameters for the bi-linear model

To find the distribution of an observed data set, probability paper plots are used to compare the observations to a predicted fitted distribution in cumulative distribution plot (Benjamin and Cornell, 1970). For example, Figure 4.7 shows the probability papers for Normal (N), Log-normal (LN), Gumbel and Weibull distributions for the initial slope ($\boldsymbol{K_o}$). The distribution parameters were calculated by method of moments (Benjamin and Cornell, 1970). This figure shows that, the distribution of $\boldsymbol{K_o}$ can be described as Log-normal or Gumbell distribution. However, for comparing the differences between the observations with the fitted distribution in the tail region, it is not advantageous to use such papers as they rarely depict that region clearly. To investigate further, the Anderson-Darling Goodness-of-fit (GOF) statistical test (Anderson & Darling, 1954) was performed for every data set. The Anderson-Darling procedure is a general test to compare the fit of an observed cumulative distribution function to an expected cumulative distribution function. This test gives more weight to the tails than the Kolmogorov-Smirnov test (Massey, 1951). If the Anderson-Darling statistic (ADs) is smaller than the Anderson-Darling critical value (CV) then the null hypothesis cannot be rejected. The smaller the ADs, the better the predicted theoretical distribution is. The critical value depends on the number of observations (which is 0.74 in these cases as there were 35 test samples for each parameter). From this statistical hypothesis test, the null hypothesis could not be rejected at 5% significance level that the parameters follow the distributions mentioned in Table 4.1. The Anderson-Darling statistic (ADs) is shown in the parentheses of the distributions. No distribution is provided for the data-driven estimations since there is no statistically significant difference between the arbitrary and

data-driven estimation as mentioned above. Shanmugham et al. (2009) also proposed log-normal distribution for uplift capacity (failure capacity) and normal distribution for initial stiffness. However, they proposed Weibull distribution for failure displacement, which is different than the finding of the present study. Figure 4.8 shows both the empirical and theoretical cumulative distribution functions for different parameters. These figures show that, the theoretical distributions predicted by probability paper plots and confirmed by Anderson-Darling Goodness-of-Fit test actually match well with the empirical cumulative distribution functions.

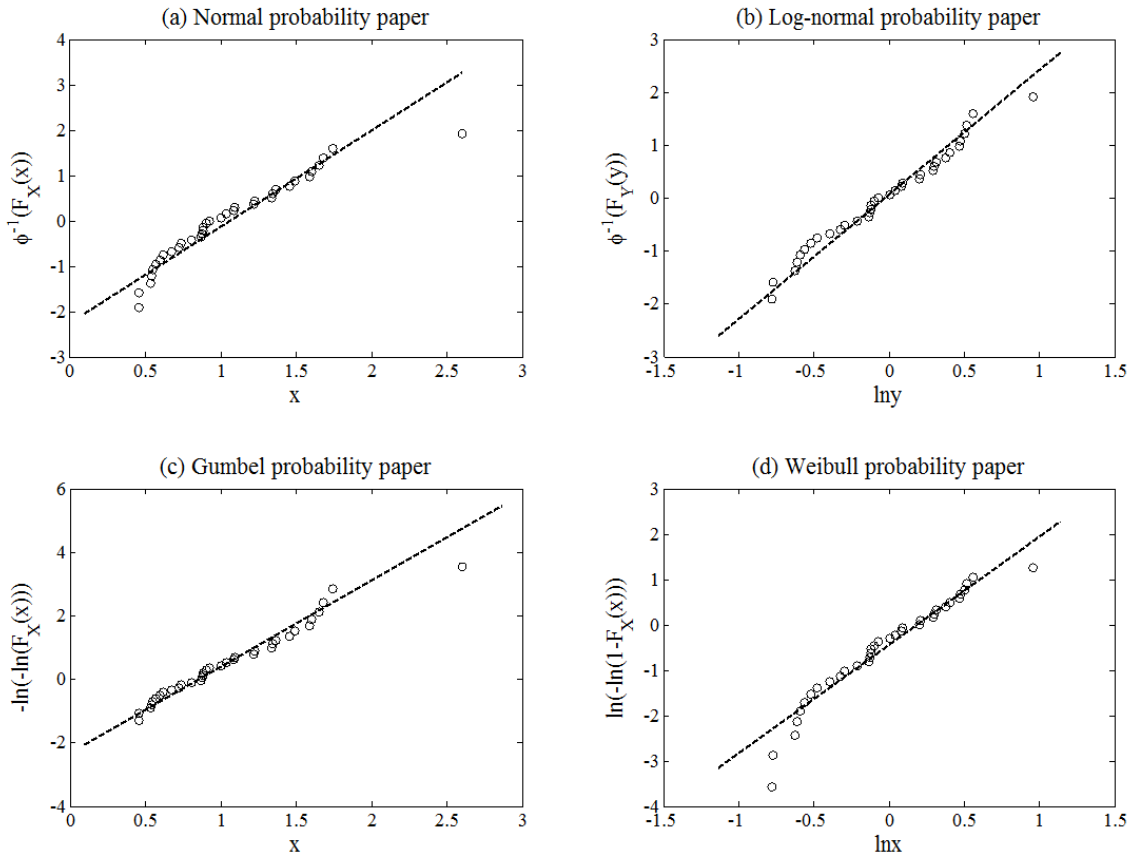

Figure 4.7 Normal, Log-normal, Gumbel and Weibull probability paper for initial slope ($\boldsymbol{K_o}$).

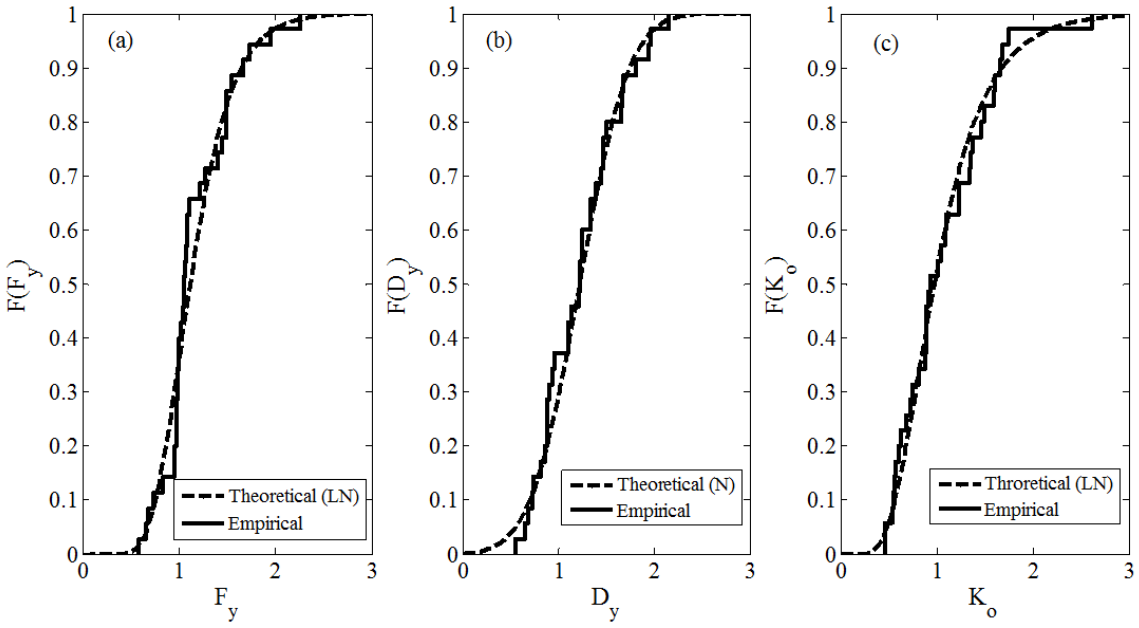

Figure 4.8.a Theoretical and Empirical cumulative distribution function for (a) yield capacity ($\boldsymbol{F_y}$), (b) yield displacement ($\boldsymbol{D_y}$) and (c) initial slope ($\boldsymbol{K_o}$) (for arbitrary estimation).

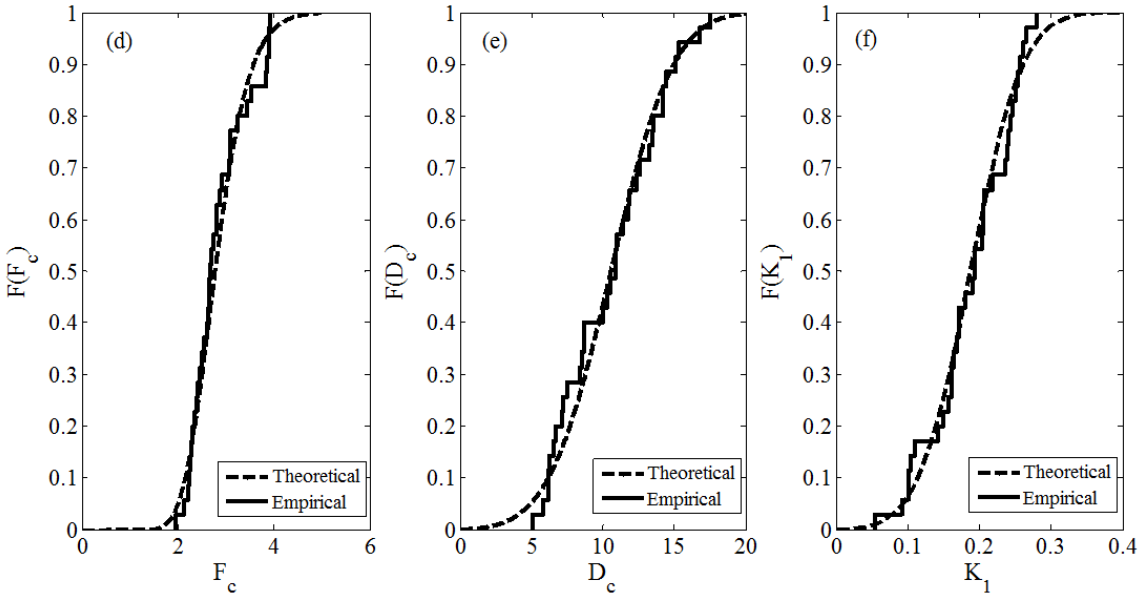

Figure 4.8.b Theoretical and Empirical cumulative distribution function for (d) failure capacity ($\boldsymbol{F_c}$), (e) failure displacement ($\boldsymbol{F_c}$) and (f) secondary slope ($\boldsymbol{K_1}$) (for arbitrary estimation).

4.2.5 Correlation between parameters for the bi-linear model

Table 4.3 show the correlation coefficients between the different model parameters. Relatively high correlations were observed between initial slope and yield capacity (0.64) and between initial slope and yield displacement (-0.69). Moderate correlations were observed between failure capacity to failure displacement (0.49) and failure displacement to secondary slope (-0.48). Surprisingly, the correlation between the initial slope and the failure capacity is very low (0.08) and also noting the fact that, the COV of the initial slope is substantially higher than the secondary slope (Table 4.1 & 4.2). This means that, a connection may have a very high initial stiffness but it may not have a high failure capacity and for the same failure capacity of different connections, the load-displacement behavior could be different. These correlations and COV of the parameters actually explain the high variability in toe-nailed connection behavior.

These experimentally obtained values, and the proposed distributions for the different parameters described above, could be used to predict the load-displacement behavior of toe-nail connections with finite element or analytical modeling. However, no further analysis is given since this is beyond the scope of the current work.

Table 4.3 Correlation coefficients between different parameters for ramp loading tests (arbitrary estimation)

Parameters	Yield capacity, F_y (kN)	Yield displacement, D_y (mm)	Initial slope, K_o (kN/mm)	Failure capacity, F_c (kN)	Failure displacement, D_c (mm)	Secondary slope, K_1 (kN/mm)
Yield capacity, F_y (kN)	1.00	0.05	0.64	0.22	-0.17	-0.35
Yield displacement, D_y (mm)	0.05	1.00	-0.69	0.15	0.43	-0.33
Initial slope, K_o (kN/mm)	0.64	-0.69	1.00	0.08	-0.42	0.03
Failure capacity, F_c (kN)	0.22	0.15	0.08	1.00	0.49	0.21
Failure displacement, D_c (mm)	-0.17	0.43	-0.42	0.49	1.00	-0.48
Secondary slope, K_1 (kN/mm)	-0.35	-0.33	0.03	0.21	-0.48	1.00

4.3 Fluctuating wind loads on individual toe-nails

Individual fluctuating load tests confirmed that RTWCs are withdrawn incrementally, as shown by Figure 4.9. These vertical permanent increments occur due to applied local peak loads (Morrison & Kopp, 2011). However, not all the peaks can substantially damage a connection. The peak loads which are responsible for substantial slip (withdrawal) of the connection are referred to as damaging peaks (Figure 4.9). From the 35 individual fluctuating wind loading toe-nail tests, it was found that there are 20 unique damaging peak loads (Figure 4.10) in the current loading time history. These damaging peak loads cause withdrawals of the connections in the range from 0.2mm to 8mm, prior failure (i.e., complete withdrawal). However, from analysis of the data, it has been found that, on average it takes 10.6 damaging peaks to fail a toe-nail connection. The weakest connection sustained 1305s and the strongest connection sustained 2253s for

the fluctuating wind loads applied to the individual toe-nail connections, based on the time histories shown in the figures below.

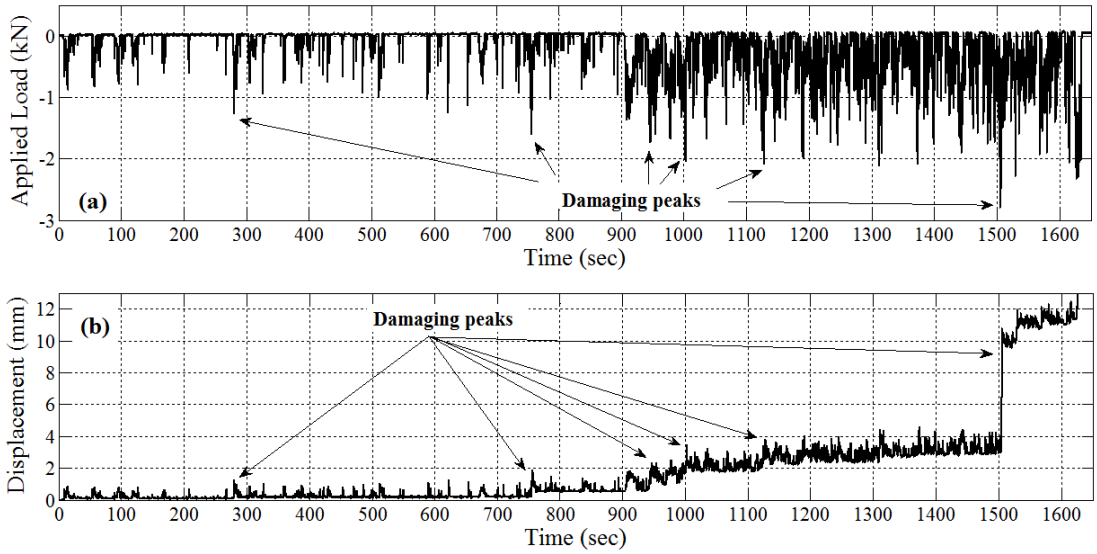

Figure 4.9 Applied fluctuating wind loads to a RTWC (a) and the response of vertical displacement for that applied fluctuating wind loading (b).

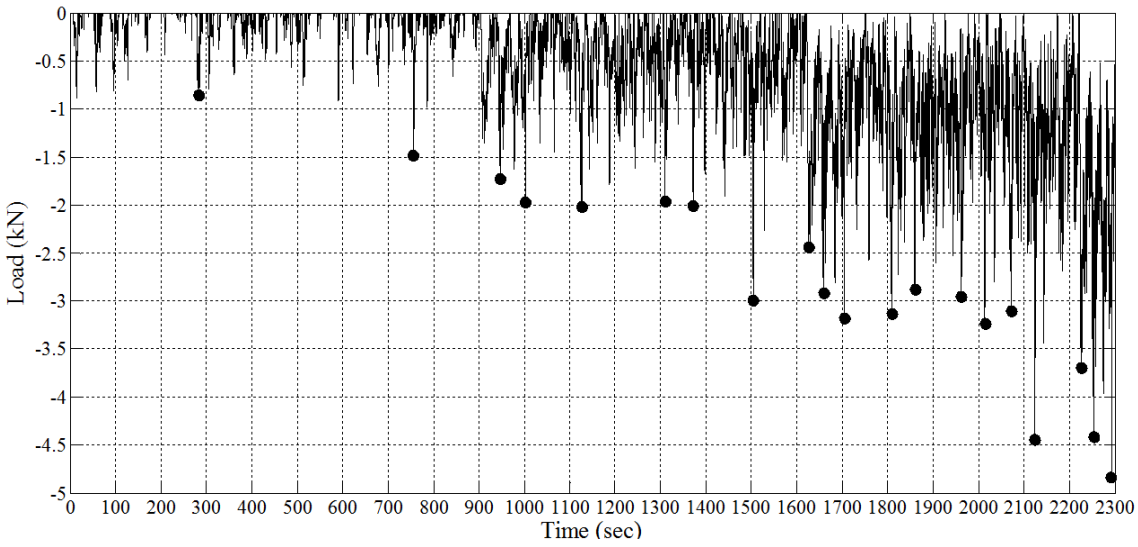

Figure 4.10 Fluctuating wind loading time history used in the individual toe-nail tests as well as in the system tests. The damaging peaks (20) are marked by the black circles.

Figure 4.11 shows the load-displacement behavior of two individual toe-nail connections for the same applied fluctuating wind loads. The envelopes of the two curves are similar to typical ramp load results, however, the unloading during the fluctuating load tests results in the incremental behavior in the plastic range.

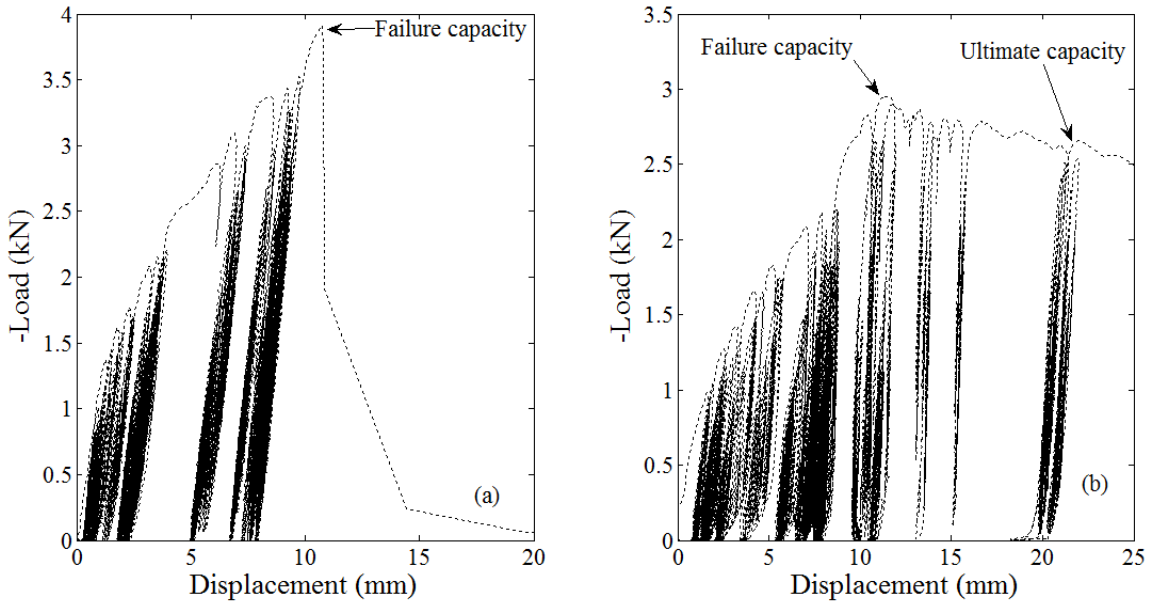

Figure 4.11 Load-displacement behavior for two RTWCs for fluctuating wind loads (experimental): (a) the connection fails at the maximum applied load; (b) the connection fails at a lower applied load than the maximum loads.

From the experiments it has been found that for the fluctuating wind load, the connection does not fail at the maximum applied load (i.e., the failure capacity (F_c)) in all cases; rather it can take some more load cycles and eventually fails at a lower applied load (e.g., Figure 4.11 (b)). This behavior is caused by the fact that the load peaks are of short duration, so it is different from the gradually increasing ramp loading tests (e.g., Figure 4.1). As a result, the connection can sustain a longer duration, until the next peak, when pullout of the connection from the top plate finally occurs. Thus, the connection

will fail at a lower peak load (which can be defined as ultimate capacity) than the previously applied maximum load, consistent with what would be observed during displacement control experiments, rather than the current load control experiments.

Most of the test specimen (60% of the total) had a failure capacity which was larger than the ultimate capacity, while the rest had failure capacity which equalled the ultimate capacity. A linear regression analysis was performed between the ultimate capacity and the failure capacity, the results of which are shown in Figure 4.12. The correlation coefficient between them is 0.90 which is a very good correlation. The standard error between the actual value and the predicted values from the linear equation was found to be small (standard error = 0.21kN). However, in all the calculations later on this document, the maximum applied load to the connection is considered as a failure capacity (F_c) as one would be concerned primarily with this value for design.

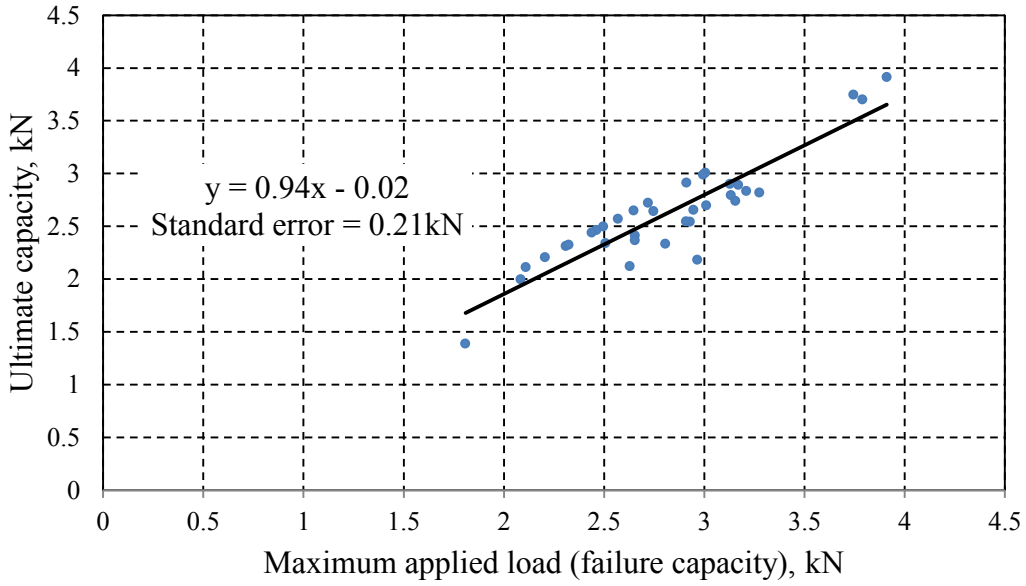

Figure 4.12 Regression analyses between the failure capacity and ultimate capacity for realistic wind load.

4.4 Comparison of load-displacement behavior in the individual and system tests

In this section, the initial slopes in the toe-nail models ($\boldsymbol{K_o}$) are compared for the data from the system and the individual toe-nail, ramp load tests. As well, a discussion of failure capacity and failure displacement for all loading type and test type will be given. Following this, the probability density and cumulative distribution functions of these parameters will be analyzed.

4.4.1 Initial slope

Similar to individual toe-nail test results for 8kN/min ramp load, the initial slope ($\boldsymbol{K_o}$) for the system tests were determined for each of the toe-nail connections from the test data to verify that they are not altered by being in the system. It is to be noted that, although the load applied (P) to each of the connection within a system is same, the actual measured loads (R) is may differ from the applied loads due to load-sharing which occurs through the steel beams which interconnect the RTWCs. The analysis of load-sharing will be discussed in the next chapter. The yield capacity (F_y) for each of the connections were calculated at the fixed yield displacement, D_y=1.22 mm (Figure 4.13). The mean value for the less stiff system and the stiffer system were 0.875kN/mm and 0.936kN/mm respectively. The coefficients of variation (COV) were 0.31 and 0.30 respectively. Since, in the present experimental system, point loads were applied to the connections, the toe-nail connection properties should not change due to the beams which interconnect the connections. To confirm this, a null hypothesis was formed that the mean values of the initial slopes for individual and system tests (less stiff and stiffer beams) are equal. Indeed, a one-way analysis of variance (ANOVA) (Spiegel, 1990)

confirmed that, statistically, there is no difference between mean values of the initial slopes for individual and system tests (less stiff and stiffer beams).

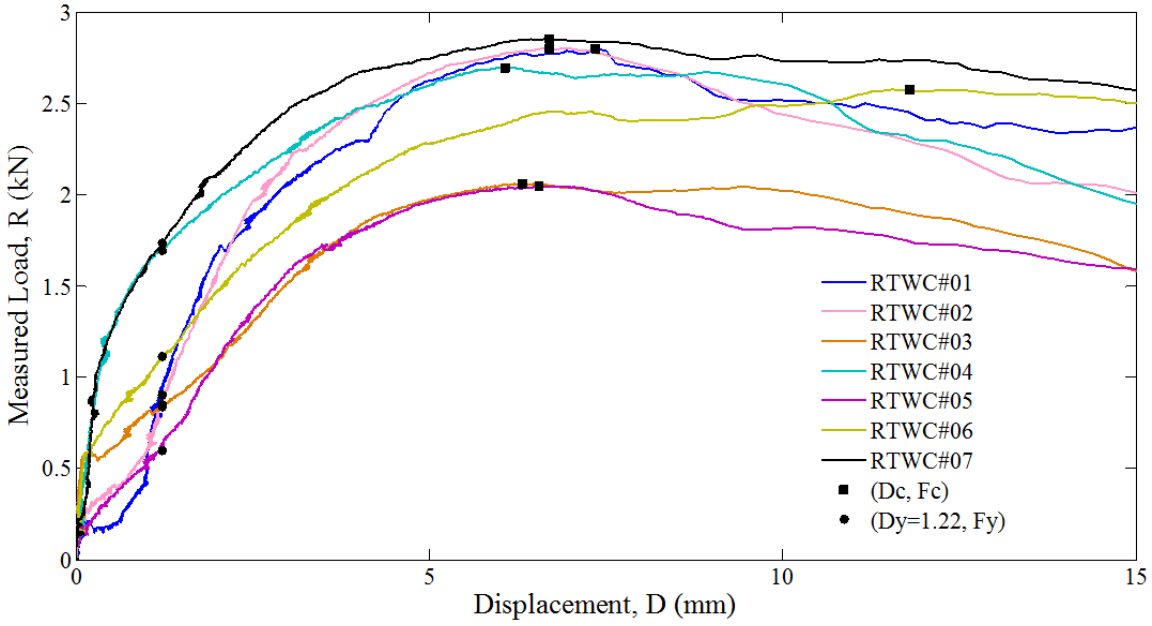

Figure 4.13 Measured loads vs. displacement for seven RTWCs in the less stiff system during one ramp loading test. Squares indicate the failure capacity (F_c) and failure displacement (D_c) for each connection; circles indicate the yield capacity (F_y) at fixed yield displacement ($D_y = 1.22mm$).

4.4.2 Failure capacity (F_c) and failure displacement (D_c)

Figures 4.14 & 4.15 show box-and-whisker diagrams (also known as box plots) of the failure capacities and failure displacements for 35 RTWCs for different loading and test types. It is to be noted that, box plots are helpful to understand data graphically between multiple groups through their five-number summaries (Q1, Q2, Q3, L and U). In each box, the central mark is the median (Q2), the lower quartile is the 25th percentile (Q1) and the upper quartile is the 75th percentile (Q3). So, within the box, 50% data of the total data set in accounted for. The difference between the upper and lower quartile is

called as interquartile range (IQR). The whiskers are extended up to the lowest observed datum and the highest datum if the lower adjacent (L=Q1-1.5*IQR) and upper adjacent (U=Q3+1.5*IQR) exceeds the lowest and highest datum of the data set. However, if any data exceeds or go below the upper adjacent or lower adjacent values then they are known as outliers and represented in the figure outside the adjacent with markers. Since, six different test types (including the loading type and system type) were conducted, the data range for each test type is represented in these figures. The analysis of the test results and the comparison between the test types is discussed below.

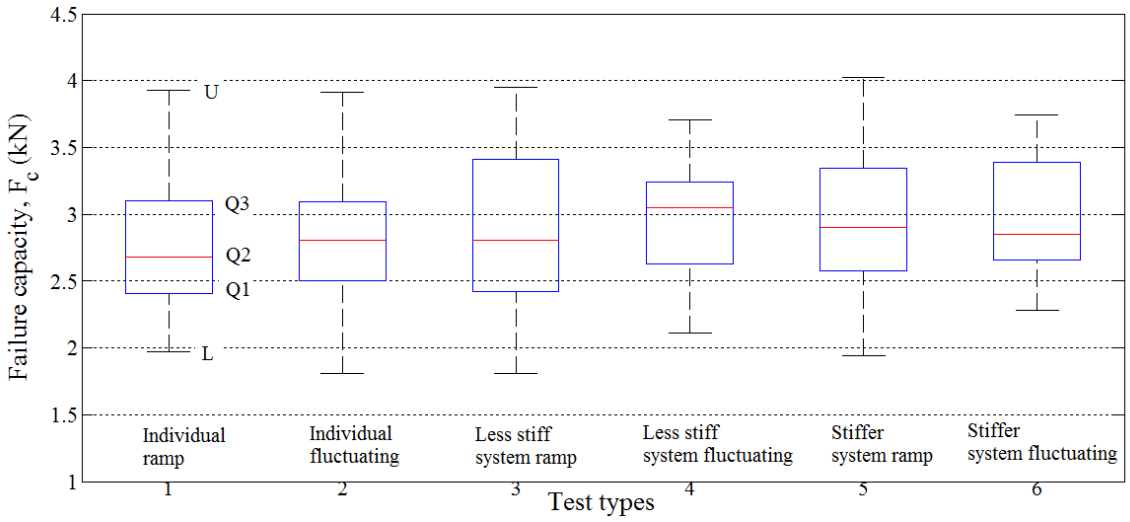

Figure 4.14 Box-and-whisker diagrams for failure capacities from the six test types.

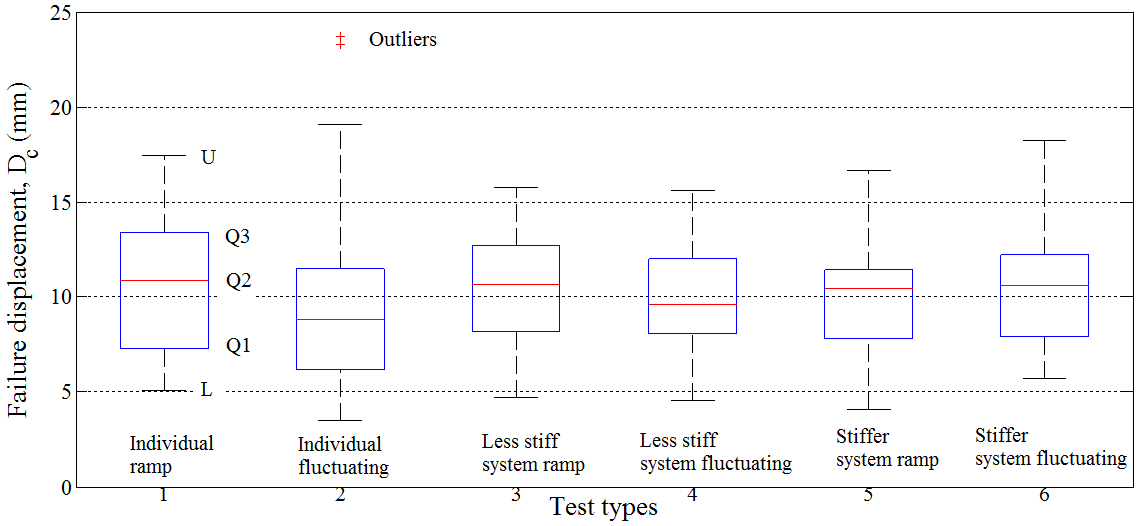

Figure 4.15 Box-and-whisker diagrams for failure displacements from the six test types.

The mean failure capacity of the RTWCs for different types of tests and loading histories ranges from 2.81kN to 3.01kN (Table 4.4). The mean failure displacement of RTWCs for different types of tests and loading histories ranges from 9.66mm to 10.45mm. Table 4.4 shows that the mean failure capacity of system RTWCs are slightly higher than the individual RTWCs results. It is also to be noted that, the mean failure capacity of RTWCs by system with higher stiffness (6.35cm x 6.35cm x 0.476cm beams) is slightly higher than the less stiff system (3.8cm x 3.8cm x 0.635cm beams).

The coefficient of variation (COV) of failure displacements is higher than the coefficient of variation (COV) of failure capacity for every test type. This result can also be seen from the box-and-whisker plots (Figure 4.14 and 4.15). The COV of failure capacities for individual ramp loading tests is 0.20, which is close to Cheng (2004) (COV=0.16) for two16d box nails and Reed et al. (1997) (COV=0.23) for three 8d nails. The variation of failure capacities reduced with the increase of the system stiffness for the fluctuating wind load case. Also, the variation of the failure displacement for system

fluctuating tests (COV=0.29) is substantially lower than individual fluctuating tests (COV=0.50). This is because of Load-sharing, which is discussed in the subsequent chapter. The minimum and maximum failure capacities considering all the tests type and loading methods are 1.81kN and 4.03kN. Similarly, the minimum and maximum displacements were found 3.48mm and 23.73mm.

Since the mean values of failure capacity (F_c) and failure displacement (D_c) are close, a null hypothesis was formed that the mean failure capacities for different loading type (i.e. ramp or fluctuating) and test type (individual or system) are equal. The failure capacity (F_c) and failure displacement of the toe-nails for different loading and test type has been considered independent to each other. Again, one-way analysis of variance (ANOVA) (Spiegel, 1990) which compares the means of two or more groups of data is used to justify the null hypothesis described above. From this, it was found that the null hypothesis could not be rejected at the 5% significance level that the mean failure capacities are same for all the loading and test type. A similar null hypothesis was made for the mean failure displacements, with the same conclusion that the values are the same.

Table 4.4 Statistics of the failure capacities & failure displacements for different test types

Test type	Parameters	Mean	Minimum	Maximum	Standard deviation	COV
Individual ramp	Failure capacity (kN)	2.84	1.97	3.93	0.57	0.20
	Failure displacement (mm)	10.57	5.06	17.48	3.41	0.32
Individual fluctuating	Failure capacity (kN)	2.81	1.81	3.91	0.47	0.17
	Failure displacement (mm)	9.66	3.48	23.73	4.86	0.50
System ramp (3.8cm x 3.8cm x 0.635cm beams)	Failure capacity (kN)	2.91	1.81	3.95	0.60	0.20
	Failure displacement (mm)	10.22	4.71	15.81	2.90	0.28
System fluctuating (3.8cm x 3.8cm x 0.635cm beams)	Failure capacity (kN)	2.94	2.11	3.71	0.46	0.16
	Failure displacement (mm)	10.07	4.53	15.64	2.77	0.28
System ramp (6.35cm x 6.35cm x 0.476cm beams)	Failure capacity (kN)	2.95	1.94	4.03	0.54	0.18
	Failure displacement (mm)	10.07	4.09	16.65	2.82	0.28
System fluctuating (6.35cm x 6.35cm x 0.476cm beams)	Failure capacity (kN)	3.01	2.28	3.75	0.43	0.14
	Failure displacement (mm)	10.45	5.70	18.27	3.08	0.29

4.4.3 Distributions of failure capacity (F_c) and failure displacement (D_c)

Figures 4.16 to 4.19 show the PDFs and CDFs of the failure capacities and failure displacements for all test and loading types. By using Anderson-Darling goodness of fit test (Anderson & Darling, 1954), the null hypothesis could not be rejected at 5% significance level that, failure capacity (F_c) and failure displacement (D_c) for all six different type of tests follow the distributions mentioned in Table 4.5.

Table 4.5 Anderson-Darling critical value and Anderson-Darling statistics for failure capacities & failure displacements for different test types

Test type	Parameters	Anderson-Darling critical value (CV)	Distribution (Anderson-Darling statistic, ADs)
Individual ramp	Failure capacity (kN)	0.74	LN (0.61)
	Failure displacement (mm)	0.74	N (0.42) LN (0.58)
Individual fluctuating	Failure capacity (kN)	0.74	N (0.31) LN (0.28)
	Failure displacement (mm)	0.74	LN (0.21)
System ramp (3.8cm x 3.8cm x 0.635cm beams)	Failure capacity (kN)	0.74	N (0.43) LN (0.50)
	Failure displacement (mm)	0.74	N (0.45) LN (0.63)
System fluctuating (3.8cm x 3.8cm x 0.635cm beams)	Failure capacity (kN)	0.74	N (0.41) LN (0.70)
	Failure displacement (mm)	0.74	N (0.54) LN (0.24)
System ramp (6.35cm x 6.35cm x 0.476cm beams)	Failure capacity (kN)	0.74	N (0.22) LN (0.26)
	Failure displacement (mm)	0.74	N (0.47) LN (0.36)
System fluctuating (6.35cm x 6.35cm x 0.476cm beams)	Failure capacity (kN)	0.74	LN (0.72)
	Failure displacement (mm)	0.74	N (0.43) LN (0.34)

From the PDF and CDF plots (Figure 4.16 and 4.17) of the failure capacity it can be seen that, for any test type, the distribution is slightly broader for the ramp loading test compared to the fluctuating load tests, which is similar to the findings of Morrison & Kopp (2011). This means that higher variability is associated with ramp loading tests. While comparing the plots between fluctuating wind loading tests, it was found that the system with higher stiffness (6.35cm x 6.35cm x 0.476cm beams) shows higher failure capacity with less variability. However, Anderson-Darling K-sample test (Scholz & Stephens, 1987; Trujillo-Ortiz et al., 2007) was performed to address if all the data came from the same distribution or not. The null hypothesis could not be rejected at 5% significance level that, all the data are coming from the same parent distribution. The

probability associated to the Anderson-Darling rank statistic was found 0.32 which is above the significance level (α=0.05). This indicates that, with the current data, the failure capacities for each loading and test type can be represented by the same distribution.

From the PDF and CDF plots of failure displacements (Figure 4.18 and 4.19), the distribution is broader for individual fluctuating, individual ramp, less stiff system ramp loads test while others show identical distribution. Similar to failure capacity, a null hypothesis was formed stating that, with the current data, the failure displacements for each loading and test type can be represented by the same distribution.

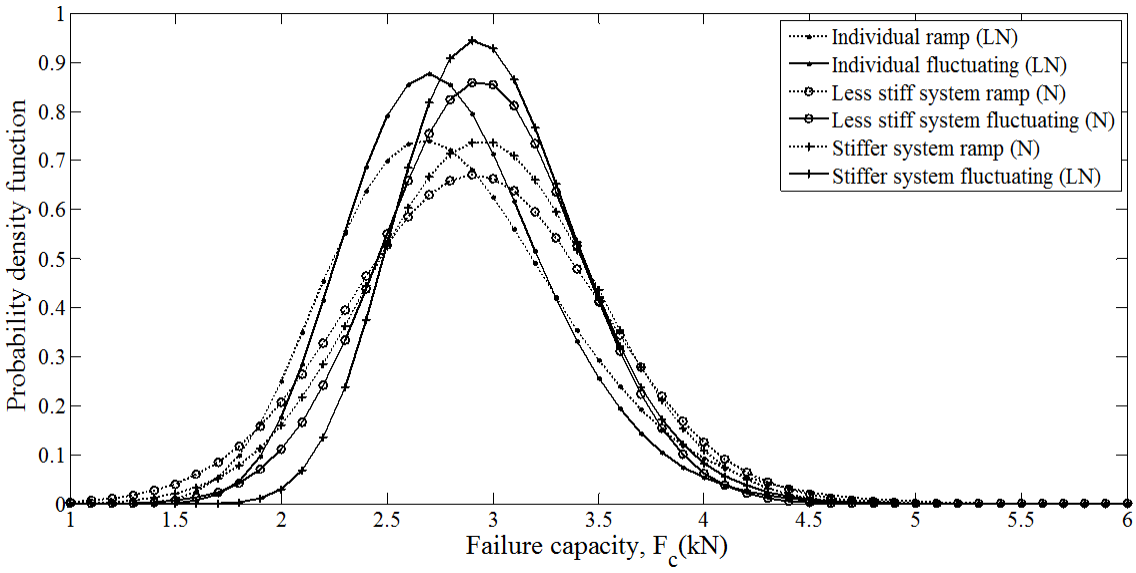

Figure 4.16 Probability density function (PDF) of failure capacities of six different test types.

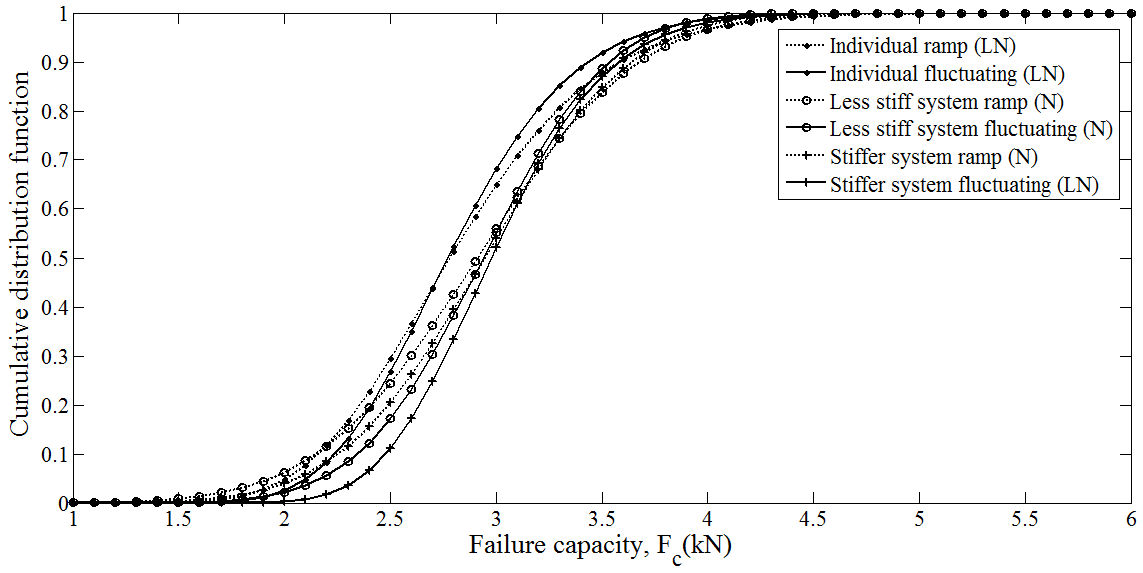

Figure 4.17 Cumulative distribution function (CDF) of failure capacities of six different test types.

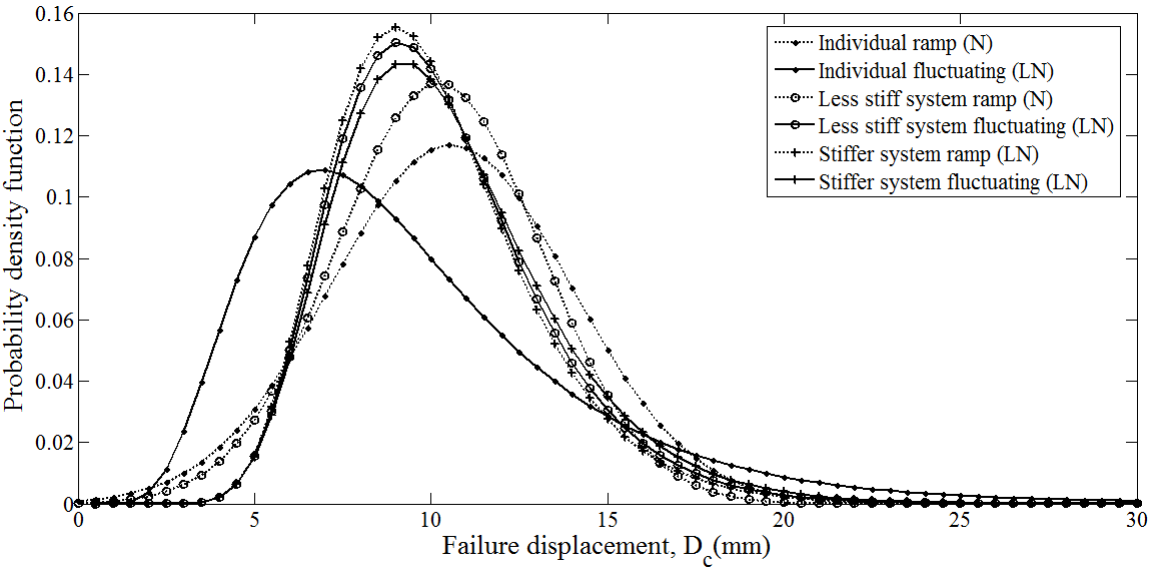

Figure 4.18 Probability density function (PDF) of failure displacements of six different test types.

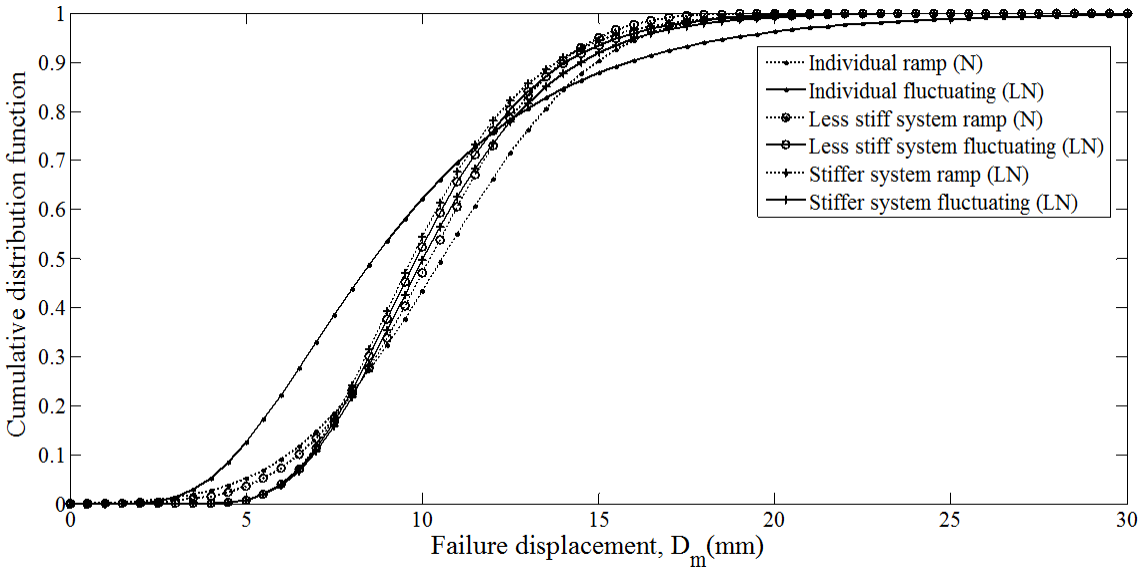

Figure 4.19 Cumulative distribution function (CDF) of failure displacements of six different test types.

The null hypothesis could not be rejected at 5% significance level that, all the data are coming from the same distribution. The probability associated to the Anderson-Darling rank statistic was found 0.46 which is above the significance level (α=0.05). Once again, this indicates that the failure displacements for each loading and test type can be represented by the same distribution.

So, it is clear that the current experiments were well-behaved, with no incorrect or unaccounted for variations occurring between the various tests. Thus, the mean failure capacities and mean failure displacements of toe-nail connections are independent of loading and test types.

4.5 Failure types

There were two types of basic failures, namely "pull out" or "splitting". "Pull out" means that the nails in the rafter are withdrawn from the top plate and remain in the rafter, whereas "splitting" means that the nails (or a single nail) remain attached to the top plate with the lower portion of the split lumber from the rafter. In total, five different possibilities of these two basics modes were observed during the tests: i) all nails pulled out ii) all nails split iii) d-nails split iv) s-nail split & v) d-nail split. Photographs are shown in Figure 4.20.

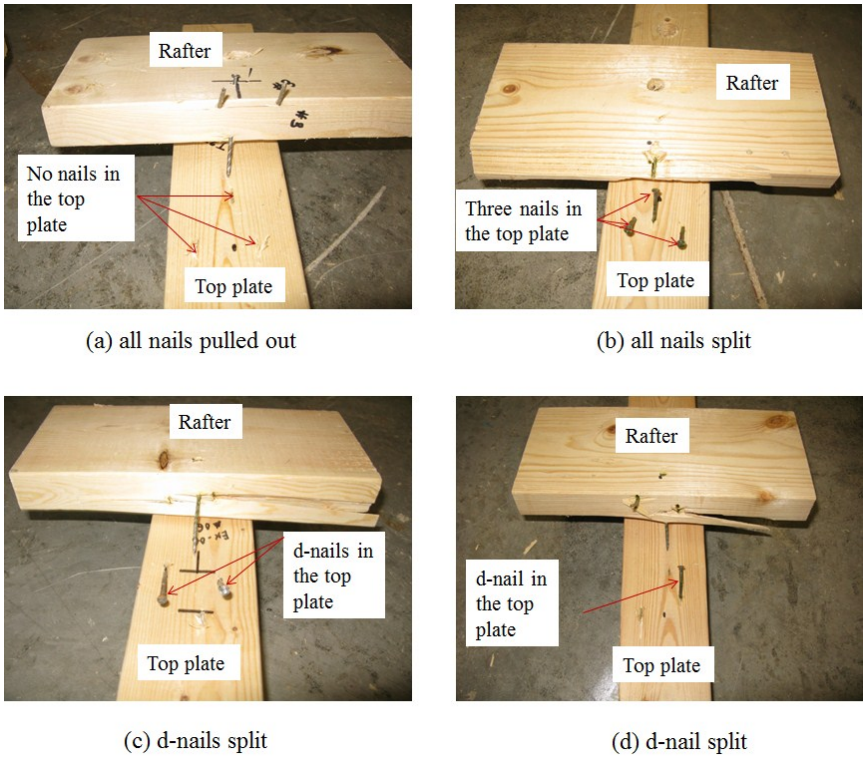

Figure 4.20 Different types of toe-nail connection failure (s-nail split failure is not shown here)

Among the five failure types, the most common type of failure (70%, considering all tests) was when all nails pulled out of the top plate. This mode was found to have the

lowest mean failure capacity, when compared to the others, as shown in Table 4.6. The second most common type of failure (21%, considering all tests) was found to be when the d-nails split. All nails splitting failure was found only 1.4% of the time. Notable differences in mean failure capacity were not found between the splitting failures, although the number of samples with this mode is very small. This result is also consistent with Shanmugam et al. (2009) who found 81% pure nail withdrawal, 16% combined failure and 3% splitting failure. Morrison and Kopp (2011) found similar results.

Table 4.6 Mean and standard deviation of the failure capacities for different failure types and different test types

Test type	All nails pulled out (mean, standard deviation)	All nails split (mean, standard deviation)	d-nails split (mean, standard deviation))	s-nail split (mean, standard deviation)	d-nail split (mean, standard deviation)
Individual ramp	18 (2.68, 0.53)	0	13 (3.06, 0.50)	1 (3.91)	3 (2.50, 0.29)
Individual fluctuating	30 (2.75, 0.45)	1 (3.91)	4 (2.97, 0.24)	0	0
System ramp (3.8cm x 3.8cm x 0.635cm beams)	22 (2.68, 0.55)	2 (3.44, 0.73)	4 (3.22, 0.57)	4 (3.38, 0.45)	3 (3.25, 0.40)
System fluctuating (3.8cm x 3.8cm x 0.635cm beams)	28 (2.86, 0.46)	0	6 (3.32, 0.29)	0	1 (2.90)
System ramp (6.35cm x 6.35cm x 0.476cm beams)	24 (2.87, 0.56)	0	9 (3.1, 0.54)	0	2 (3.16, 0.26)
System fluctuating (6.35cm x 6.35cm x 0.476cm beams)	25 (2.95, 0.45)	0	8 (3.18, 0.39)	0	2 (3.02, 0.23)

4.6 Moisture content

Although the lumbers were bought from the same batch, the moisture content of the lumber varied in between 6.3% to 14%. A two prong moisture meter was used to measure the moisture content. However, no correlation (0.03) was found between the

moisture content and the failure capacity. Shanmugham et al. (2009) also found low correlation between the moisture content and the failure capacity. Since, the construction of toe-nail connection itself contains a lot of variability and slight variations in nailing angle or nailing height could result different failure capacities, the variation in moisture content seems to have minimal effect on the toe-nail connection properties in the laboratory environment with a small range of this parameter.

4.7 Conclusions

In this chapter bi-linear and curvilinear load-displacement model of individual toe-nail connections for 8kN/min ramp loads have been discussed extensively based on previous studies and the parameters which define these models have been proposed from experimental results analysis. The high coefficient of variation (COV) in the parameters and small correlation between the parameters indicates the high variability of individual toe-nail connections. Load-displacement behavior of individual toe-nail connections for fluctuating wind loads showed that toe-nail connections fail with incremental withdrawal from the top plate. Permanent withdrawal occurs due to the localized, large peaks in the wind loads. No statistically significant differences were found between different loading and test type for mean failure capacities and mean failure displacements. The variations of the failure displacements were found to be higher than the variations of failure capacities for any loading or test type. Failure displacements for individual fluctuating wind loads showed broader distribution compared to others.

Chapter 5: Analysis of Load-sharing

5.1 Introduction

Toe-nail load-displacement behavior is highly variable, as shown in Chapter 4. Although different toe-nail connections may follow similar load-displacement behavior, they may have different magnitude of displacement for the same applied load. As a result, when multiple RTWCs are connected via steel beams the differential load-displacement behavior will cause load differences (denoted as ΔR) between the applied load (denoted as P) and actual reaction (measured load; denoted as R) for any connection. The schematic diagram shown in Figure 5.1 explains more about the load-sharing. In this figure, there are two RTWCs interconnected via a steel beam. The toe-nail connections can be approximated as non-linear spring support. Hence, this system will satisfy both force equilibrium ($\sum F_y = 0$) and moment equilibrium ($\sum M$=0). Here, for the same applied load (i.e. P1(t)=P2(t)), RTWC#02 displaces more than RTWC#01 (D2>D1). D is denoted as for the displacement of that connection. Since, the RTWCs are connected through the beam, RTWC#02's reaction load (R2 (t)) will not be equal to the applied load (P2(t)) due to internal moment which is generated for differential displacements between the connections. Thus, RTWC#02 will transfer some of its applied load to RTWC#01. As a result there will be a load difference (ΔR) between the measured load and applied load for both the connections. This load difference can be denoted as:

$$\Delta R = R - P$$

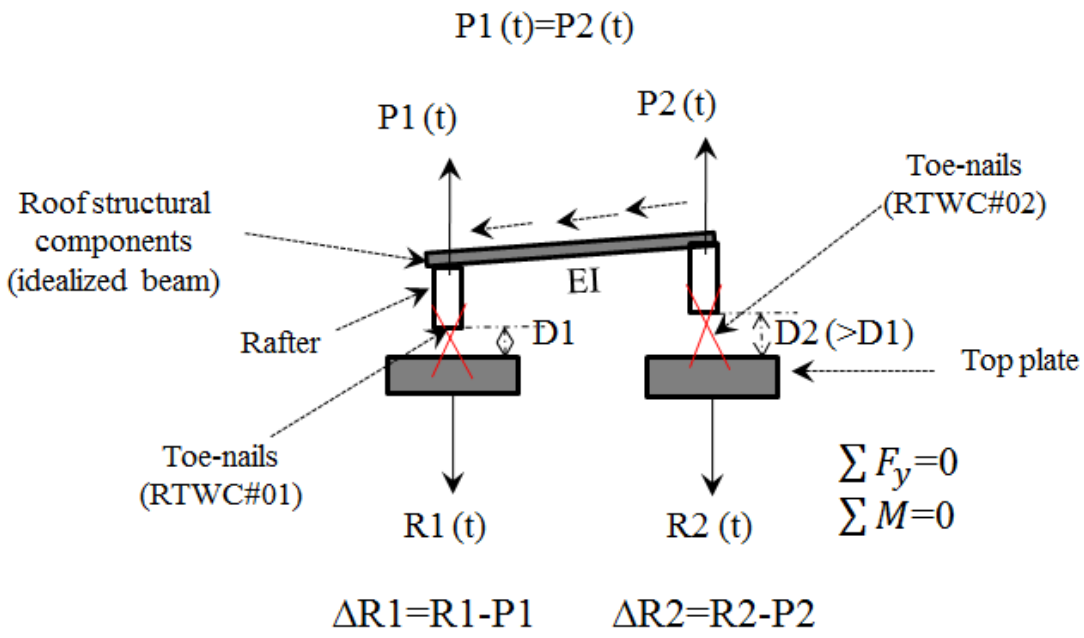

Figure 5.1 Load-sharing schematic diagram between two RTWCs.

Since there are seven connections interconnected via steel beams in the present experimental set up and they are subjected to identical loads (ramp or fluctuating) there could be a load difference of each connection which will depend on the adjacent connections load-displacement behavior, steel beam stiffness and the center to center distance between RTWCs. The load difference for each connection can be denoted as $\Delta R_1,\ \Delta R_2, \ldots, \Delta R_7$.

5.2 Load-sharing between stronger and weaker connections for ramp loads

To understand the load-sharing behaviors between a strong and a weak connection, two tests were performed with the stiffer system described in chapter 3. In these tests, all the RTWCs were made with three 12d nails except RTWC#04. In the first test, RTWC#04 was made with four 12d nails (i.e., stronger connection) and in the

second test RTWC#04 was made with two 12d nails (i.e., weaker connection). Identical 8kN/min ramp loads were applied (i.e. P1=P2=…=P7) to each connection simultaneously during the tests. From these tests, it has been confirmed that the stronger connection takes up load from the adjacent weaker connections (Figure 5.2) while the weaker connection sheds its load to the adjacent stronger connections (Figure 5.4). Figures 5.2 & 5.4 show the applied and measured load time series for three adjacent connections (RTWC#03~RTWC#05). These figures show that the difference between measured (R) and applied (P) load increases with load level (and time, since it is a ramp load time history) and that around failure the maximum load difference, ΔR occurs (Figure 5.3 (c)). In these particular tests, the stronger connection take up to maximum 33% higher loads than its applied load, whereas the weak connection shed up to maximum 50% of its applied load. Once the weakest connection fails, it will (obviously) shed its entire load to the neighbouring stronger connections to satisfy moment equilibrium. For this reason, the measured load for RTWC#04 in Figure 5.4 becomes flatter and shows ductile behavior when it reaches its failure capacity.

Figure 5.3 and Figure 5.5 shows the applied load (P) vs. displacement (D), measured load (R) vs. displacement (D) and load difference (ΔR) vs. displacement (D) plots for the same experiments shown in Figure 5.2 and Figure 5.4 respectively. For the same applied load there will be a difference in displacement magnitudes for different connections. As a result there will be load-sharing between the adjacent connections and hence the measured load (R) will be different from applied load (P) at the same displacement (D) of the connections. The load difference (ΔR) vs. displacement (D) plots shows that, the load difference (ΔR) changes with the increasing displacement of the

connections. The positive values indicate that the connection is shedding its load to the neighbours (i.e. R<P) whereas negative values indicate that the connection actually taking up loads from the neighbours (i.e. R>P). That is why ΔR for RTWC#04 is positive in Figure 5.5 (c) and negative in Figure 5.3 (c). It is to be noted that, up to certain displacements (i.e., yield displacement, $\boldsymbol{D_y}$=1.22 mm), the load differences (ΔR) are less, and perhaps negligible. After yield displacement, the measured load vs. displacement shows higher load differences, which is practically important.

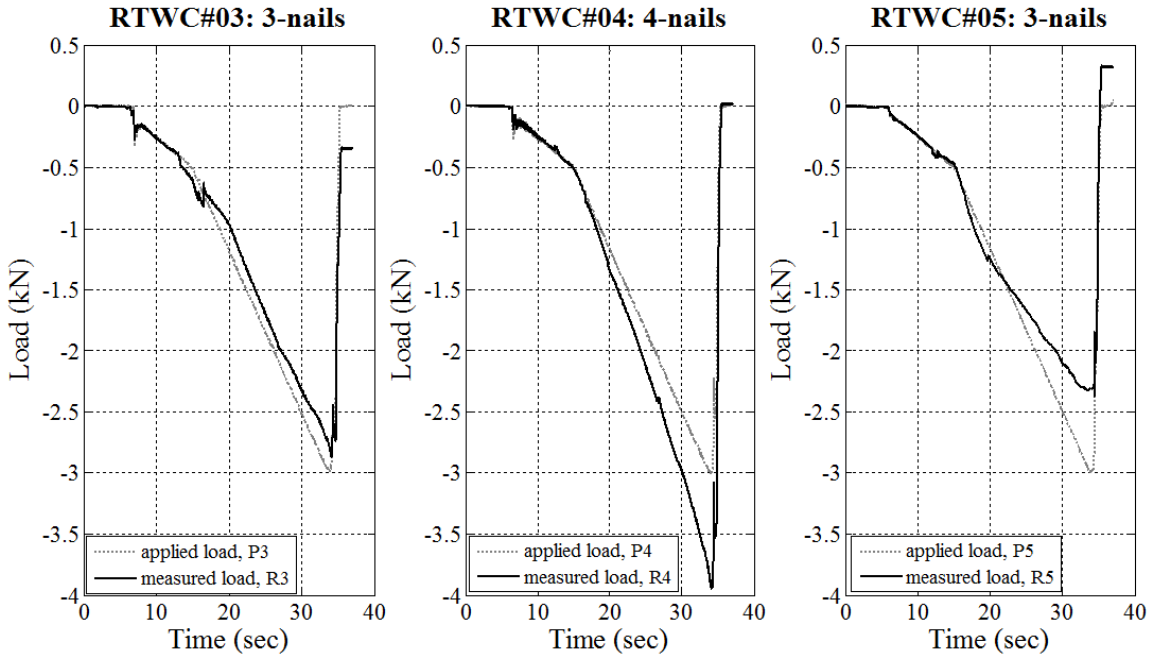

Figure 5.2 Applied (P) and measured load (R) time series for RTWC#03~RTWC#05; RTWC#03 and RTWC#05 constructed with 3 nails whereas RTWC#04 constructed with 4 nails.

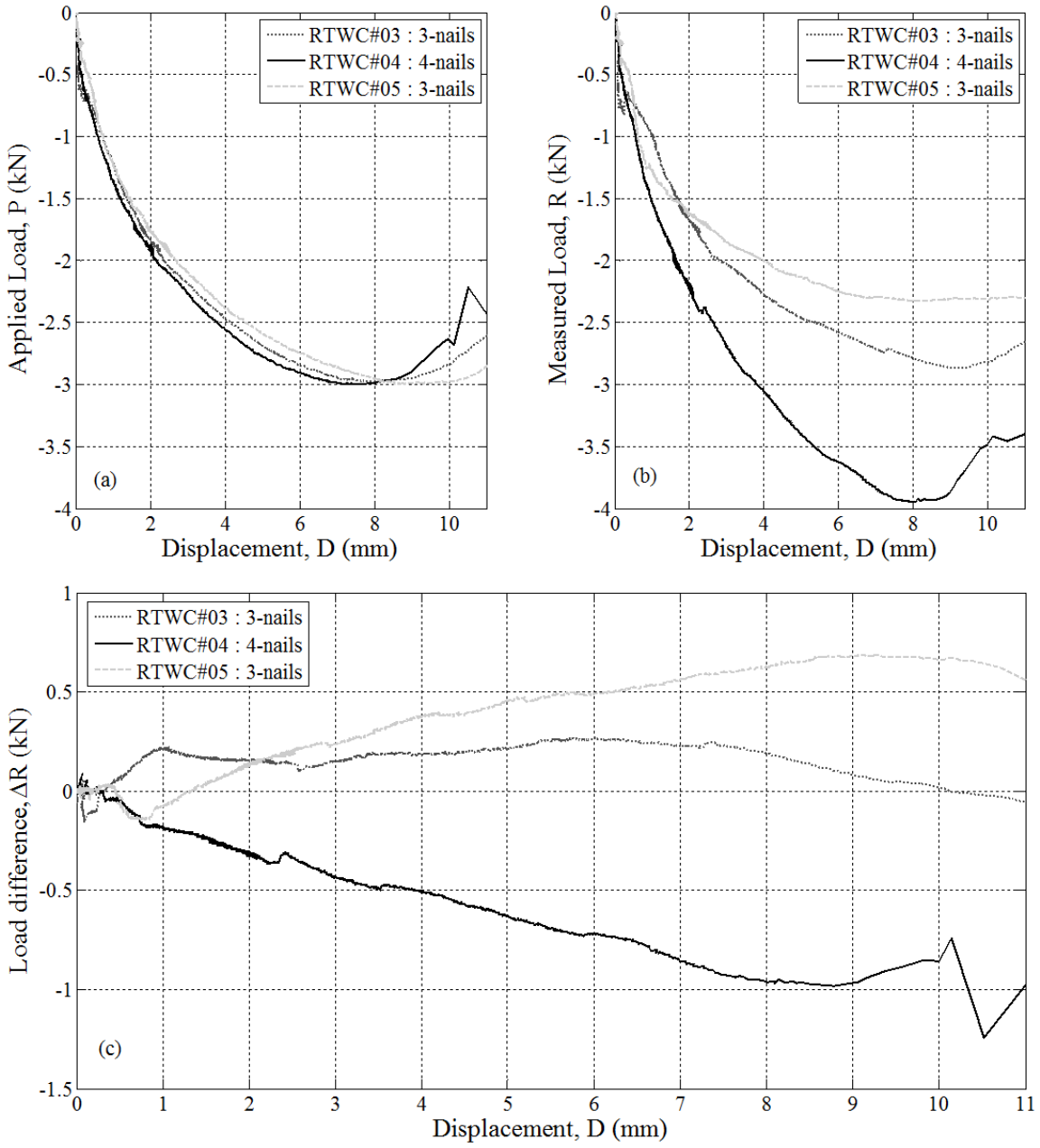

Figure 5.3 (a) Applied load (P) vs. displacement (D); (b) measured load (R) vs. displacement (D); and (c) load difference (ΔR) vs. displacement (D) for RTWC#03~RTWC#05 for the same experiment of Figure 5.2.

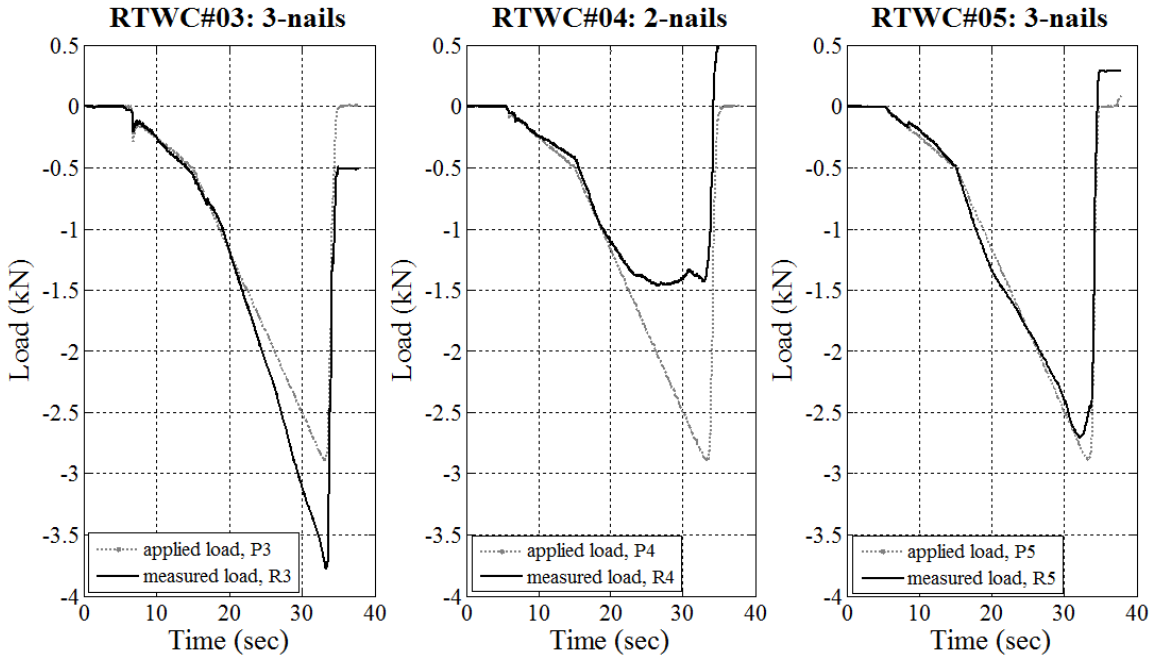

Figure 5.4 Applied (P) and measured (R) load time series for RTWC#03~RTWC#05; RTWC#03 and RTWC#05 constructed with 3 nails whereas RTWC#04 constructed with 2 nails.

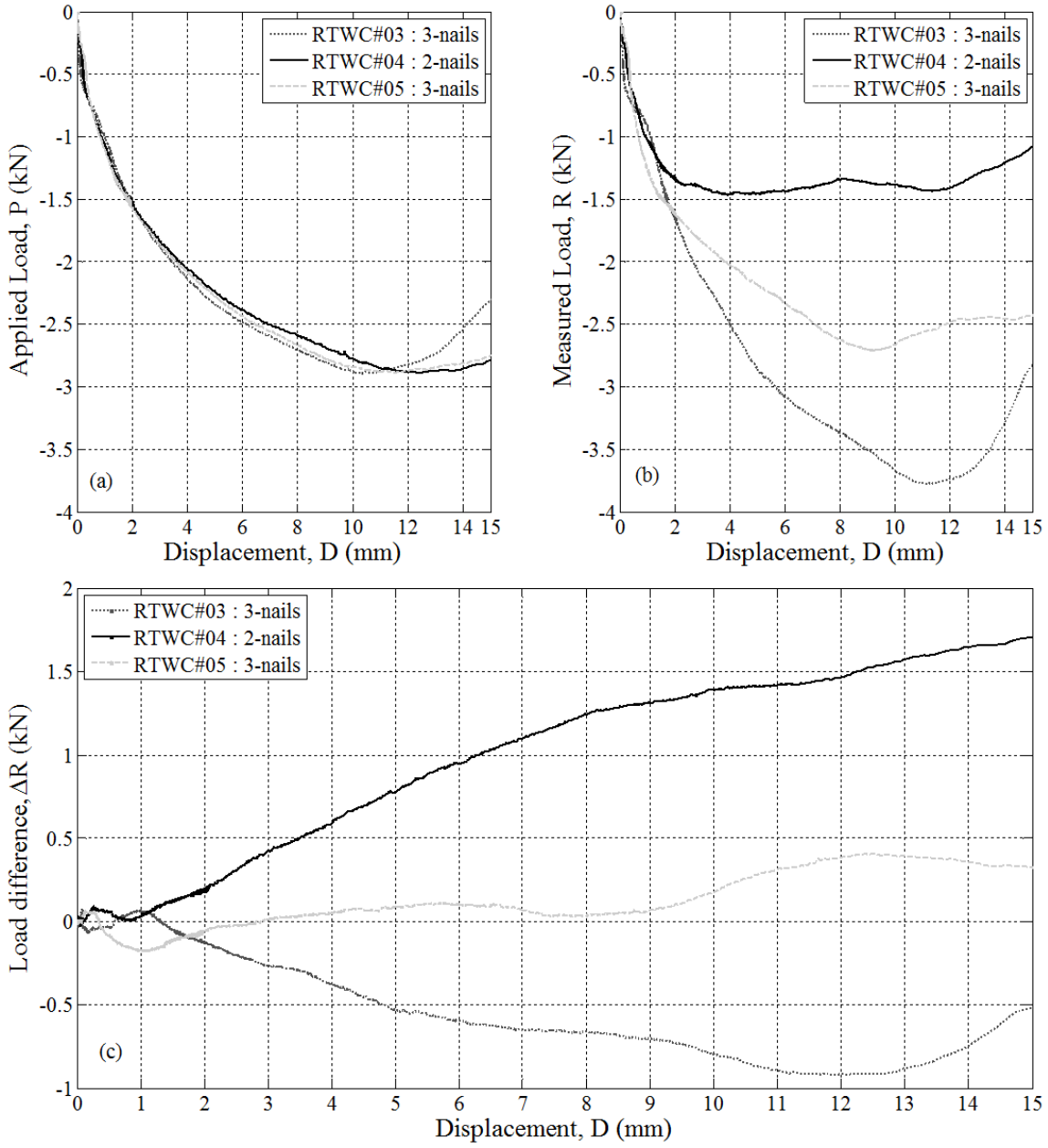

Figure 5.5 Applied load vs. displacement (a) and measured load vs. displacement (b) for RTWC#03~RTWC#05 for the same experiment of Figure 5.4.

5.3 Effect of beam bending stiffness on load-sharing for identical ramp loads

Identical, 8kN/min ramp loads (shown in Figure 3.5) were applied to each of the connections in the system. Note that these tests were different than the above mentioned

tests since all the connections were made with 3-nails. Five repeated tests were performed for each set of beams. Figure 5.6 shows the response (applied load and measured load) of three consecutive RTWCs, of the seven connections during one experiment for the less stiff system. Figure 5.7 shows the applied load vs. displacement, measured load vs. displacement and load difference vs. displacement plots for the same test results shown in Figure 5.6. From the applied load (P) vs. displacement plot (D), it can be clearly seen that for same loading history applied to all the connections, different connection exhibits different magnitude of displacement resulting in load transfer between the connections. As a result of this continuous load-sharing, the measured (R) and applied (P) load plotted against displacement (D) follows a different trend as shown in Figures 5.7 (a & b). Figure 5.7 (c) shows that, the load difference is not constant, rather it is changing with increasing displacement of each connection. It is to be noted that, load-sharing (i.e. load difference) starts from the very beginning between RTWCs (although the magnitude is very small at the beginning) and it increases with the incremental damage of the connections. In most cases load difference is maximum prior the failure of the connection (or the whole system). This behavior is observed because, even though same load was applied to each connection, the differential displacement between connections increases with time as shown in Figure 5.7 (a).

For example, from Figure 5.6, the measured load time series for RTWC#04 shows that, it is subjected to a lower measured load (i.e. load shedding), R4, than the applied load, P4, initially at small applied load (up to 13s), and then it receives extra load from the neighbours (from 13s to 24s), again it shed loads to the neighbours (from 24s to 32s) and finally it get extra loads from the neighbours (from 32s to failure). The load

difference vs. displacement plot shown in Figure 5.7 (c) explains even better. This figure shows that the load difference of RTWC#04 changes with its incremental damage and prior failure the load difference is maximum (around 12mm). This behavior is consistent with Wolfe and LaBissoniere (1991). They also speculated that, this load-sharing or load redistribution can be occurred up to three to four adjacent connections on either side for a given connection which cannot be specified in these current experiments. Similar type of changing load-sharing (i.e. load difference) behavior is observed for RTWC#03 (Figure 5.7 (c)). RTWC#05 always shed its applied load to the neighbouring connections and prior failure it get the maximum load difference. These behaviors are also observed for the rest of the connections.

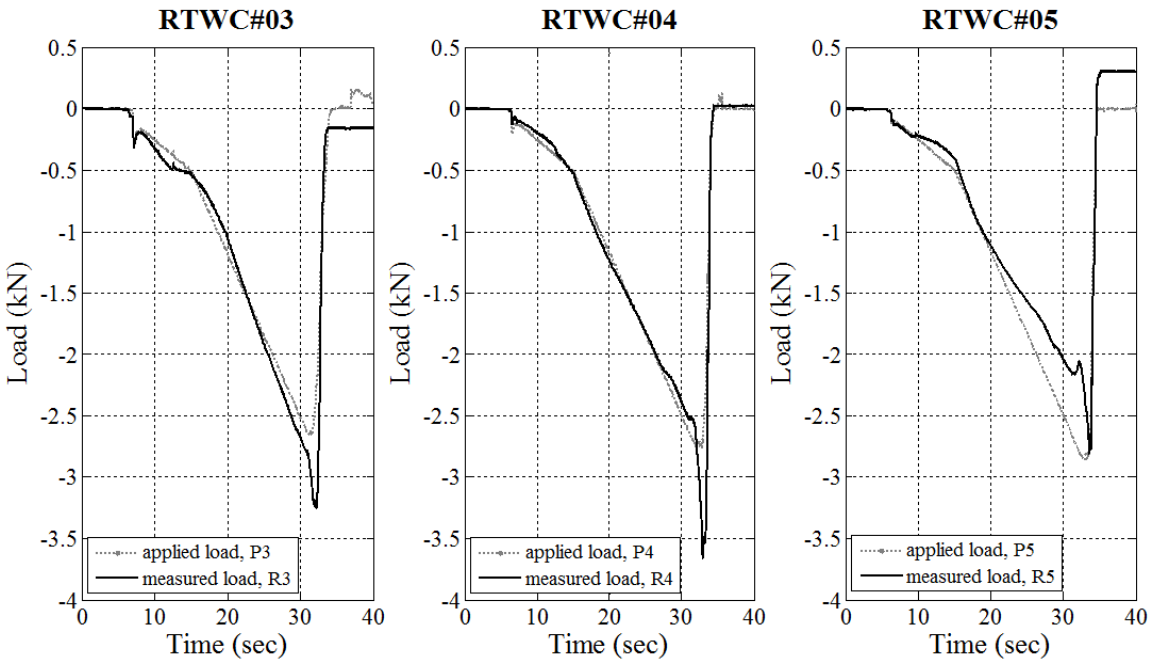

Figure 5.6 Applied and measured load time series for RTWC#03~RTWC#05 for the less stiff system.

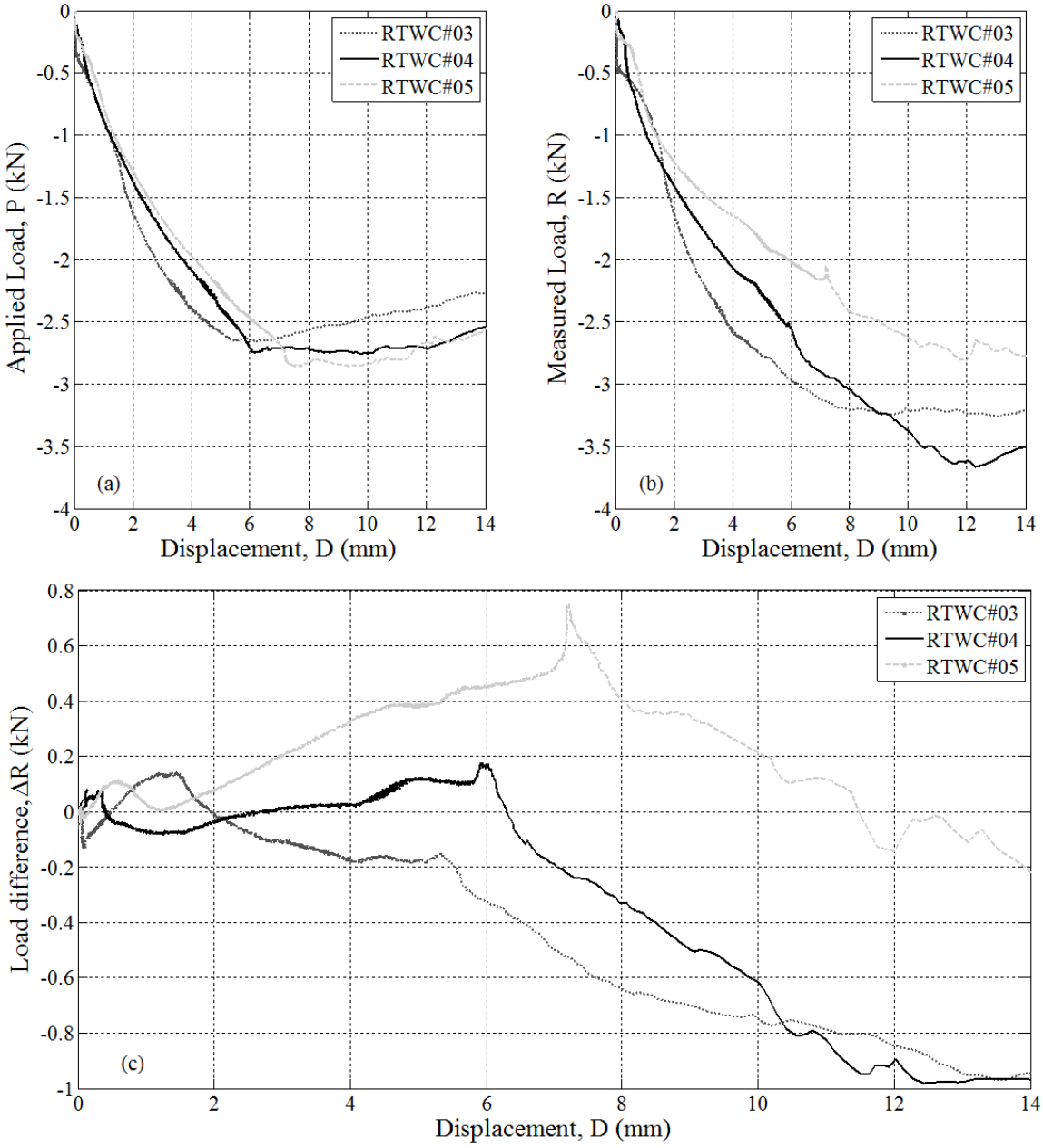

Figure 5.7 Applied load (P) vs. displacement (D) and measured load (R) vs. displacement (D) for RTWC#03~RTWC#05 for the same experiment as Figure 5.6.

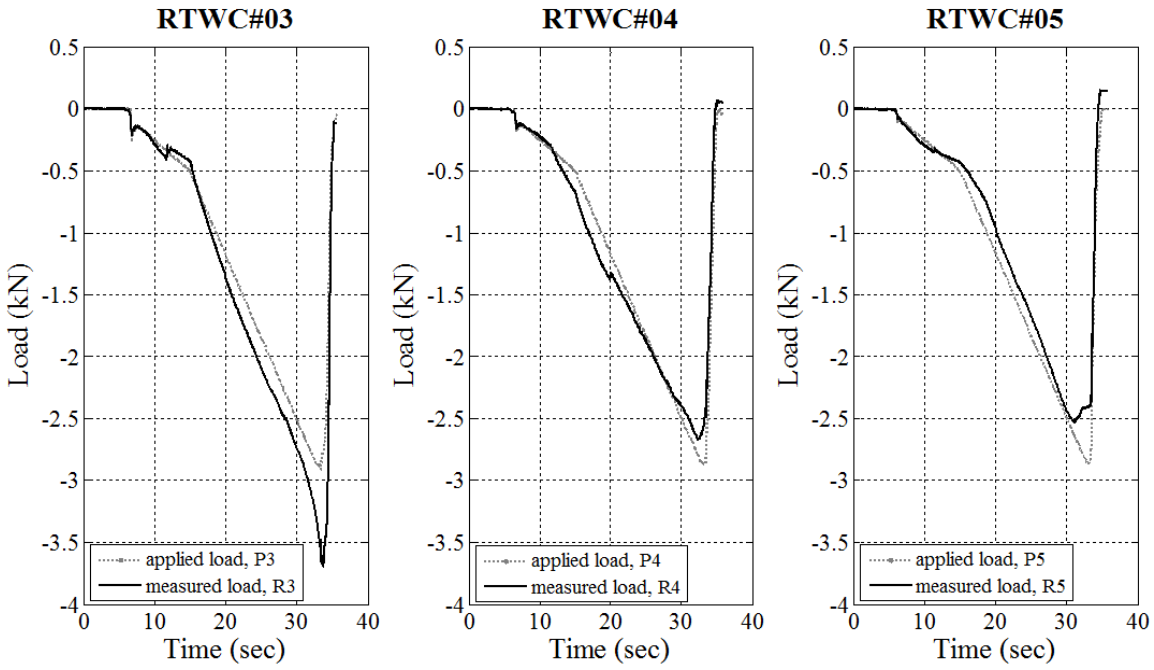

Figure 5.8 Applied (P) and measured (R) load time series for RTWC#03~RTWC#5 for stiffer system.

For the stiffer system, similar type of changing load-sharing behavior is observed as described above for the less stiff system. For example, Figure 5.8 & 5.9 shows the load-sharing behavior of three consecutive connections during one test for the stiffer system. These plots also show that load-sharing (i.e. load difference) changes with time, and prior to failure of any connection or system, the load differences are maximum.

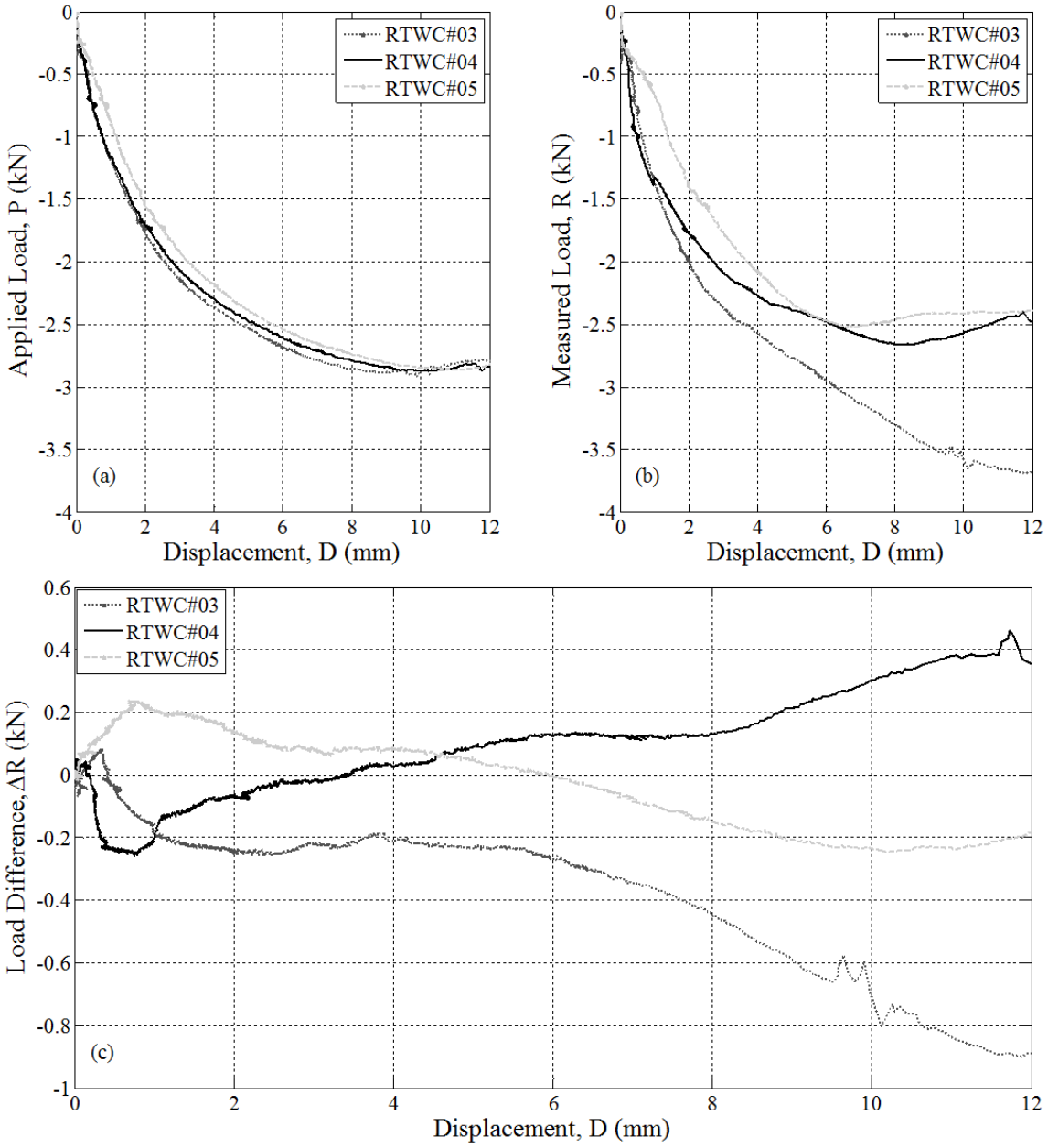

Figure 5.9 Applied load and measured load vs. displacement for RTWC#03~RTWC#05 for the same experiment of Figure 5.8.

Since load difference changes with the connection's increasing damage, it is very challenging to quantify load difference for comparison between the system tests. However, an attempt was made to find any significant difference in load-sharing between the two beam stiffnesses. The maximum absolute load differences (positive or negative)

up to mean yield displacement ($\boldsymbol{D_y}$=1.22mm) for all the connections were calculated. For the less stiff beam the mean maximum absolute load difference for 35 connections (i.e., 5 tests with 7 connections each) was found to be 0.13kN, whereas for the stiff beam it was found 0.16kN. A two-sample t-test (Spiegel, 1990) was performed to accept or reject the null hypothesis that these mean values are equal for both the systems. It was found that the null hypothesis could not be rejected at 5% significance level that the mean maximum absolute load difference is equal up to the yield displacement for both systems.

Again, the maximum absolute load difference from the yield displacement ($\boldsymbol{D_y}$=1.22mm) to the point where the weakest connection within a system started to fail was calculated. It is to be noted that, except for the end connections (i.e. RTWC#01 or RTWC#07), the rest of the connections have two adjacent connections. As a result, when any of the two end connections weaken, the failure initiates there first since it has only one adjacent connection to share its applied load with. The mean maximum absolute load differences were found 0.24kN and 0.31kN, for the less stiff and stiffer beams, respectively. As before, a two-sample t-test (Spiegel, 1990) was performed to accept or reject the null hypothesis that these mean values are equal for both the systems. In this case, the null hypothesis could be rejected at 5% significance level. This means that it can be said that the mean maximum absolute load difference for the stiffer beam is significantly higher than for the less stiff system from the yield displacement to the point where the weakest connection starts to fail. This intrinsically means that the load-sharing is higher for the stiffer system, as expected.

5.4 Load-sharing for fluctuating wind loads

Identical 'S3' fluctuating wind loads (shown in Figure 3.6 or, Figure 4.9) were applied to each connection. Figure 5.10 shows the applied load (P5), load difference (ΔR5) and displacement (D5) time series for one toe-nail connection (RTWC#05) out of the seven connections in the less stiff system. Similar to individual fluctuating load tests, the connection is withdrawn incrementally by the local peak loads. The applied load (P5) and measured load (R5) were found to differ (i.e., ΔR5 in Figure 5.10 (b)). During applied peak wind loads, even at the lower load levels, the load difference also shows peaks. The peak load difference shows both positive and negative values during a peak applied load. Due to the fractional time difference in applying peak loads between adjacent connections the load difference shows positive and negative peaks. Figure 5.11 (a) shows that the peak loads are applied to RTWC#06 and RTWC#04 slightly before RTWC#05 – thus, the PLA timing is not perfect. Hence they distribute their load to RTWC#05 and the load difference is negative (at 589.5s). On the other hand, when peak load is applied to RTWC#05, it distributes its load to its neighbours (i.e. RTWC#04 or RTWC#06). As a result, the load difference is positive (at 589.9s). Load difference also changes with the incremental damage which is explained below. While this asynchronous timing was not intended (and cannot be avoided), it is consistent with the nature of real loading which is also not generally synchronous across the roof. In any case, this is the explanation for the load differences at the lower load levels.

Now at the higher load levels (say after 900s) the load difference is negative. At around 1500s, due to high peak applied load the connection displace substantially and the

load difference also changes substantially with that. This changing load difference with incremental permanent withdrawal can be explained even better from Figure 5.12.

Figure 5.12 shows the load-displacement plot for the same connection shown in Figure 5.10. If there were no adjacent connections attached with it through the beams, there would not be any difference between applied and measured load vs. displacement plots. However, due to the difference in load-displacement behavior of individual connections, there will be difference in applied load and measured load. It is to be noted that, the load difference does not vary that much before the connection started to yield (around 2mm). After the yield displacement the load difference increases with the permanent incremental displacements at 2.5mm, 3mm, 4mm, 5mm, 7.5mm, 9mm etc. In between these permanent incremental displacements the load difference is almost constant which can be seen from Figure 5.11 (b).

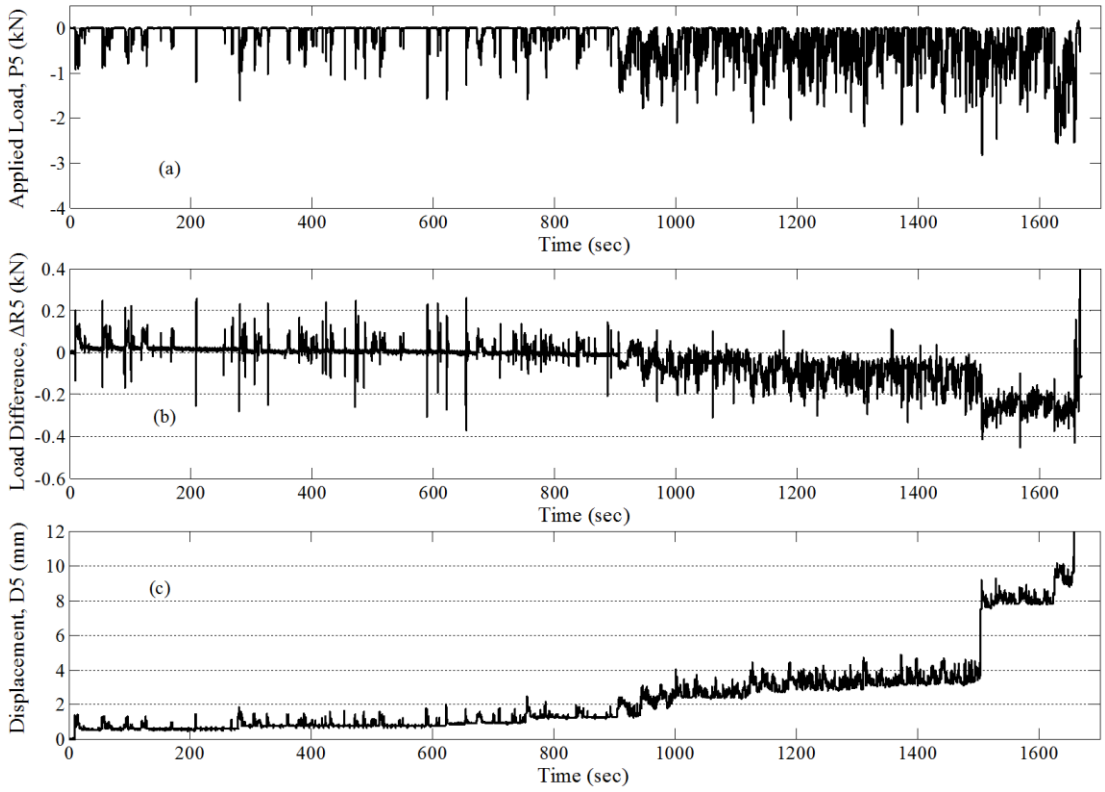

Figure 5.10 Applied load (a), load difference (b) and displacement (c) time series for one toe-nail connection (RTWC#05) in the less stiff system for identical fluctuating 'S3' wind loads

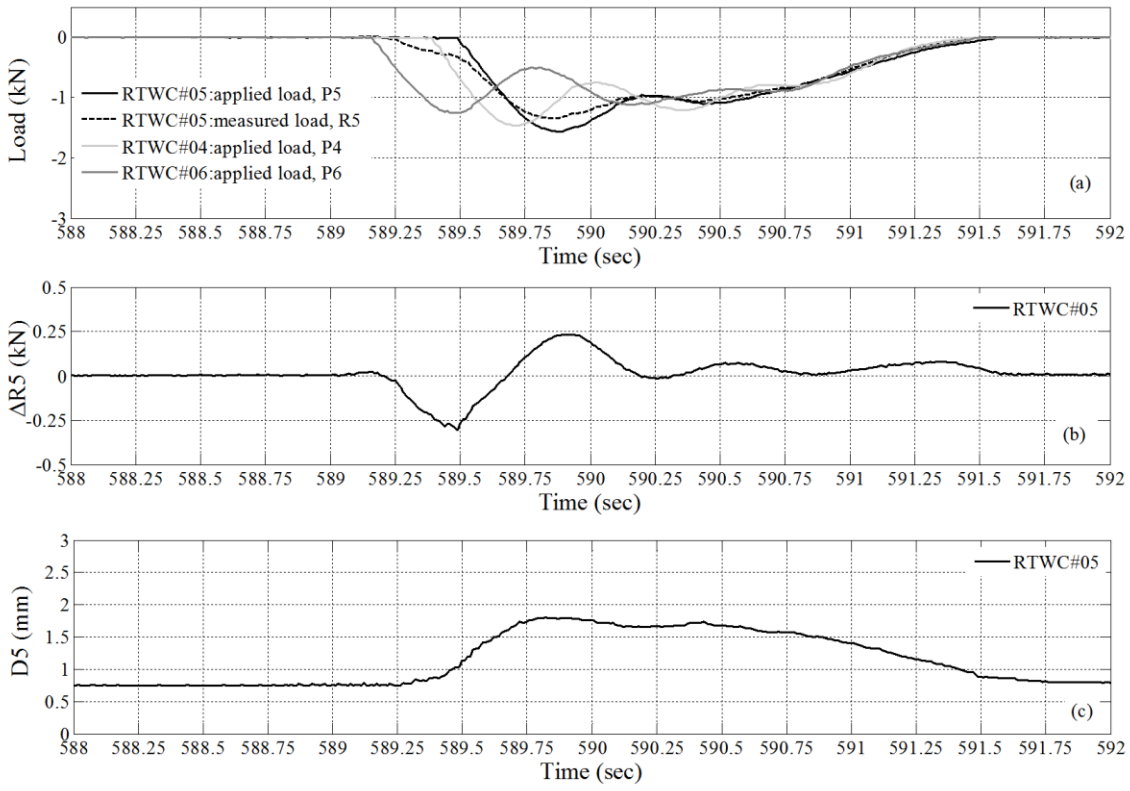

Figure 5.11 (a) Applied load (P4, P5 & P6) and measured load (R5); (b) load difference (ΔR5) and (c) displacement (D5) for t=588s to 592s for the same experiment shown in Figure 5.10.

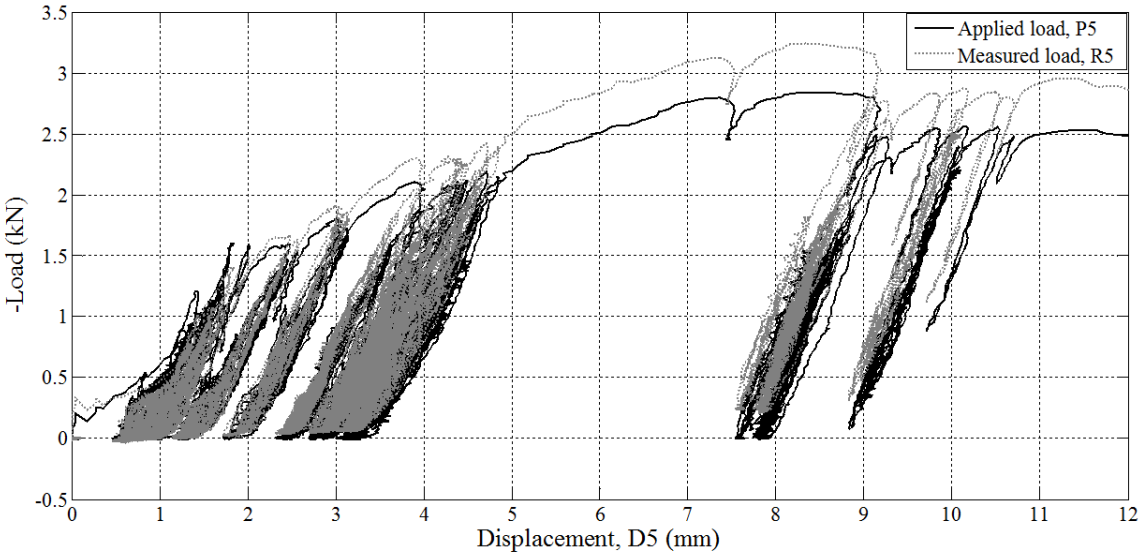

Figure 5.12 Load-displacement behavior for the same connection shown in Figure 5.10.

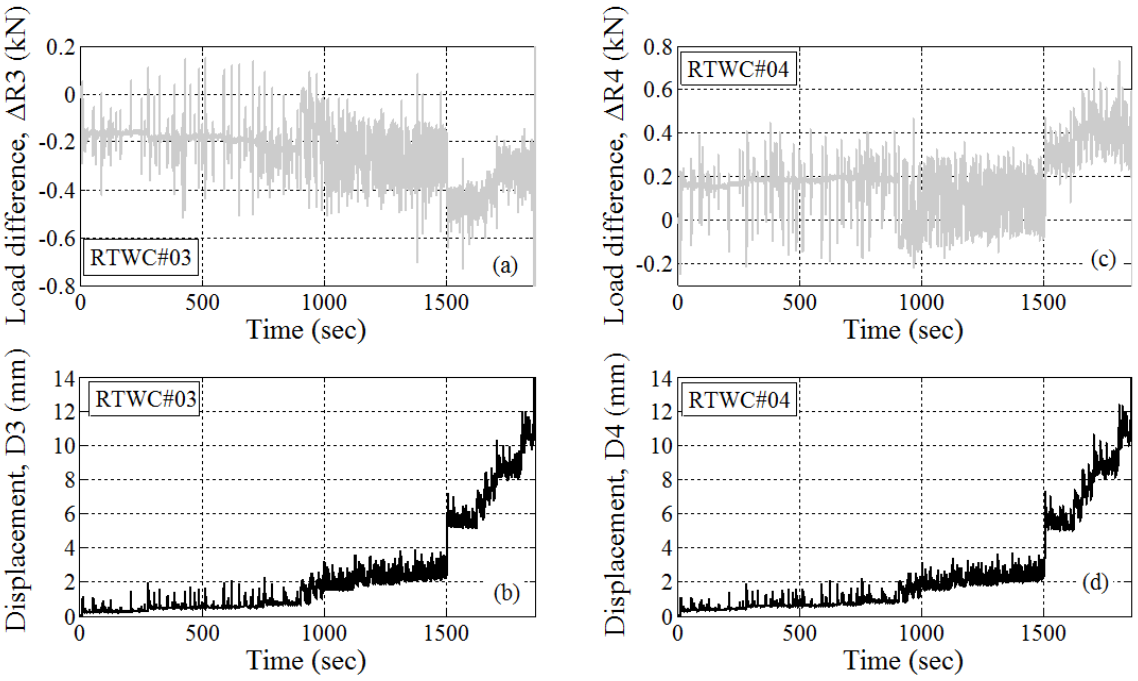

Figure 5.13 Load difference vs. time (a, c) and Displacement vs. time (b, d) for RTWC#03 and RTWC#04 respectively for one fluctuating wind loading system test with 6.35cm x 6.35cm x 0.476cm beams.

Figure 5.13 show the measured responses to the applied load for two of the consecutive connections out of seven during one fluctuating wind loading test for the stiffer system. Although the load difference is fairly constant for both the connections before the first damaging peak (nail withdrawal at 900s), it changes substantially with this first large damaging peak. (The reasons for the spikes (peaks) of load difference have been explained earlier pertaining to the asynchronous loading.) However, these load-sharing remains relatively constant until the next damaging peak around 1500 sec when the load-sharing changes again for both the connections. After 1500 sec, the damage (i.e., displacement) continues to accumulate and the load difference changes with it, similar to what was observed by Henderson et al. (2011) in their full-scale roof tests. Note that, in the entire loading history of these two connections, RTWC#03 gets extra load from its

neighbours, whereas RTWC#04 sheds its load to the neighbours. That means, RTWC#03 is relatively stronger than RTWC#04 in this case. This load distribution during peak loads helps to keep the displacements at each connection similar (D3, D4 in Figure 5.13), allowing the weakest connections to survive longer, while the stronger may fail earlier because of the additional load they must take-up. Thus, the structural system, as represented by the beam connecting the RTWCs in the current experiments, reduces the effects of the variability of the individual connections. This behavior is consistent with Wolfe & LaBissoniere (1991). The change in load difference with incremental displacement behavior is consistent with the full-scale test results (Henderson et al., 2011; Morrison et al., 2012).

Similar to the system ramp loading tests described earlier, the maximum absolute load differences up to mean yield displacement ($\boldsymbol{D_y}$=1.22mm) for all the connections were calculated. For the less stiff system, the mean maximum absolute load difference for the 35 tested connections were found 0.23kN with a coefficient of variation of 0.41, whereas for the stiffer system it was found 0.36kN with a coefficient of variation of 0.47. This 50% increase for the stiffer system is statistically significant.

Again, the maximum absolute load difference from the yield displacement ($\boldsymbol{D_y}$=1.22mm) to the point where the weakest connection within a system started to fail was determined. For the less stiff and stiffer systems the mean maximum absolute load difference were found to be 0.45kN with a coefficient of variation of 0.75 and 0.66kN with a coefficient of variation of 0.39, respectively. Thus, it can be said that the mean maximum absolute load difference for the stiffer system is significantly higher than the less stiff system from the yield displacement to the point where the weakest connection

starts to fail. This intrinsically means that the load-sharing is higher for the stiffer system; in this case it is more than 40% higher.

Figure 5.14 & 5.15 shows the load difference vs. displacement for seven RTWCs within a system (less stiff system and stiffer system respectively) for two experiments. From these figures it can be easily seen that the load-sharing is extended for the stiffer system (Figure 5.15) and actually higher in magnitude in the failure region (around 12mm-15mm) than the less stiff system (Figure 5.14). Load-sharing is extended for the stiffer connection due to higher duration of the system failure compared to less stiff system. The reason for higher duration for stiffer system is explained in Section 5.4.2.

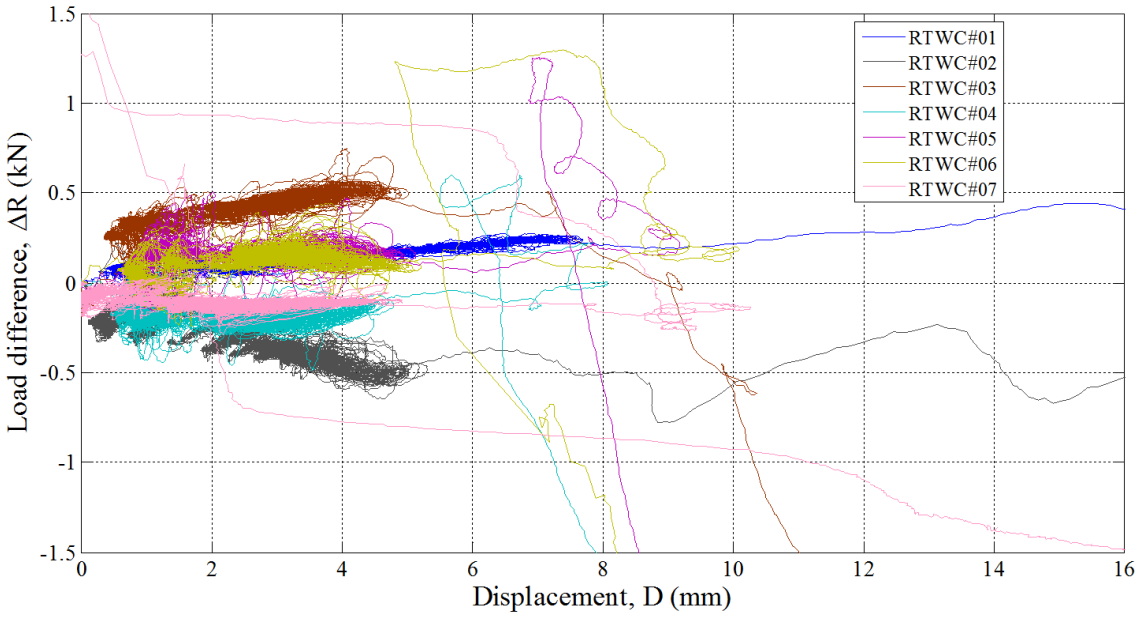

Figure 5.14 Load difference vs. displacement for seven RTWCs within the less stiff system during one experiment.

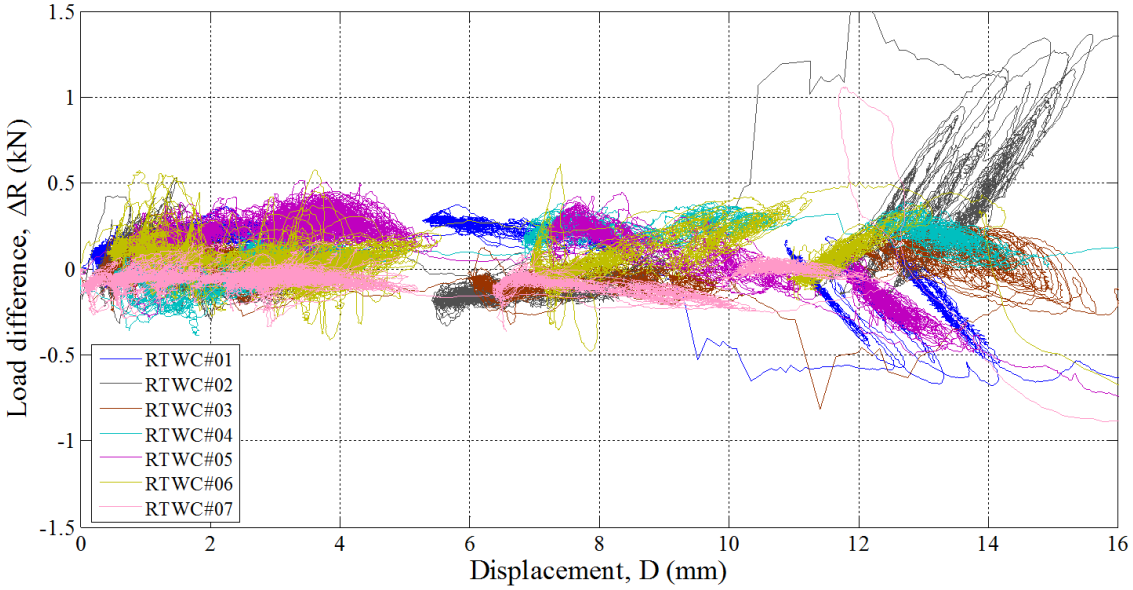

Figure 5.15 Load difference vs. displacement for seven RTWCs within the stiffer system during one experiment.

5.4.1 Variation of displacements for RTWCs within the system

In this section the variation of the displacements for the same applied fluctuating wind loads to the individual connections and the connections within a system will be discussed. Figure 5.16 shows the box-and-whisker diagram for the mean displacements at different time segments shown in Table 5.1. In total, 18 time segments (groups) were chosen and for each time segment the mean displacements were calculated. These time segments were selected to be in the region of relatively constant offset, between the damaging peak loads where the connection displaces substantially. Since different connections sustained different duration (especially for the individual test cases), the number of samples at different groups may differ as well (see Table 5.1). From the plot, it can be seen that for individual fluctuating tests, the variation is higher in the individual

tests, compared to the system tests. Table 5.1 shows that for each group the coefficient of variation for individual fluctuating tests is higher than any of the system tests.

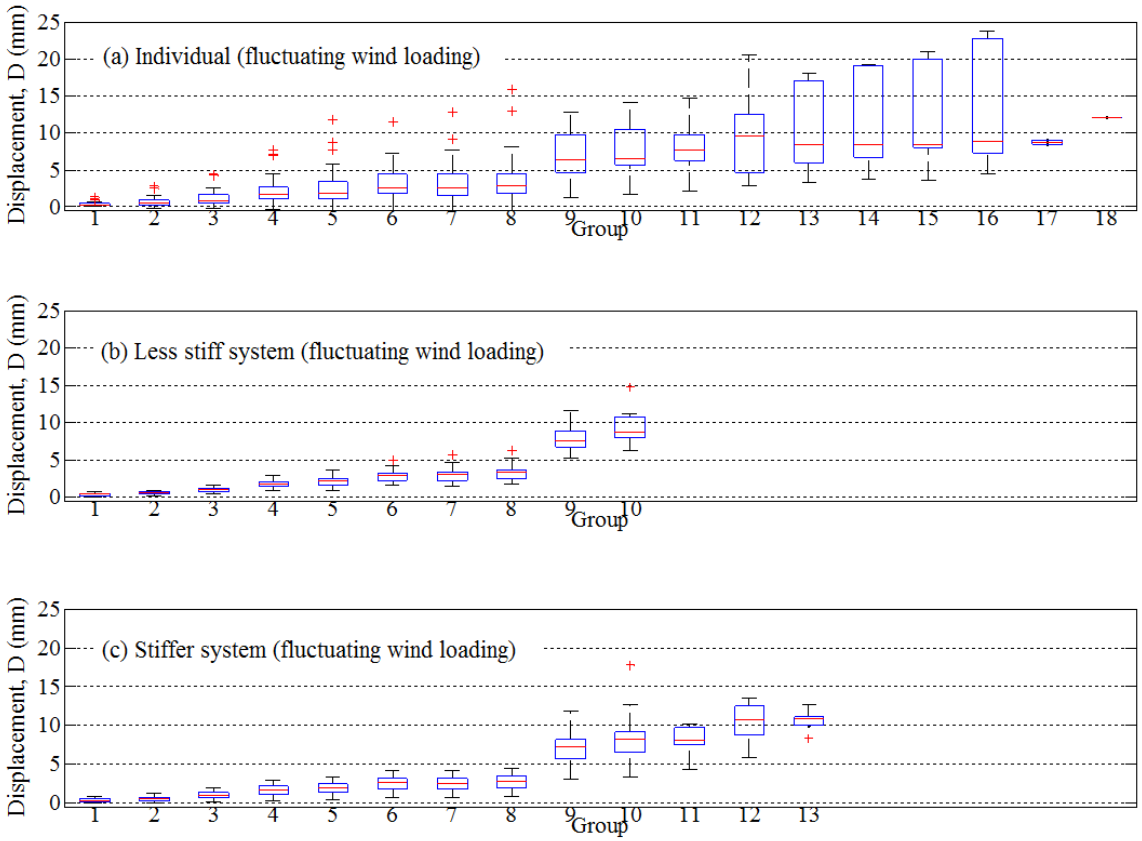

Figure 5.16 Box-and-whisker diagrams for mean displacements at different time segments (groups) mentioned in Table 5.1 for (a) individual fluctuating, (b) less stiff system fluctuating and (c) stiffer system fluctuating wind loads.

One-way analysis of variance (ANOVA) (Spiegel, 1990) test was performed to find the differences in mean displacements between these tests are significant or not. At 5% significance level the null hypothesis could not be rejected that the mean displacements are equal between the individual and system test in any group shown in Table 5.1.

Note that, the variation of failure displacements for individual fluctuating wind loading tests are substantially higher (COV=0.50) than the variation of any system tests (COV=0.28) for fluctuating wind loads (Table 4.4). For the same reason the distribution of failure displacements (Figure 4.17) for individual fluctuating wind loading tests was found broader than the distribution of any system tests. Thus, the beams which interconnect the RTWCs reduce the variation of displacement among them for the same identical applied fluctuating wind loading.

Table 5.1 Mean displacement (D) and coefficient of variation (COV) of mean displacements at different time segments (groups) for the individual and system fluctuating wind loading tests

Group	Time	Individual fluctuating			Less stiff system fluctuating			Stiffer system fluctuating		
		Number of samples	Mean, D (mm)	COV	Number of samples	Mean, D (mm)	COV	Number of samples	Mean, D (mm)	COV
1	20s-274s	35	0.30	0.97	35	0.35	0.56	35	0.32	0.72
2	294s-745s	35	0.61	1.04	35	0.55	0.39	35	0.54	0.65
3	765s-936s	35	1.13	1.02	35	1.01	0.29	35	0.99	0.48
4	956s-991s	35	2.07	0.93	35	1.82	0.23	35	1.72	0.41
5	1011s-1117s	35	2.54	1.03	35	2.10	0.26	35	1.97	0.39
6	1137s-1300s	34	3.18	0.9	35	2.82	0.26	35	2.52	0.35
7	1320s-1362s	33	3.14	0.92	35	2.94	0.3	35	2.50	0.35
8	1382s-1494s	33	3.64	0.97	35	3.26	0.29	35	2.75	0.34
9	1514s-1616s	22	6.97	0.48	7	7.91	0.24	35	7.10	0.28
10	1636s-1649s	18	7.29	0.47	7	9.50	0.27	28	8.33	0.33
11	1714s-1799s	14	8.25	0.46	x	x	x	14	8.07	0.2
12	1819s-1850s	10	9.69	0.53	x	x	x	14	10.39	0.23
13	1870s-1952s	7	10.93	0.52	x	x	x	7	10.58	0.11
14	1972s-2004s	6	10.90	0.56	x	x	x	x	x	x
15	2024s-2062s	6	11.54	0.57	x	x	x	x	x	x
16	2082s-2114s	5	13.75	0.6	x	x	x	x	x	x
17	2134s-2215s	2	8.72	0.03	x	x	x	x	x	x
18	2235s-2243s	1	12.13	0	x	x	x	x	x	x

5.4.2 Effect of bending stiffness on the time duration to failure

As explained earlier, load-sharing is extended (Figure 5.15) for the stiffer system due to higher duration of the system failure compared to the less stiff system (Figure 5.14). In this section a detailed discussion on the failure duration for the less stiff system and the stiffer system will be presented. For the less stiff system, the failure duration (while the first connection fails) for five tests were 1504s, 1504s, 1504s, 1529s and 1658s. For the stiffer system the failure duration of the system for the five tests were 1630s, 1658s, 1684s, 1807s and 1860s. For the less stiff system, in 80% of the cases the system fails during the 25 m/s segment of the loading history (time = 901s to 1620s). For the stiffer system, no connection failed during the 25m/s segment; rather, all of them failed during wind loading history of 30m/s (time = 1621s to 2220s). Longer duration and increased wind speeds for the stiffer system means that, on average, the number of damaging peaks required to fail a connection is higher for a stiffer system. With the current time history, on average11.2 damaging peaks were required to fail a connection in the stiffer system, whereas, on average, 9.2 damaging peaks are required to fail a connection in the less stiff system.

Figures 5.17 and 5.18 shows the displacement vs. time for seven RTWCs in the systems for the same experiments shown in Figure 5.14 & 5.15 respectively. Since the less stiff system has less flexural rigidity (EI=23.1kN-m^2) and the end connection (RTWC#01 in Figure 5.17) has only one adjacent connection it cannot transfer its load to the connection that are far from it. As a result, when the end connection is sufficiently damaged, it will fail. But other connections that are still in the system will try to resist the failure of the whole system. From Figure 5.17 (b) it can be seen that the first connection

(RTWC#01) failed at around 1504s and the last connection (RTWC#07) failed at 1514s. So, it took 10s (Δt) to fail the first to last connection. Considering 5 repetitive system tests it also took 10s on average to fail the first to last connection. On the other hand, the stiffer system has higher flexural rigidity (EI=91kN-m^2) and hence even though the end connection has one adjacent connection it will distribute its load to multiple connections that are far away. For this reason, the whole system needs more incremental steps (displacement) to weaken all the connections (Figure 5.18 (a)) and thus fail the whole system. Since, all the connections are displaced (damaged) enough it took only 4sec (considering 5 repetitive system tests) on average to fail the first to last connection. For this reason the mean failure duration of the less stiff system (1539.8s) is lower compared to the stiffer system (1727.8s). Thus, for a stiffer system load-sharing is higher and extended to multiple connections for higher flexural rigidity of the beams in compared to a less stiff system as shown in Figure 5.14 & 5.15.

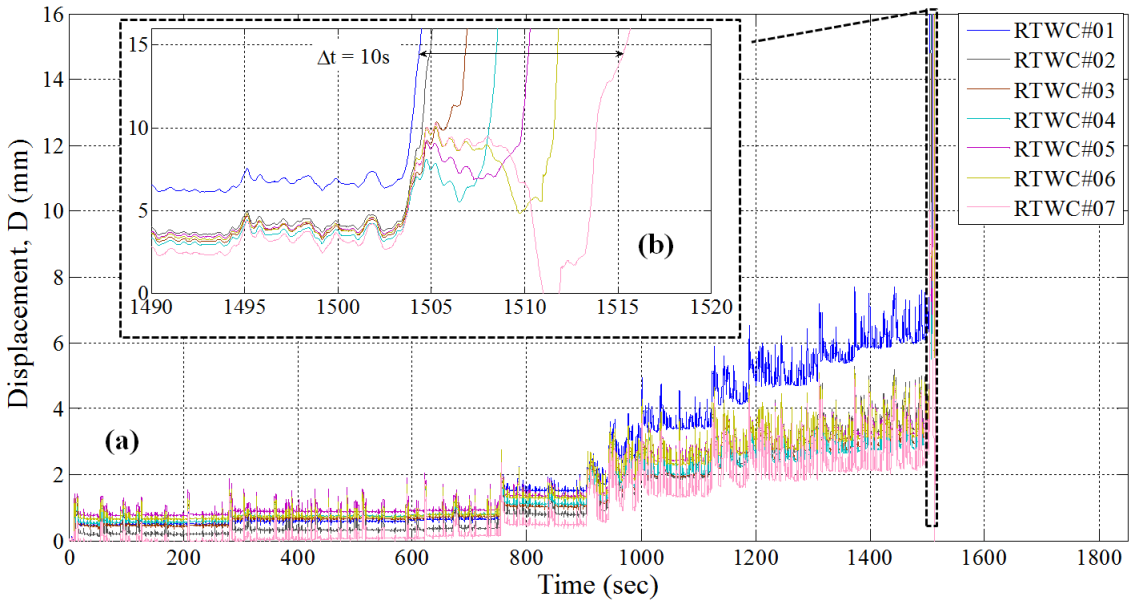

Figure 5.17 (a) Displacement vs. time for all the connections in the less stiff system during one fluctuating wind loads test. (b) Inset showing the same plot from 1490s to1520s.

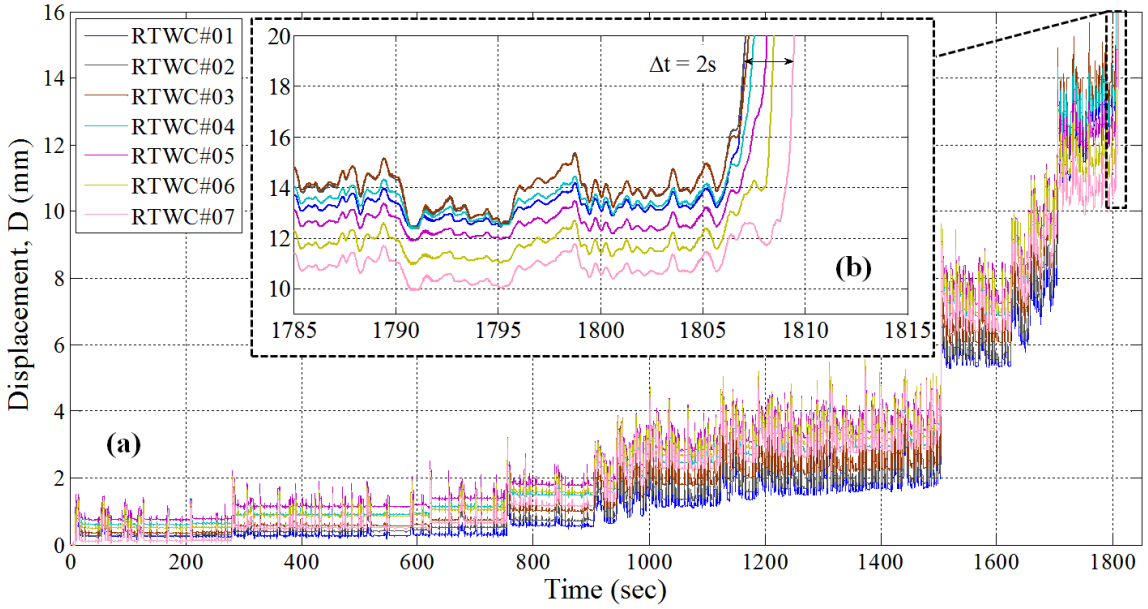

Figure 5.18 (a) Displacement vs. time for all the connections in the stiffer system during one fluctuating wind loads test. (b) Inset showing the same plot from 1785s to1815s.

Chapter 6: CONCLUSIONS & RECOMMENDATIONS

An experimental set-up was developed which investigates the load-sharing behavior between toe-nailed, roof-to-wall connections in idealized wood-framed roofs during high winds. Two types of loading, viz., ramp and fluctuating wind loading, were applied to a series of 7 roof-to-wall connections (RTWCs) that were connected with two steel beams which simulated the roof bending stiffness. Two types of beams which ideally represent two types of roof stiffness (i.e. less stiff roof system and stiffer roof system) were used for these loading types. Individual RTWCs were also subjected to ramp and fluctuating wind loads to define the load-displacement behavior of toe-nail connections and to make comparisons with the results found from the RTWCs of the systems.

6.1 Conclusions

The conclusions of the major findings from this project are summarized below:

1. The load-displacement behavior of a toe-nail connection for ramp loads is highly variable. Fits to the experimental data are provided for both bi-linear and curvilinear load-displacements models. No notable correlation between the initial slope and the failure capacity was found. In addition, the COV (0.45) of the slope of the first linear region in the bi-linear model is higher than the COV (0.31) of the slope of the second linear region.

2. Individual fluctuating wind loading tests shows that the toe-nail connections fail by incremental withdrawal from the top plate. Permanent withdrawal occurs due to the localized, large peaks in the wind loads.
3. The differences in mean failure capacities of the toe-nail connections between individual and system tests were found to be statistically negligible, as theory requires.
4. The failure displacement of the toe-nail connection for every test type has been found to vary more (higher COV) than failure capacities of that test type. The distribution of toe-nail's failure displacement for individual fluctuating wind loading test has been found broader than the distribution of failure displacements of fluctuating wind loading test within a system.
5. From the tests conducted, it has been found that, in a group of toe-nail connections subjected to similar ramp loading, the weaker connection sheds its load to the adjacent stronger connections, and vice versa. For example, a stronger connection (e.g., 4-nails) may get 33% higher than its applied load while a weaker connection (e.g., 2-nails) may shed up to 50% of its applied load. Extra nails (i.e., 4-nails in the connection) or missing nails (i.e., 2-nails) during construction of RTWCs are a common error. So, when there is variation in toe-nail construction, the load-sharing between adjacent connections can be very high.
6. From the ramp loading tests it has been found that, load-sharing or load-differences vary with time, depending on the load-displacement behavior of individual connections. However, the load differences prior to the yield

displacement have been found to be small, while just prior to the failure of the system, the load-difference has been found maximum.

7. Load-sharing (i.e., load differences) is higher for the stiffer system compared to the less stiff system. This result is consistent with Wolfe and LaBissoniere (1991). With the current systems, it appears that increasing the beam bending stiffness four times increases the load transfers by more than 40%. The load-sharing is greatest during the short duration, damaging peak loads. Load-sharing changes and increases continuously with the permanent displacements during damaging peak loads.
8. Individual connections displacement variability for the same applied load is reduced by the system (i.e. beams) due to load-sharing between the connections through the beams.
9. In addition to the changes in load-sharing caused by the bending stiffness of the beam connecting the RTWCs, there are also substantial duration effects. Systems with higher bending stiffness sustain the load for longer periods than less stiff systems; in other words, a great number of damaging peaks are required to fail the stiffer system.

6.2 Recommendations for future research

1. Since the wind field on the roof of a low-rise building varies both spatially and temporally, the roof-to-wall connections will be subjected to dissimilar loading at different time. So, it is suggested that tests with

different wind loading history applied on different connections can be conducted to investigate the load-sharing phenomenon.

2. Gable end roof-to-wall connections are usually much stronger than the internal connections due to additional hold-downs at the gable end wall and due to the additional dead weight of the brick veneer wall. Therefore, to ideally mimic this end roof-to-wall configuration, the end connections in the present experimental set-up can be made much stronger using more number of nails.
3. Since, missing nails or extra nails during construction of houses are common; test can be performed with this current setup to isolate the load-sharing behavior for different number of nails in different connections.
4. The effect of truss spacing and the number of effective trusses that are involved in load transfer is not examined here. So it is recommended to examine both of them for different beam bending stiffness.
5. The statistical parameters of the roof-to-wall connections reported in this study can be used to develop fragility based analysis of the interconnected roof-to-wall connections using analytical models.
6. The findings of this study with regards to the load-sharing behavior of the roof-to-wall connections can be used to improve the load-sharing predictions using numerical techniques such as finite element analysis.

REFERENCES

Anderson, T. W. and Darling, D. A. (1954). "A Test of Goodness of Fit." *Journal of the American Statistical Association*, Vol. 49, No. 268. (Dec., 1954), pp. 765-769.

ASTM-D1761-06 (2008). "Annual book of ASTM standards-standard test methods for mechanical fasteners in wood." ASTM International.

Benjamin, J. R. and Cornell, C. A. (1970). "Probability, Statistics and decision for Civil Engineers." McGraw-Hill, New York, USA.

Board on Natural Disasters (1999). "Mitigation emerges as major strategy for reducing losses caused by natural disasters." *Science* 284, 1943-1947.

Cheng, J. (2004). "Testing and analysis of the toe-nailed connection in the residential roof-to-wall system." *Forrest Products Journal*, 54, 58-65.

Chui, Y. H., Ni, C., and Jiang, L. (1998). "Finite element model for nailed wood joints under reversed cyclic load." *Journal of Structural Engineering*, ASCE, 124(1), pp 96-103.

Emanuel, K., (2005). "Increasing destructiveness of tropical cyclones over the past 30 years." *Nature*, 436, 686-686. (DOI:10.1038/nature03906).

Foschi, R. O. (2000). "Modeling the hysteretic response of mechanical connections for wood structures." Proc., *World Conf. on Timber Engg*., Dept. of Wood Sci., ed., University of British Columbia, Vancouver.

GIIS (Georgia Insurance Information Service). (2004). "The Insurance Industry: Globally, Across the U.S.A. and In Georgia." [http://www.giis.org/giis/giis_pc_facts.shtml]

Ginger. J. D and Holmes J. D. (2003). "Effect of building length on wind loads on low-rise buildings with a steep roof pitch." *Journal of Wind Engineering and Industrial Aerodynamics* 91 (2003) 1377–1400.

Groom, K. M. and Leichti, R. J. (1993). "Load withdrawal displacement characteristics of nails." *Forest Products Journal*, 43(1), pp. 51-54.

Guikema, S. D. (2009). "Infrastructure Design Issues in Disaster-Prone Regions." *Science*, 323, 1302-1303. (DOI:10.11206/science.1169057).

He, W. (2010). "Numerical Assessment of Roof Panel Uplift Capacity under Wind Load." PhD Thesis, Department of Engineering, The University of Western Ontario London, Ontario, Canada.

Henderson, D. J., Morrison, M. J. and Kopp, G. A. (2011). "Spatially and temporally varying wind loads applied to a full scale, timber-framed, hip roof." *Proceedings of the 13th International Conference on Wind Engineering, Amsterdam*.

Ho, T. C. E., Surry, D., Morrish, D. and Kopp, G. A., (2005). "The UWO contribution to the NIST aerodynamic database for wind loads on low buildings: Part1. Archiving format and basic aerodynamic data." *Journal of Wind Engineering and Industrial Aerodynamics*, 93, 1-30

Housing and Urban Development (HUD) (1993). "Wind-borne debris impact resistance of residential glazing." NAHB Research Center, Inc. Upper Marlboro, Maryland.

Knabb, R. D., Rhome, J. R., and Brown, D. P. (2005). "Tropical Cyclone Report Hurricane Katrina 23-30 August 2005." *National Hurricane Center.*

Kopp, G. A., Morrison, M. J. and Henderson, D. J. (2012). "Full-scale testing of low-rise, residential buildings with realistic wind loads." *Journal of Wind Engineering and Industrial Aerodynamics*, vol. 104-106, pp. 25-39.

Kopp, G. A., Morrison, M. J., Gavanski, E., Henderson, D. J. and Hong, H. P. (2010). "Three Little Pigs" Project: Hurricane Risk Mitigation by Integrated Wind Tunnel and Full-Scale Laboratory Tests." *Natural Hazards Review*, 11, 151-161.

Kopp, G. A., Morrison, M. J., Kordi, B. and Miller, C., (2011). "A Method to Assess Peak Storm Wind Speeds Using Detailed Damage Surveys." *Engineering Structures*, Submitted April 2010 Volume 33, Issue 1, January 2011, Pages 90–98

Kopp, G. A., Oh, J. H. and Inculet, D. R. (2008). "Wind-induced internal pressures in houses." *Journal of Structural Engineering*, 134, 1129-1138.

Lee, K. H. and Rosowsky, D. V. (2005). "Fragility assessment for roof sheathing failure in high wind regions." *Engineering Structures* 27 (2005) 857–868.

Mani, S. (1997). "Influence functions for evaluating design loads on roof-truss to wall connections in low-rise buildings." M.S. Thesis, Clemson University, Clemson, South Carolina, United States.

Massey, F. J. (1951). "The Kolmogorov-Smirnov Test for Goodness of Fit." *Journal of the American Statistical Association*. Vol. 46, No. 253, 1951, pp. 68–78

Mensah, A. F., Datin, P. L., Prevatt, D. O., Gupta, R. and Lindt, J. W. (2011). "Database-assisted design methodology to predict wind-induced structural behavior of a light-framed wood building." *Engineering Structures*, vol. 33, 674-684.

Minor, J. E. (1994). "Windborne debris and the building envelope." *Journal of Wind Engineering and Industrial Aerodynamics* 53, 207-227.

Morrison, M. J. (2010). "Response of a Two-Story Residential House Under Realistic Fluctuating Wind Loads." PhD Thesis, Department of Engineering, The University of Western Ontario, London, Ontario, Canada.

Morrison, M. J. and Kopp, G. A. (2011). "Performance of toe-nail connections under realistic wind loading." *Engineering Structures*, vol. 33, pp. 69-76.

Morrison, M. J., Henderson, D. J. and Kopp, G. A. (2012). "The response of a wood-frame, gable roof to fluctuating wind loads." *Engineering Structures*, vol. 41, pp. 498-509.

Mtenga P. V., Cramer S. M., Peyrot A. H. and Wolfe R. W. (1995). "System factors for light-frame wood truss assemblies." *Journal of Structural Engineering*; 121(2):290-300.

National Design Specification for Wood Construction (NDS), 2005.

Ontario Building Code (2006). 2006 Building code compendium/Ministry of Municipal Affairs and Housing, Building and Development; Toronto, Ontario, Canada.

Pielke, R. A. Jr., Gratz, J., Landsea, C. W., Collins, D., Saunders, M. A., Musulin, R. (2008). "Normalized Hurricane Damage in the United States: 1900-2005." *Natural Hazards Review*, 9, 29-42. (DOI:10.1061/(ASCE)1527-6988(2008)9:1(29)).

Reardon, G., Henderson, D., Ginger, J., (1999). "A structural assessment of the effects of Cyclone Vance on houses in Exmouth WA", CTS, James Cook University Australlia, Technical Report No. 48.

Reed, T. D., Rosowsky, D. V. and Schiff, S. D. (1997). "Uplift capacity of light-frame rafter to top plate connections." *Journal of Architectural Engineering*, 3, 156-163.

Riley, M. A. and Sadek, F. (2003). "Experimental Testing of Roof to Wall Connections in Wood Frame Houses." National Institute of Standards and Technology, Technical Report NISTIR 6938.

Rosowsky, D. V. and Reinhold, T. A. (1999). "Rate-of-load and duration-of-load effects for wood fasteners." *Journal of Structural Engineering*, ASCE-125, 719-724.

Scholz, F. W. and Stephens, M. A. (1987). "K-Sample Anderson-Darling Tests." *Journal of the American Statistical Association*, 82:918-924.

Shanmugam, B., Nielson, B. G., Prevatt, D. O. (2009). "Statistical and analytical models for roof components in existing light-framed wood structures." *Engineering Structures*, vol. 31, Issue 11, Pages 2607-2616.

Simiu, E. and Scanlan, R. H. (1996). "Wind Effects on Structures, Fundamentals and Application to Design." New York: John Wiley.

Sparks, P. R., Schiff, S.D., Reinhold, T. A. (1994). "Wind damage to envelopes of houses and consequent insurance losses." *Journal of Wind Engineering and Industrial Aerodynamics* 53, 145-155.

Spiegel, M. R. (1990). "Theory and Problems of Statistics." Schaum's Outline Series, McGraw-Hill Inc. New York, USA.

Surry, D., Ho, T. C. E., and Lythe, G. R. (1999). "Simulation requirements for roof wind loads near the corners of low buildings with low-slope roofs.", *ASCE Structures Congress*, ASCE, New Orleans.

Trenberth, K. (2005). "Uncertainty in Hurricanes and Global Warming." *Science*, 308, 1753-1754. (DOI:10.1126/science.1112551).

Trujillo-Ortiz, A., R. Hernandez-Walls, K. Barba-Rojo, L. Cupul-Magana and R.C. Zavala-Garcia. (2007). "AnDarksamtest: Anderson-Darling k-sample procedure to test the hypothesis that the populations of the drawn groups are identical." A MATLAB file. [WWW document]. http://www.mathworks.com/matlabcentral/fileexchange/loadFile.do?objectId=17451.

Wheeler, A. J & Ganji, A. R. (1996). "Introduction to Engineering Experimentation." New Jersey, Prentice Hall

Wolfe, R. W. and LaBissoniere, T. (1991). "Structural Performance of Light-Frame Roof Assemblies II. Conventional Truss Assemblies." *Forrest Products Laboratory*, Research Paper: FPL-RP-499.

Zisis, I. and Stathopoulos, T. (2009). "Wind-induced cladding and structural loads on a low wooden building." *Journal of Structural Engineering*-ASCE 135 (4), 437-447.

Appendix A

A.1 Construction of Specimens

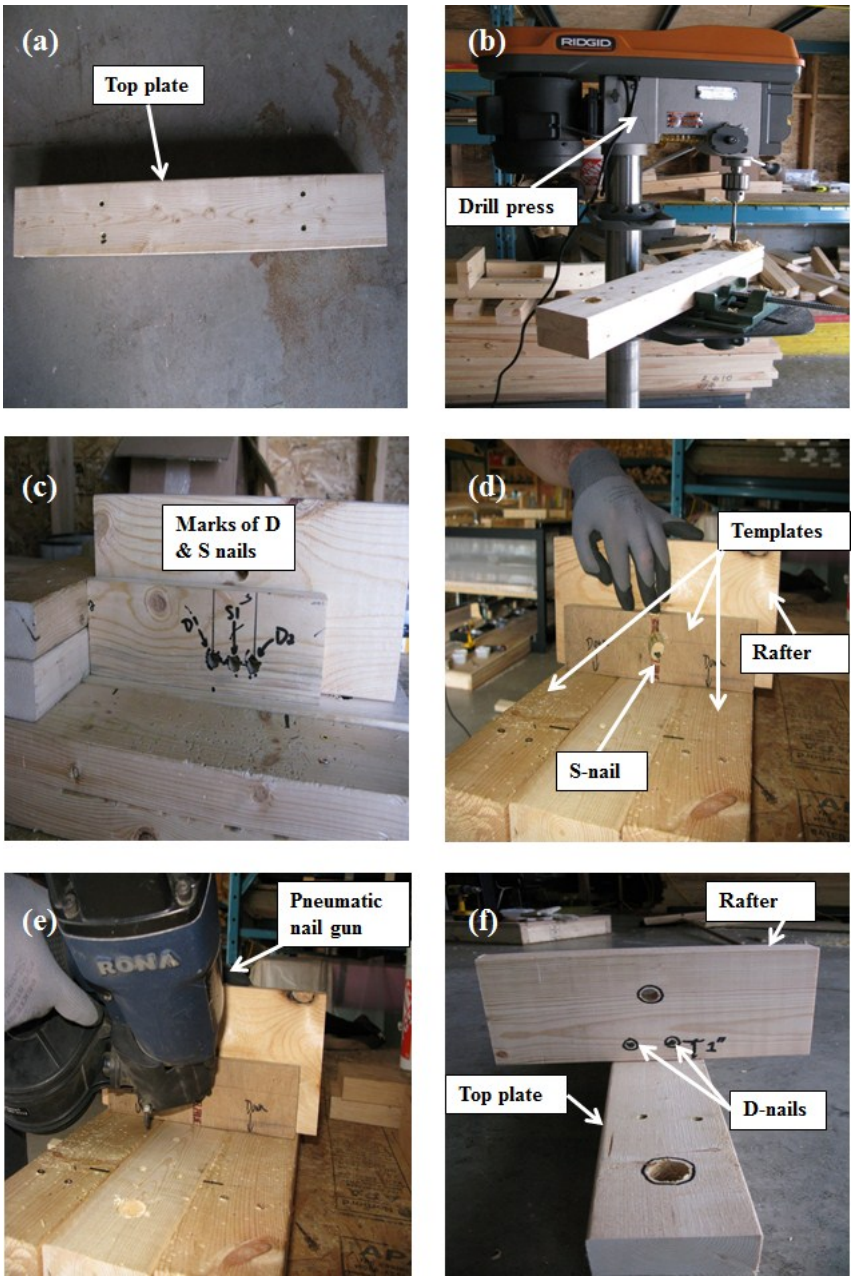

Figure A.1 Construction of a roof-to-wall toe nail connection.

Procedure:

1) 2 2x4 lumbers are attached together by 4 nails (Figure A.1 (a)). This is known as top plate.
2) Two holes are made by drill press (Figure A.1 (b)) in order to bolt the top plate to the bending beam load cells firmly (not shown in the figure) so that it does not move.
3) There is another hole in the rafter (Figure A.1 (c)) which is used to fasten the rafter to the tension load cell (not shown in the figure).
4) 3-12d nails are used. On one side of the rafter there are 2 nails which are referred to as d-nails (d1 & d2) (Figure A.1 (d)) and on the other side of the rafter there is one nail which is referred to as s-nail. Templates or form works were used to minimize the human error (Figure A.1 (e)).
5) All the nails are driven by a pneumatic gun nail (Figure A.1 (f)) with an inclination of 45 degree with the top plate.
6) The distance of the nail heads from the surface of the top plate should be one inch (25.4mm) (Figure A.1 (g)).

Appendix B

B.1 Load cells calibration

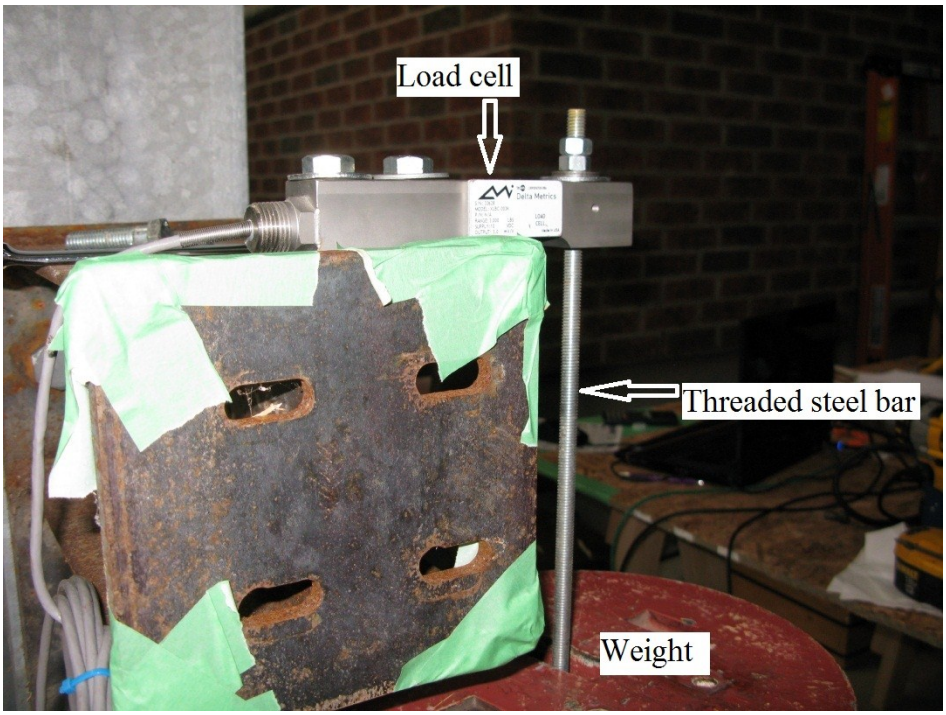

Figure B.1 Load cell calibration technique

The bending beam load cell (BBLC) is attached to a rigid elevated steel angle by bolts. A 0.91meter (3feet) long threaded bar (Figure B.1) was used to hold the weight as well as it transfers the load to the load cell. The BBLC is then wired to the National Instruments Data Acquisition System (NI-DAQ) which read the data in terms of voltage. A LABVIEW program was used to operate the tests. By putting different weight, different voltage excitation could be found. A voltage excitation vs. applied load will help to develop the linear equation and by doing mathematical calculations the slope and y intercept for applied load (kN) vs. voltage excitation (VDC) could be determined. So, if

we apply any load the load cell will measure the voltage excitation and NI-DAQ will show us the real applied load in kN during an experiment. A maximum of 230Kg weight was used for calibrating the load cells. Similar procedure was used to calibrate the tension load cell (TLC).

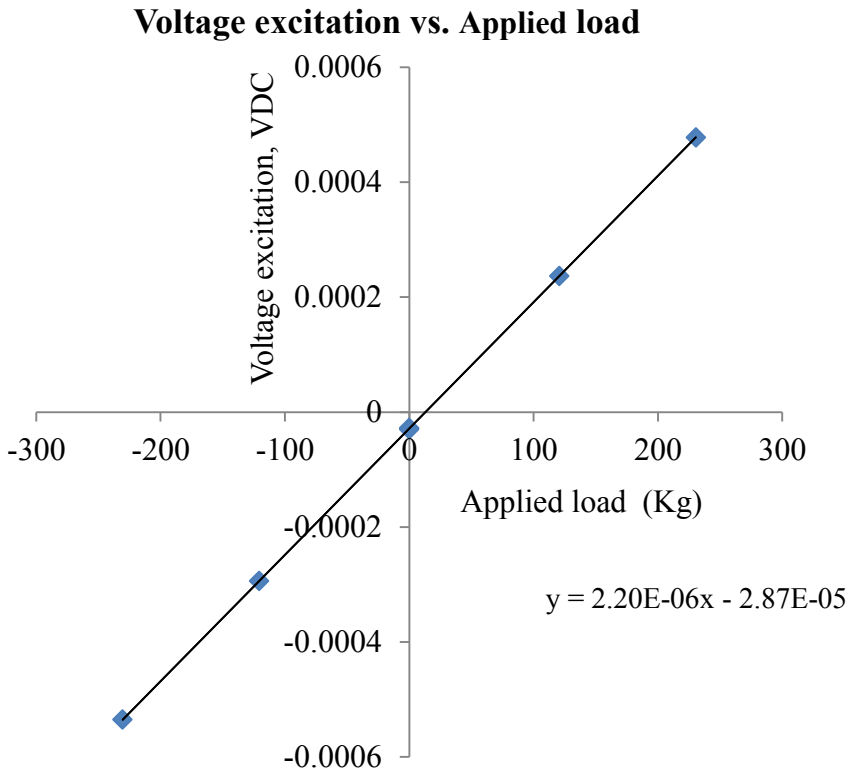

Figure B.2 A plot of voltage excitation measurements versus corresponding applied load with a least-squares line overlaid.

B.2 Pressure transducer calibration

A 2ft x 2ft calibration box and a manometer (Figure B.3) are used to calibrate the pressure transducers. The pressure transducers are put into the calibration box. There is a tube which is filled with water is put on the same calibration box. Using Putty (a program

which is used to command the PLA to operate at a certain pressure), the PLA is turned on and each time the valve is moved to a certain value, the pressure on putty is recorded (in KPa) and the height of water (manometer reading) is also recorded. By using a LABVIEW program the voltage excitation for each pressure transducer is recorded for individual applied pressure. So, for a large number of pressure range, individual voltage excitation for different pressure transducer will be recorded. Voltage excitation vs. pressure for each pressure transducers (Figure B.4) will give the slope and intercept of the linear equation which we use for the experiments.

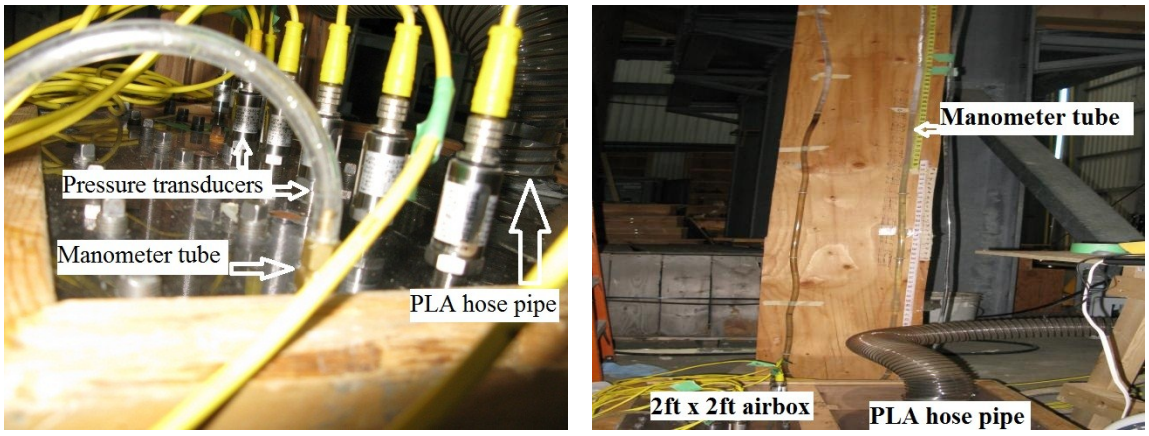

Figure B.3 Experimental set up for pressure transducer calibration.

However, the data from pressure transducer during experiments were not used. Since, we are looking at the load-sharing between the connections and the load cells are representing the data accurately, no uncertainty analysis for pressure transducers was carried out. The calibration of the pressure transducer is important because it will generate the demand force to the tension load cell accurately.

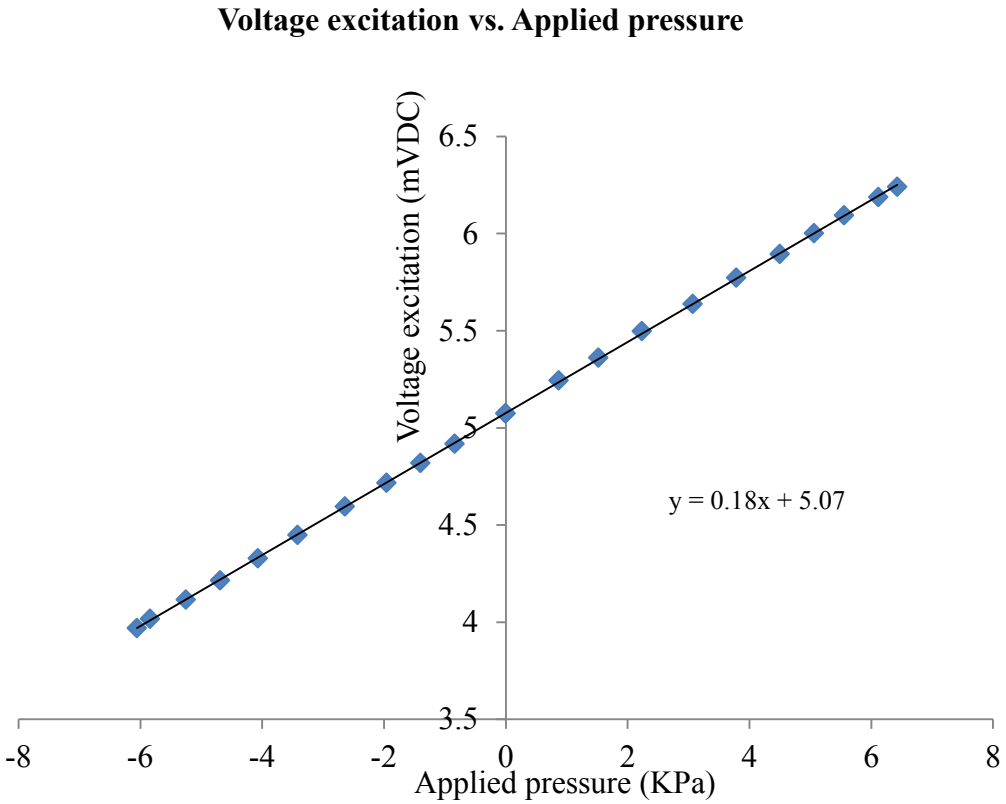

Figure B.4 A plot of voltage excitation measurements versus corresponding applied pressure with a least-squares line overlaid.

B.3 Linear Variable Differential Transformer (LVDT) Calibration

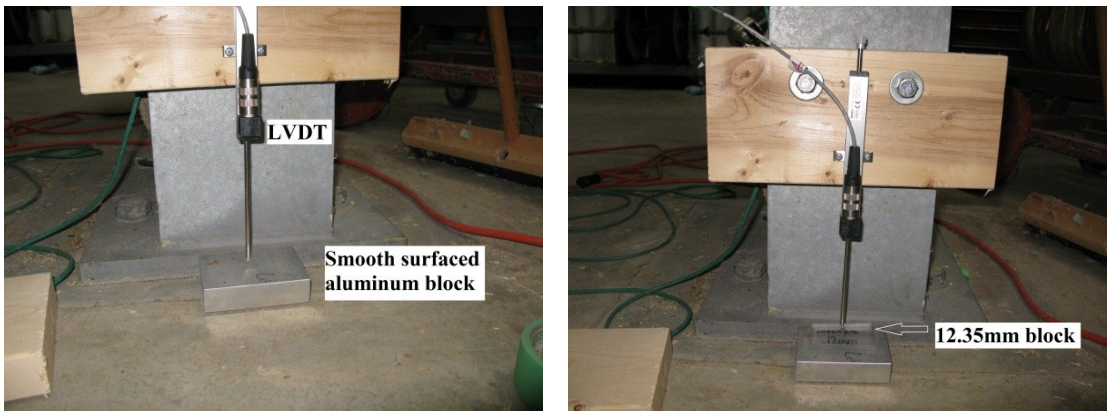

Figure B.5 LVDT calibration technique.

Similar procedure is used to calibrate the LVDTs. LVDT is fixed through a system. A smooth surface (aluminium block surface) is chosen as the zero reading (Figure B.5). The NI-DAQ system will read the data in terms of voltage. Now a 5.2mm and a 12.35mm block is inserted in between the aluminium block and the tip of the LVDT and then measurement is taken by NI-DAQ (voltage) again. These data will be used to find the slope of displacement vs. voltage excitation graph (Figure B.6). Once the slope is known displacement can be found by knowing the voltage excitation during tests.

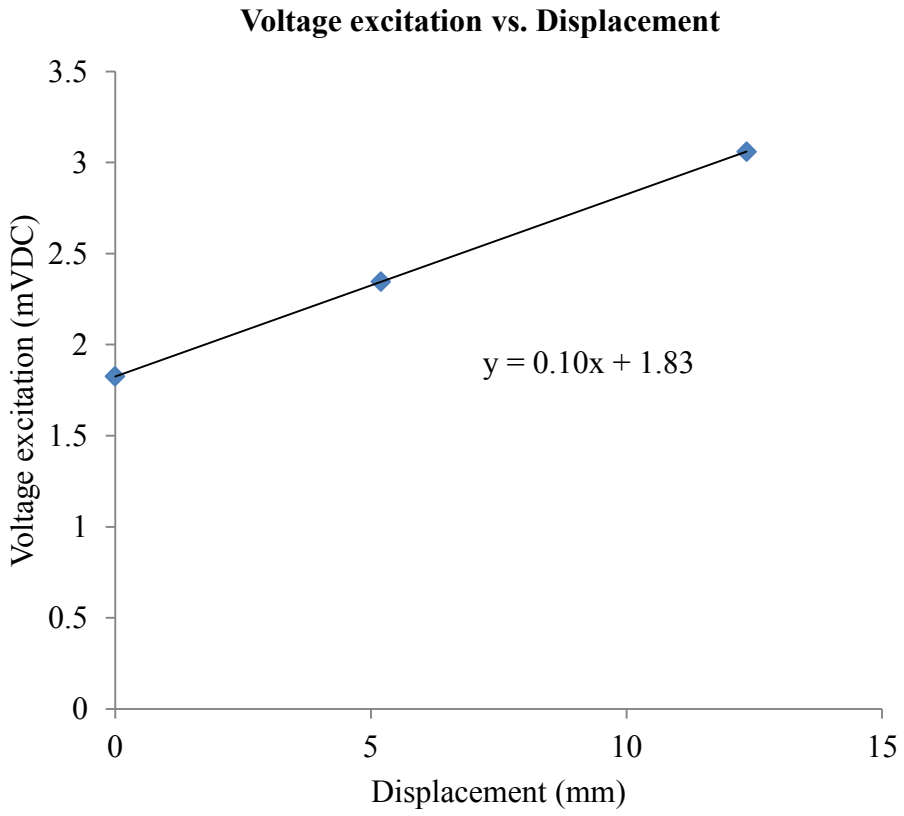

Figure B.6 A plot of voltage excitation measurements versus corresponding displacement with a least-squares line overlaid.

Appendix C

C.1 Measurement uncertainty

Experimental measurements always associated with some kind of variability or randomness and this randomness can affect the concluding results. In this particular project uncertainty comes from the measuring devices itself. The uncertainty can be defined as follows (adapted from Wheeler, A. J & Ganji, A. R. (1996))

$$w = (B^2 + P^2)^{1/2} \quad [C.1]$$

Where, B is known as bias error and P is known as precision error.

The precision error basically depends on the sample size and it is random in individual measurements whereas the bias error doesn't vary in repeated measurements and independent on the sample size.

C.2 Precision uncertainty (linearity error) for load sensors

The slope (m) and the intercept (b) between the two variables R and X must be known in order to get the final results. For a few number of known values of R, X is determined by DAQ system. Linear regression analysis is used to find m and b. So, statistically there is an error between the results from the predicted equation (linear regression) and the original results which is known as linearity error. This error can be calculated as follows:

$$\Delta R_i = |(mX_i + b) - R_a| \quad [C.2]$$

where, R_a is the actual result. If, $S_{\Delta R}$ is the standard deviation of linearity errors for all the data, the precision uncertainty can be calculated as follows:

$$P = t * S_{\Delta R} \quad [C.3]$$

where, t can be determined from students t-Table for selected 95% confidence level and degrees of freedom ν=N-1, where N=total number of data points.

C.3 Bias uncertainty for load sensors

If the output results R has a linear relationship with the sensors response X:

$$R = mX + b \quad [C.4]$$

The bias uncertainty can be calculated as follows:

$$B = X_u * \frac{dR}{dX} = X_u * m \quad [C.5]$$

where, X_u is the measurement uncertainty of the sensing device.

Table C.1 Uncertainties associated with individual Tension Load Cells (TLC).

TLC#	Uncertainties, kN
101327	0.0565
101328	0.0626
101329	0.0580
101330	0.0649
101331	0.0569
101332	0.0591

101333	0.0570
Mean	0.0593

Table C.2 Uncertainties associated with individual Bending Beam Load Cells (BLC).

BLC#	Uncertainties, kN
32634	0.0396
32599	0.0372
32601	0.0392
32603	0.0439
32609	0.0384
32610	0.0397
32612	0.0479
32613	0.0376
32614	0.0440
32623	0.0444
32625	0.0422
32628	0.0419
32630	0.0407
32633	0.0383
Mean	0.0411

Appendix D

D.1 Roof idealization

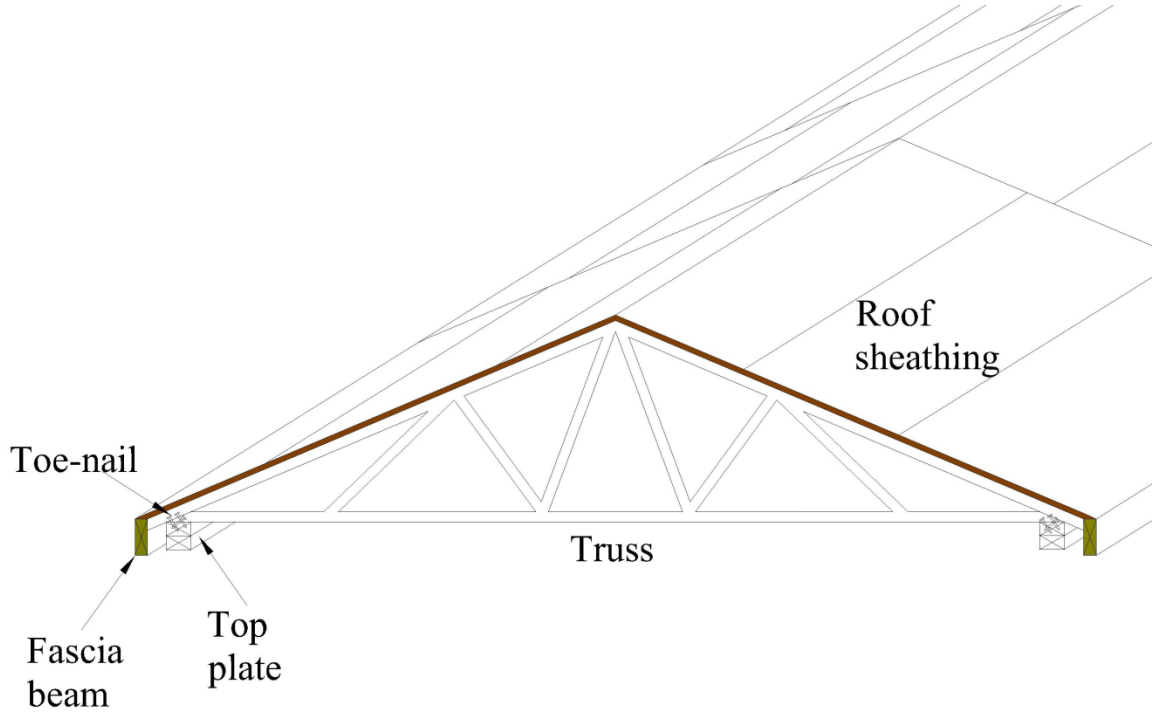

Figure D.1 Roof system. The truss of the roof is nailed to the top plate by three-12d nails (toe-nail). The end of the trusses is interconnected via a fascia beam.

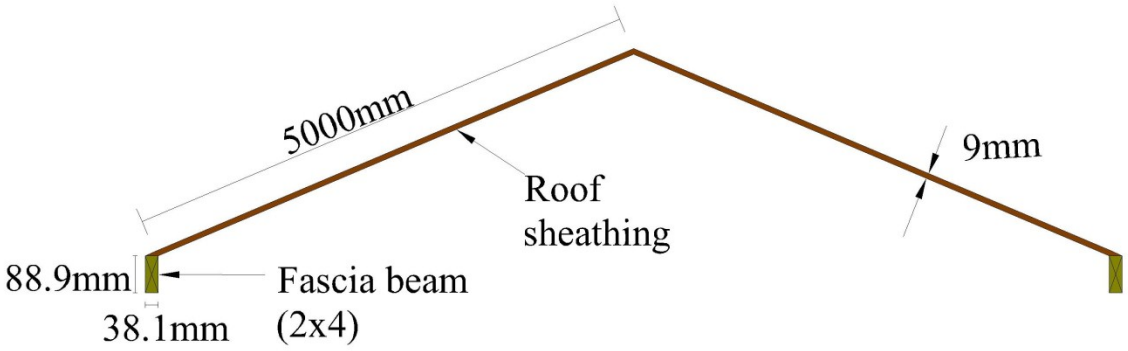

Figure D.2 Roof sheathing and fascia beam are considered for roof bending stiffness.

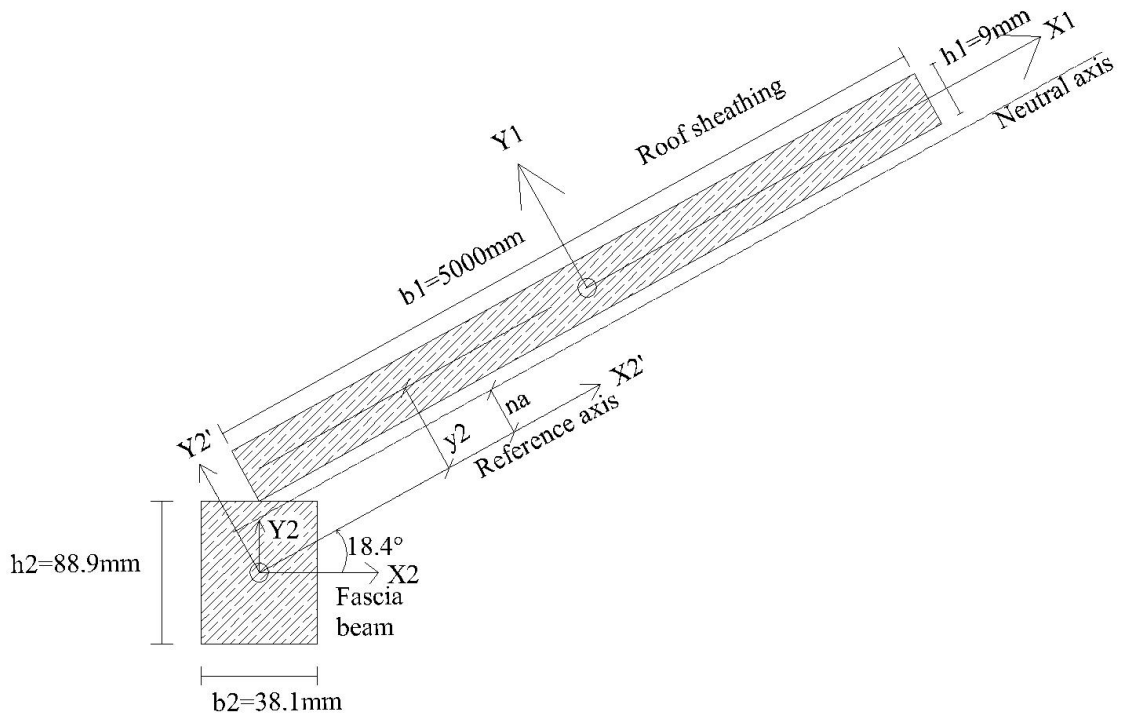

Figure D.3 Cross section of 5000mm long, 9mm thick roof sheathing and 2x4 fascia beam.

Figure D.3 shows the cross section of 5000mm long, 9mm thick roof sheathing and 2x4 fascia beam (38.1mm x 88.9mm). Note that this figure does not show all the details of a simple roof of a house. However, roof sheathing and fascia beams appear to be the most important element which contributes the flexural rigidity of the roof along the direction perpendicular to the trusses. The flexural rigidity of this composite element (as shown in Figure D.3) can be calculated as follows:

Distance from the fascia beam to the ridge, b1=5000mm (Figure D.3);

Thickness of the plywood, h1=9mm (Figure D.3);

Fascia beam's width, b2=1.5*25.4=38.1mm;

Fascia beam's height, h2=3.5*25.4=88.9mm;

Along the centroid of the fascia beam the moment of inertia with respect to X2 axis, I_{X_2} = b2*h2^3/12;

Along the centroid of the fascia beam the moment of inertia with respect to Y2 axis, I_{Y_2} = h2*b2^3/12;

Moment of inertia with respect to transformed axis X2', $I_{X_2}' = I_{X_2}*\cos^2\Theta + I_{Y_2}*\sin^2\Theta$;

Along the centroid of roof sheathing, the moment of inertia with respect to X axis, I_{X_1}=b1*h1^3/12;

Distance from the reference axis to the centroid of roof sheathing, y1=0.5*h1+0.5*h2*Cos Θ;

Distance from the reference axis to the centroid of fascia beam, y2=0;

Area of roof sheathing, A1=b1*h1;

Area of fascia beam, A2=b2*h2;

Distance from the reference axis to neutral axis of the composite section, na=(A1*y1+A2*y2)/(A1+A2)

Moment of inertia of roof sheathing with respect to neutral axis, $I_1 = I_{X_1} + A1*(y1-na)^2$;

Moment of inertia of roof sheathing with respect to neutral axis, $I_2 = I_{X_2}' + A2*(y2-na)^2$;

Modulus of elasticity of roof sheathing (plywood), E_1=11000 N/mm^2.

Modulus of elasticity of fascia beam, E_2=10000 N/mm^2.

Flexural rigidity of the composite section, $EI = E_1I_1 + E_2I_2$= 92.95 kN-m^2.

So, the flexural rigidity of the composite section which is constructed by 5000mm long, 9mm thick roof sheathing and 2x4 fascia beam is 92.95kN- m^2. By using the same approach described above and by keeping the roof sheathing same and changing the

fascia from 2x4 to 2x6 the flexural rigidity was found 322.89kN- m^2. So, by changing the fascia from 2x4 to 2x6 the flexural rigidity of the composite section is increased around 3.5 times.

Since the procedure described above does not include all the details of a simple roof and the actual roof bending stiffness is very challenging to quantify, the beams cross section was chosen based on the availability of the materials and accessibility of installation under the airbags. Two types of beams have been used in the experiments. The cross sections of the beams are 38.1mm x 38.1mm x 6.35mm and 63.5mm x 63.5 mm x 4.76mm (shown in Figure D.4). The bending stiffness of the stiffer beams is chosen purposefully four times higher than the bending stiffness of the less stiff beams.

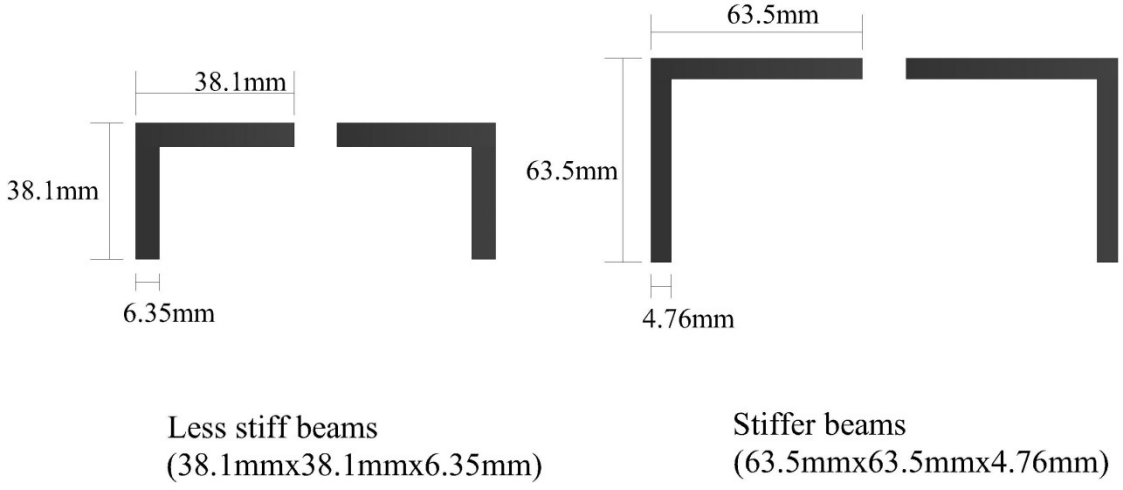

Figure D.4 Cross sections of the steel beams which have been used in the present study (less stiff system and stiffer system).

D.2 Flexural rigidity of less stiff beams

Modulus of elasticity of Steel, E=200000 N/mm^2

Moment of inertia of the steel angle section, I= $5.7658x10^4 mm^4$

Flexural rigidity of the steel angle, EI= 1.1532×10^{10} N-mm^2.

Flexural rigidity of two steel angle sections=$2 \times 1.1532 \times 10^{10}$ N-mm^2=23.1kN-m^2.

D.3 Flexural rigidity of stiffer beams

Modulus of elasticity of Steel, E=200000 N/mm^2

Moment of inertia of the steel angle section, I= 2.2749×10^5 mm^4

Flexural rigidity of the steel angle, EI= 4.5498×10^{10} N-mm^2.

Flexural rigidity of two steel angle sections=$2 \times 4.5498 \times 10^{10}$ N-mm^2 =91kN-m^2.

Appendix E

E.1 Illustration of two-sample t-test

The formula for the t-test for independent samples is:

$$t = \frac{\bar{X}-\bar{Y}}{S_{\bar{X}-\bar{Y}}} \quad [E.1]$$

where the numerator equals the difference between two sample means $(\bar{X}, \bar{Y})$, and the denominator, $S_{\bar{X}-\bar{Y}}$ called the 'standard error of difference' which equals the combined standard deviation of both samples. The formula for 'standard error of difference' is:

$$S_{\bar{X}-\bar{Y}} = \sqrt{\frac{(n_x-1){S_x}^2+(n_y-1){S_y}^2}{n_x+n_y-2} * [\frac{1}{n_x}+\frac{1}{n_y}]} \quad [E.2]$$

where (S_x, S_y) are the samples standard deviations and (n_x, n_y) are the samples sizes.

The null hypothesis for two-sample t-test for independent data is defined as:

$$H_o: \mu_1 = \mu_2 \quad [E.3]$$

$$H_A: \mu_1 \neq \mu_2 \quad [E.4]$$

Reject the null hypothesis that the two means are equal (i.e. H_o) if,

$$|t| > t_{1-\frac{\alpha}{2},\vartheta} \quad [E.5]$$

where, α=significance level=5%

ϑ=degree of freedom=$n_x + n_y - 2$

Here, $t_{1-\frac{\alpha}{2},\vartheta}$ = critical t-statistic, which depends on the significance level and the degree of freedom. This value can be determined from student's t-distribution.

Example

A null hypothesis was formed (i.e. equation E.1) that there is no difference in mean values between arbitrary (X) and data-driven (Y) estimation of initial slope for 8kN/min ramp loads. The means and standard deviations of initial slopes for arbitrary ($n_x = 35$ samples) and data-driven estimation ($n_y = 35$ samples) are $\bar{X} = 1.062\text{kN/mm}$, $\bar{Y} = 0.972\text{kN/mm}$ and $S_x = 0.474\text{kN/mm}$, $S_y = 0.369\text{kN/mm}$ respectively. The t-statistic was calculated by equation E.2 and E.1 and found 0.892. The critical t-statistic for significance level, α=5% and 68 degrees of freedom was found to be 1.995 (from student t-distribution). The t-statistic is lower than the critical t-statistic in this case which is opposite to equation E.5. So, the null hypothesis could not be rejected at 5%. Thus, it means that, statistically there is no difference in mean values between the arbitrary and data-driven estimation.

E.2 Illustration of one-way analysis of variance (ANOVA)

The logic used in ANOVA (analysis of variance) to compare means of multiple groups is similar to that used with the t-test to compare means of two independent groups. When one-way ANOVA is applied to the special case of two groups, one-way ANOVA gives identical results as the t-test. The logic of this approach extends directly to one-way analysis of variance with **K** groups. We can use our data to calculate two independent estimates of the population variance: one is the pooled variance of scores within groups,

and the other is based on the observed variance between group means. These two estimates are expected to be equal if the population means are equal for all **K** groups (null hypothesis, H_0: $\mu_1 = \mu_2 = \ldots = \mu_k$), but the estimates are expected to differ if the population means are not all the same or at least one is different (alternate hypothesis: H_A).

The estimate of the population variance based on the variability between group means is considerably larger than the estimate based on variability within groups. We should like to know how likely it is that two estimates of the same population variance would differ so widely if all of our assumptions are valid (i.e. $\mu_1 = \mu_2 = \ldots = \mu_k$). The F-statistic is designed to test the null hypothesis. F-statistic can be determined as follows:

$$F\ (df_{BG}, df_{WG}) = \frac{Between\ Groups\ estimate\ of \sigma_y^2}{Within\ Groups\ estimate\ of \sigma_y^2} = \frac{MS_{BG}}{MS_{WG}} \qquad \text{E.6}$$

where df_{BG}, df_{WG} stands for degrees of freedoms of Between Group and Within Group respectively and MS_{BG}, MS_{WG} stands for Mean Squares Between Groups and Mean Squares Within Groups respectively. These parameters can be estimated as follows:

$$MS_{BG} = \frac{SS_{BG}}{df_{BG}} = \frac{\sum_j n_j(\bar{y}_j - \bar{y})^2}{(K-1)} \qquad \text{E.7}$$

$$MS_{WG} = \frac{SS_{WG}}{df_{WG}} = \frac{\sum_{ij}(y_{ij} - \bar{y}_j)^2}{\sum_j(n_j - 1)} \qquad \text{E.8}$$

where, j stands for the group number, n stands for the sample size within a group, K stands for the total number of groups and $\bar{y}$ represents the grand mean of the data considering all groups. However, SS_{BG} represents Sum of Squared deviations for each

group mean about the grand mean and SS_{WG} represents Sum of squared deviations for all observations within each group from that group mean, summed across all groups.

Reject the null hypothesis that the means of k groups are equal (i.e. H_o) if,

$$F > F_{\alpha,df_{BG},df_{WG}} \quad [E.9]$$

where, α=significance level=5%

Here, $F_{\alpha,df_{BG},df_{WG}}$ = critical F-statistic, which depends on the significance level (α) and the degree of freedoms of Between Groups (df_{BG}) and Within Group (df_{WG}). This value can be determined from F-distribution.

Example:

A null hypothesis was formed (i.e. H_0) that the mean failure capacities for different loading type (i.e. ramp or fluctuating) and test type (individual or system) are equal. So there are six groups (K) in total and in each group there are 35 samples (n). From this statistical hypothesis test described above the F-statistic was found 0.71. The critical F-statistic was found 2.26 for $\alpha = 5\%, df_{BG} = 5 \; and \; df_{WG} = 204$. The F-statistic is smaller than the critical F-statistic which is opposite to equation E.1. Thus, the null hypothesis could not be rejected at the 5% significance level that the mean failure capacities are same for all the loading and test type.

E.3 Anderson-Darling Goodness-of-Fit test

Testing a Normal distribution using Anderson-Darling Goodness-of-Fit test (AD GoF)

The AD GoF test for Normality has the functional form:

$$AD = \sum_{i=1}^{n} \frac{1-2i}{n} \left\{ \ln\left(F_o\left[Z_{(i)}\right]\right) + \ln\left(1 - F_o\left[Z_{(n+1-i)}\right]\right) \right\} - n \qquad \text{E.10}$$

Where F_o is the assumed (Normal) distribution with the assumed or sample estimated parameters (μ, σ); $Z_{(i)}$ is the ith sorted, standardized, sample value; "n" is the sample size. The null hypothesis, that the true distribution is F_o with the assumed parameters, is then rejected (at significance level α=0.05, for sample size n) if the AD test statistic is greater than the critical value (AD_{CV}). The rejection rule is:

Reject if:

$$AD > AD_{CV} = \frac{0.752}{\left(1 + \frac{0.75}{n} + \frac{2.25}{n^2}\right)} \qquad \text{E.11}$$

Testing a Log-normal distribution using Anderson-Darling Goodness-of-Fit test (AD GoF)

To fit a Log-normal distribution the logarithm of the data can be taken and then by following the above described procedure the null hypothesis can be checked or rejected.

Testing a Weibull distribution using Anderson-Darling Goodness-of-Fit test (AD GoF)

The Weibull version of the AD GoF test statistic is different from the Normality test described above. Anderson-Darling statistic can be determined as follows:

$$AD = \sum_{i=1}^{n} \frac{1-2i}{n} \left\{ \ln(1 - \exp(-Z_{(i)})) - Z_{(n+1-i)} \right\} - n \qquad \text{E.12}$$

Modified Anderson-darling statistic:

$$AD^* = \left(1 + \frac{0.2}{\sqrt{n}}\right) * AD \qquad \text{E.13}$$

where $Z_{(i)} = [\frac{x_{(i)}}{\alpha}]^{\beta}$; α=scale parameter of Weibull distribution ; β=shape parameter of Weibull distribution. The OSL (observed significance level) probability (p-value) is now used for testing the Weibull assumption. If OSL<0.05 then the Weibull assumption is rejected and the error committed is less than 5%. The OSL formula is given by:

$$OSL = \frac{1}{1+\exp[-0.1+1.24\ln(AD^*)+4.48(AD^*)]} \qquad \text{E.14}$$

Curriculum Vitae

Name:	Mohammad Abrar Alam Khan
Post-secondary Education and Degrees:	Bangladesh University of Engineering & Technology Dhaka, Bangladesh 2004-2009, BSc. The University of Western Ontario London, Ontario, Canada 2010-2012 MESc.
Honours and Awards:	Graduate Thesis Research Award 2012 Alan G. Davenport Graduate Award 2011 Western Graduate Research Scholarship (WGRS) 2010-2012
Related Work Experience	Teaching Assistant The University of Western Ontario 2010-2012

Conference Proceedings:

Kopp, G. A., Khan, M. A. A., Henderson, D. J. and Morrison, M. J. (2012). *"Analysis of wood-framed, roof failures under realistic hurricane wind loads."* The Applied Technology Council (ATC) and the Structural Engineering Institute (SEI) of the American Society of Civil Engineers (ASCE), Advances in Hurricane Engineering Conference, 2012. Miami, Florida, USA (to be presented)

Khan, M. A. A., Henderson, D. J., Morrison, M. J. and Kopp, G. A. (2012). *"Damage accumulation and Load-sharing in residential, wood-frame roofs under fluctuating wind loads."* 2012 Joint Conference of the Engineering Mechanics Institute and the 11th ASCE Joint Specialty Conference on Probabilistic Mechanics and Structural Reliability; Notre Dame, IN, USA

Poster Presentation: Khan, M. A. A., Henderson, D. J., Morrison, M. J. and Kopp, G. A. (2012). "*Load-sharing of toe-nailed, roof-to-wall connections under extreme wind loads*." 3rd American Association for Wind Engineering Workshop Hyannis, Massachusetts, USA August 12 - 14, 2012